LIST OF PUBLICATIONS

1. **Hajra D**, Rajmani RS, Chakravortty D. (2024) Salmonella-induced SIRT1 and SIRT3 are crucial for maintaining the metabolic switch in bacteria and host for successful pathogenesis *eLife***13**: RP93125 (**In press, Elife**)
2. Roy Chowdhury A[*], **Hajra D[*]**, Mukherjee D[*], Nair AV, Chakravortty D. Functional OmpA of Salmonella Typhimurium provides protection from lysosomal degradation and inhibits autophagic processes in macrophages. J Infect Dis. 2024 Jul 30:jiae376. doi: 10.1093/infdis/jiae376. Epub ahead of print. PMID: 39078938. * Equal contribution.
3. Agharkar N.A[*], **Hajra D[*]**, Jaiswal V, Kabi P, Chakravortty D, Basu S. Evaporation of bacteria-laden surrogate respiratory fluid droplets on a hydrophilic substrate versus contact free environment confers differential bacterial infectivity. * Equal contribution. (**Accepted, *Physics of Fluids***, POF-24-AR-000158R)
4. **Hajra D**, Kirthivasan N, Chakravortty D. Symbiotic Synergy from Sponges to Humans: Microflora-host harmony is crucial for ensuring survival and shielding against invading pathogens. ACS Infectious Diseases.2023. https://doi.org/10.1021/acsinfecdis.3c00554
5. **Hajra D**, Yadav V, Singh A, Chakravortty D. SIRT1 and SIRT3 impact host mitochondrial function and host-*Salmonella* pH balance during infection. bioRxiv 2023.09.11.557159; doi: https://doi.org/10.1101/2023.09.11.557159 (**Under Revision**)
6. Ghosh S, Roy S, Baid N, Das K U, **Hajra D**, Menon S et al. A host AAA-ATPase exhibits bacteriolytic activity for clearance of microbial infection.

bioRxiv 2023.07.18.549519; doi: https://doi.org/10.1101/2023.07.18.549519. (**In communication**)

7. **Hajra D**, Mukherjee D, Vij R, Rajmani S, Tatu U, Chakravortty D. *Odoribacter splanchnicus* mitigates *Salmonella*-induced gut inflammation and its associated pathogenesis. (**Under preparation**)
8. **Hajra D**, Nair AV, Chakravortty D. Decoding the invasive nature of a tropical pathogen of concern: The invasive non-Typhoidal Salmonella strains causing host-restricted extraintestinal infections worldwide. Microbiol Res. 2023 Dec;277:127488. doi: 10.1016/j.micres.2023.127488. Epub 2023 Sep 12. PMID: 37716125.
9. Chatterjee R, Chowdhury AR, Nair AV[#], **Hajra D[#]**, Kar A, Datey A, Shankar S, Mishra RK, Chandra N, Chakravortty D. Salmonella Typhimurium PgtE is an essential arsenal to defend against the host resident antimicrobial peptides. Microbiol Res. 2023 Jun;271:127351. doi: 10.1016/j.micres.2023.127351. Epub 2023 Mar 11.PMID: 36931126 #-Equal contribution.
10. **Hajra D**, Nair AV, Roy Chowdhury A, Mukherjee S, Chatterjee R, Chakravortty D. Salmonella Typhimurium U32 peptidase, YdcP, promotes bacterial survival by conferring protection against in vitro and in vivo oxidative stress. Microb Pathog. 2022;173(Pt B):105862. doi:10.1016/j.micpath.2022.105862.
11. **Hajra D**, Nair AV, Chakravortty D. An elegant nano-injection machinery for sabotaging the host: Role of Type III secretion system in virulence of different human and animal pathogenic bacteria. Phys Life Rev. 2021 Sep;38:25-54. doi: 10.1016/j.plrev.2021.05.007. Epub 2021 May 26. PMID: 34090822.

12. **Hajra D**, Datey A, Chakravortty D. Attenuation Methods for Live Vaccines. Methods Mol Biol. 2021;2183:331-356. doi: 10.1007/978-1-0716-0795-4_17. PMID: 32959252.

Microbiology and Infectious Disease

Salmonella-induced SIRT1 and SIRT3 are crucial for maintaining the metabolic switch in bacteria and host for successful pathogenesis

Reviewed Preprint
v2 • July 16, 2024
Revised by authors

Reviewed Preprint
v1 • February 13, 2024

Dipasree Hajra, Raju S Rajmani, Ayushi Devendrasingh Chaudhary, Shashi Kumar Gupta, Dipshikha Chakravortty

Department of Microbiology & Cell Biology, Indian Institute of Science • Centre of Infectious Disease Research, Indian Institute of Science, Bangalore, India • Pharmacology Division, CSIR-Central Drug Research Institute, Lucknow, India • Academy of Scientific and Innovative Research (AcSIR), Ghaziabad, India • Adjunct Faculty, School of Biology, Indian Institute of Science Education and Research, Thiruvananthapuram

Abstract

Sirtuins are the major players in host immuno-metabolic regulation. However, the role of sirtuins in the modulation of the immune metabolism pertaining to Salmonellosis is largely unknown. Here, our investigation focussed on the role of two important sirtuins, SIRT1 and SIRT3, shedding light on their impact on intracellular *Salmonella*'s metabolic switch and pathogenesis establishment. Our study indicated the ability of the live *Salmonella* Typhimurium to differentially regulate the levels of SIRT1 and SIRT3 for maintaining the high glycolytic metabolism and low fatty acid metabolism in *Salmonella*. Perturbing SIRT1 or SIRT3 through knockdown or inhibition, resulted in a remarkable shift in the host metabolism to low fatty acid oxidation and high glycolysis. This switch led to decreased proliferation of *Salmonella* in the macrophages. Further, *Salmonella*-induced higher levels of SIRT1 and SIRT3 led to a skewed polarization state of the macrophages from a pro-inflammatory M1 state toward an immunosuppressive M2 making it more conducive for the intracellular life of *Salmonella*. Alongside, governing immunological functions by modulating p65 NF-κB acetylation, SIRT1, and SIRT3 also skew *Salmonella*-induced host metabolic switch by regulating the acetylation status of HIF-1α and PDHA1. Interestingly, though knock-down of SIRT1/3 attenuated *Salmonella* proliferation in macrophages, in *in vivo* mice-model of infection, inhibition or knockdown of SIRT1/3 led to more dissemination and higher organ burden which can be attributed to enhanced ROS and IL-6 production. Our study hence reports for the first time that *Salmonella* modulates SIRT1/3 levels to maintain its own metabolism for successful pathogenesis.

eLife assessment

This study presents **valuable** findings on the role of the sirtuins SIRT1 and SIRT3 during Salmonella Typhimurium infection. Although the work increases our understanding of the mechanisms used by this pathogen to interact with its host and may have implications for other intracellular pathogens, the reviewers found that the evidence to support the claims is **incomplete**. In particular, the discrepancy between results obtained using cultured cell lines and the animal model of infection, as well as potential indirect effects through the microbiome stand out.

https://doi.org/10.7554/eLife.93125.2.sa3

Introduction

Sirtuins are NAD+-dependent deacetylases that are present in all forms of life. Sirtuins comprise a conserved core catalytic domain that removes acetyl moiety from the lysine residues of proteins in presence of NAD+ as a cofactor [1] giving rise to 2'O-acetyl-ADP-ribose and free nicotinamide as products[2][3]. Free nicotinamide acts as a non-competitive inhibitor of sirtuins[4]. They possess variable N terminal and C terminal domains that confer different subcellular localization, substrate specificity, and functions[5]. Mammals have seven sirtuins that are responsible for regulating various biological functions such as cell survival, apoptosis, oxidative stress, metabolism, and inflammation[6][7]. SIRT1,6 and 7 have nuclear localization, SIRT2 is cytoplasmic and SIRT 3,4 and 5 comprise the mitochondrial SIRTs. In addition to their deacetylase activity, they possess ADP ribosylation (SIRT1, SIRT4, and SIRT6), desuccinylation and demalonylation (SIRT5), delipoylation (SIRT4), and demyristoylation and depalmitoylation (SIRT6) enzymatic activities [8]. Previous studies have shown that SIRT1 gets activated in response to acute immune response and it deacetylates RelA/p65 component of NFκB thereby mediating its proteasomal degradation[9]. On the other hand, it activates RelB component of NFκB pathway. RelB causes heterochromatinization of pro-inflammatory genes like TNF-α and IL-β[10]. SIRT1 activates Peroxisome proliferator-activated receptor γ (PPARγ) coactivator-1α (PGC-1α) mediating a metabolic switch from glycolysis toward fatty acid oxidation. SIRT1-mediated RelB activation, in turn, activates SIRT3 causing the promotion of mitochondrial bioenergetics[11]. PGC-1α, a major player in mitochondrial biogenesis, activates SIRT3 [12] which in turn causes activation of PGC-1α, thereby fuelling a positive feedback loop. SIRT3 accounts for the major mitochondrial deacetylase orchestrating several metabolic processes such as fatty acid oxidation, promotion of the TCA cycle, and inhibition of ROS production[13].

Salmonella enterica serovar Typhimurium is a facultative intracellular Gram-negative enteric pathogen, causing a wide array of infections ranging from self-limiting gastroenteritis to diarrhea in humans [14]. *Salmonella enterica* serovar Typhi cause systemic infection in humans with typhoidal symptoms. Recent reports reported incidences of 21 million [15] typhoid cases and 93 million of non-typhoidal [16] cases round the year. The virulence of *Salmonella* is majorly regulated by two pathogenicity islands, namely, SPI-1 and SPI-2. It uses SPI-1 encoded T3SS and the effector proteins to invade host cells [17]. Inside the macrophages, they harbour within the *Salmonella* containing vacuoles (SCV) by virtue of its SPI-2 effectors [18]. Macrophages, dendritic cells and neutrophils are responsible for successful dissemination throughout the body through the reticulo-endothelial system (RES) [17].

Macrophages, serving as an intracellular niche for *Salmonella,* exhibit several continua of polarization states. At the two extreme ends of the spectrum lie the classically polarized M1 macrophages and alternatively activated M2 macrophages. M1 macrophages comprise of the proinflammatory antimicrobial state producing IL-1β, IL-6, TNF-α,IL-12, IFN-γ cytokines and exhibit enhanced expression of CD80, CD86 surface markers. The anti-inflammatory M2 macrophages promote bacterial persistence by producing anti-inflammatory cytokines like IL-10,TGF-β and show increased expression of Arg-1, CD206 surface markers[19][20]. To sustain the continuous production of proinflammatory cytokines M1 macrophages rely on glycolysis for their energy requirements. On the other hand, M2 macrophages are fuelled by enhanced oxidative phosphorylation (OXPHOS) and fatty acid oxidation (FAO)[21].It has been previously reported that sirtuins mediated attuning of metabolism impact polarization of macrophages *in vivo*. SIRT1 has the ability to promote the polarization of M2 macrophages and inhibit inflammation in macrophages of adipose tissue[22][23][24]. SIRT3 suppresses ROS by deacetylating and activating MnSOD[25].

Several bacteria are known to subvert the host immune system toward an immunosuppressive state. *Salmonella* or *Mycobacterium* have evolved mechanisms to counteract the M1 state of the host macrophage. *Salmonella* Typhimurium uses its SPI-2 effectors to inhibit the recruitment of NADPH oxidase to the SCV, thereby preventing oxidative burst mediated microbicidal activity[26]. Similarly, *Mycobacterium bovis* bacillus Calmette-Guérin prevents NOS2 recruitment to phagosomes[27]. *Salmonella* Dublin causes inhibition of the production of pro-inflammatory cytokine like IL-18 and IL-12p70[28]. Moreover, *Mycobacteria* inhibits NFκB signalling and IFN-γ mediated downstream pathways[29]. Furthermore, *Yersinia enterocolitica* elicits an M2 response by inducing Arginase-1 expression and TGFβ1 and IL-4production[30]. *Yersinia* TTSS effector LcrV induces an M2 phenotype supposedly by IL-10 production[31].

Since SIRT1 and SIRT3 are the major modulators of the immuno-metabolic paradigm, we intend to decipher the role of SIRT1 and SIRT3 in influencing host and *Salmonella* metabolism. This study highlights the role of SIRT1 and SIRT3 in intracellular pathogen survival by promoting *Salmonella* glycolysis and concomitantly driving host metabolism towards fatty acid oxidation. Additionally, *Salmonella* trigger an immunosuppressive M2 environment conducive to its intravacuolar proliferation by modulating SIRT1 and SIRT3 levels. Here, we have shown that SIRT1 and SIRT3 knockdown cause decreased M2 surface marker expression such as CD206 along with increased production of pro-inflammatory cytokines and ROS generation, together amounting to attenuated bacterial intracellular proliferation within the infected macrophages. Moreover, SIRT1 mediated p65 NF-κB deacetylation played a vital role in immune function regulation within the *Salmonella* infected macrophages with increased interaction of SIRT1 with p65 NF-κB. SIRT1 knockdown or inhibition resulted in hyperacetylation of p65 NF-κB thereby leading to enhanced pro-inflammatory response in *S*. Typhimurium infected macrophages. Further, SIRT1 and SIRT3 knockdown or inhibition skewed the *Salmonella*-induced host metabolic shift by regulating acetylation status of HIF-1α and PDHA. This caused increased host glycolysis and reduced fatty acid oxidation. However, the *Salmonella* shows the opposing metabolic profile with increased fatty acid oxidation and reduced glycolysis upon SIRT1 or SIRT3 inhibition. In the contrary to the macrophages, in *in vivo* mice-model of infection, SIRT1 and SIRT3 inhibition resulted in increased pathogen loads in organs and triggered enhanced bacterial dissemination, together leading to increased susceptibility of the mice to *S*. Typhimurium infection owing to increased ROS and IL-6 production. To the best of our knowledge, this is the first report implying the ability of host Sirtuins in impacting intracellular bacterial metabolism crucial for successful pathogenesis.

Results

Salmonella modulates SIRT1 and SIRT3 expression along its course of infection in macrophages

Upon infection of RAW 264.7 murine macrophages with wildtype *Salmonella* Typhimurium strain 14028S, we observed an increased expression level of *SIRT 1* and *SIRT3* at initial and middle phases of infection, precisely at 2hr and 6hr post infection through qPCR (**Fig. 1**, A and B). The *SIRT1* expression level declined at later phases of infection. On the other hand, the *SIRT3* transcript levels remained elevated at all time points with respect to uninfected control with a marked increment at 16hr time point post-infection which subsided at 20hr post-infection. We even monitored the expression profile of *SIRT1* and *SIRT3* in primary macrophages like peritoneal macrophages of C57BL/6 mice and observed a similar trend of elevated expression at initial (2hr), middle (6hr), and late (16hr) time points post-infection (**Fig. 1**, C and D). In Confocal Laser Scanning Microscopy (CSLM) studies, we observed a similar increase in SIRT1 and SIRT3 expression at 6hr post infection within the infected macrophages RAW264.7 macrophages. (**Fig. 1**, E-H). Immunoblotting revealed increased protein expression of both SIRT1 and SIRT3 at 2hr post-infection in comparison to the uninfected control (Fig. S1). However, SIRT1 expression exhibits a gradual decline at the late phase of infection (Fig. S1A, C). In line with the confocal microscopy data, SIRT3 immunoblotting data shows an increased protein expression profile at 6hr and 16hr post-infection (Fig. S1, B-D). Subsequently, to ascertain whether indeed *Salmonella* could modulate SIRT1 or SIRT3 expression levels, we evaluated the *SIRT1* and *SIRT3* mRNA and SIRT1 and SIRT3 protein expression profile within RAW264.7 macrophages upon infection with wildtype *S*. Typhimurium and SPI-1 (Δ*invC*) (InvC-protein export apparatus) or SPI-2 (Δ*ssaV* and Δ*steE*) (SsaV-Structural component of SPI-2 needle apparatus, SteE-SPI-2 effector protein involved in driving M2 polarization) mutants of *S*. Typhimurium. Our results depict the ability of wildtype *S*. Typhimurium to induce the expression of both SIRT1 and SIRT3 within the infected RAW264.7 macrophages. However, infection with either SPI-1 or SPI-2 mutant abrogates the induction of *SIRT1* whereas only SPI-2 mutants (Δ*ssaV* and Δ*steE*) and not SPI-1 mutant infection caused reduction in *SIRT3* transcript level expression in the infected macrophages, implicating the role of SPI-1 and SPI-2 genes in triggering SIRT1 and SIRT3 in the infected macrophages (**Fig. 1**, I-J). However, at the protein level, only SPI-2 mutant infection resulted in a predominant decline in SIRT3 expression and a mild reduction in SIRT1 expression (Fig. S1B). Further, we examined the transcript level profile of *SIRT1* and *SIRT3* in M1 or M2 polarized RAW264.7 macrophages at 16hr post-infection and we observed 20-fold and 5-fold increase in *SIRT1* and *SIRT3* expression in M2 polarized infected macrophages as opposed to 0.5-fold and 0.4 fold downregulation in M1 polarized infected macrophages (Fig. S1C-D). Thus, an increase in expression profile both at transcript and protein levels indicates their role in *Salmonella* pathogenesis.

SIRT1 and SIRT3 play crucial role in intracellular bacterial proliferation in infected murine macrophages

As our previous *SIRT1* and *SIRT3* expression data in the polarized macrophages, hinted at the role of SIRT1 and SIRT3 in driving polarization of macrophages in the infected macrophages. We validated the intracellular replication of *S*. Typhimurium within the infected polarized macrophages. *S.* Typhimurium exhibited increased intracellular fold proliferation within anti-inflammatory M2 polarized macrophages in comparison to the pro-inflammatory M1 polarized RAW264.7 macrophages (Fig. S1 E-F). To evaluate the role of SIRT 1 and SIRT3 in the intracellular proliferation of the bacteria within murine macrophages, we have undertaken knockdown of SIRT1 and SIRT3 in RAW 264.7 (Fig. S2) macrophages through PEI-mediated transfection of shRNA plasmids directed against SIRT1 and SIRT3. Post 48hr of transfection, the transfected cells were

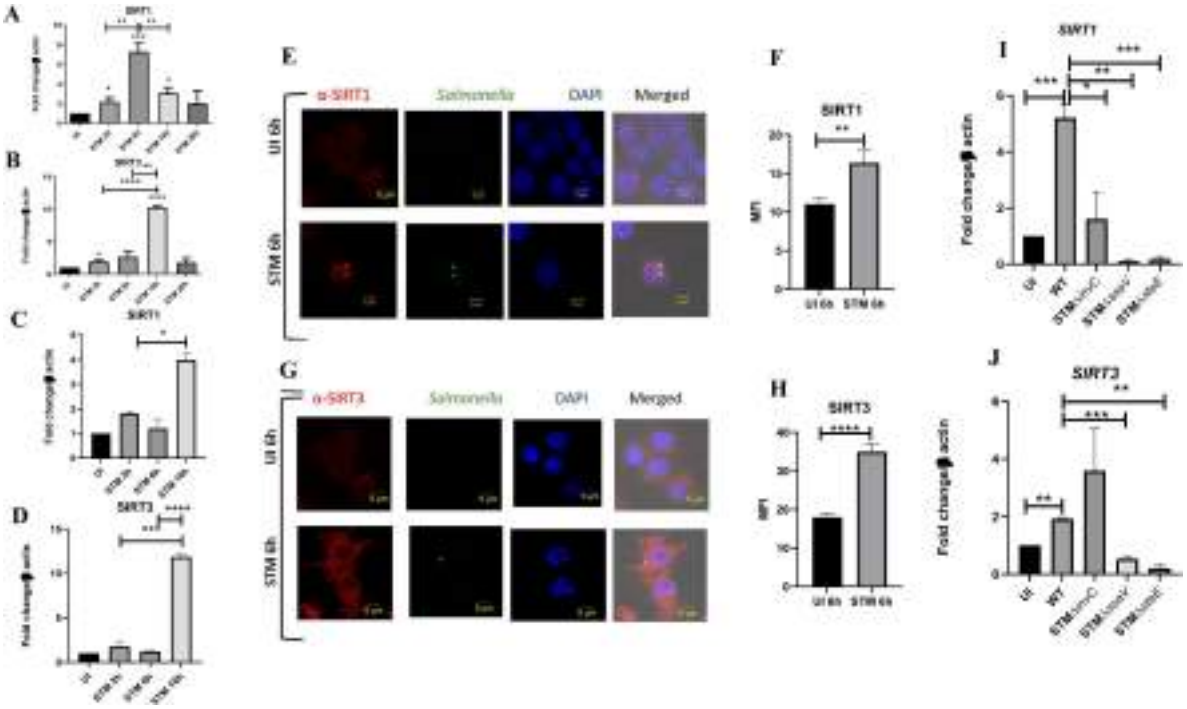

Fig. 1

– *Salmonella* modulates the expression of SIRT1 and SIRT3 along its course of infection

A-B. Expression studies of *SIRT1* and *SIRT3* through qPCR in RAW 264.7 macrophages. Data is representative of N=4, n=2. Unpaired two tailed Student's t test was performed to obtain the p values. (****p<0.0001,***p < 0.001, ** p<0.01, *p<0.05)
C-D-Expression studies of *SIRT1* and *SIRT3* through qPCR in peritoneal macrophages derived from C57BL/6. Data is representative of N=3, n=2. Unpaired two tailed Student's t test was performed to obtain the p values. (****p<0.0001,***p < 0.001, ** p<0.01, *p<0.05)
E. Representative confocal images of RAW264.7 macrophages exhibiting SIRT1 expression upon *S.* Typhimurium infection at indicated time points post infection. Data is representative of N=3, n=80 (microscopic field).
F. Quantitative representation of the expression profile as depicted in the confocal images (E) in terms of Mean Fluorescence Intensity (MFI). Unpaired two tailed Student's t test was performed to obtain the p values. (****p<0.0001,***p < 0.001, ** p<0.01)
G. Representative confocal images of RAW264.7 macrophages exhibiting SIRT3 expression upon *S.* Typhimurium infection at indicated time points post infection. Data is representative of N=3, n=80 (microscopic field).
H. Quantitative representation of the expression profile as depicted in the confocal images (G) in terms of Mean Fluorescence Intensity (MFI). Unpaired two tailed Student's t test was performed to obtain the p values. (****p<0.0001, *** p < 0.001, ** p<0.01)
I. qPCR mediated expression of *SIRT1* in RAW264.7 macrophages upon infection with wildtype *S.* Typhimurium or SPI-1 (Δ*invC*) or SPI-2 (Δ*ssaV* and Δ*steE*) *m*utants of *S.* Typhimurium. Data is representative of N=3,n=3. Unpaired two tailed Student's t test was performed to obtain the p values. (****p<0.0001,***p < 0.001, ** p<0.01)
J. qPCR mediated expression of *SIRT3* in RAW264.7 macrophages upon infection with wildtype *S.* Typhimurium or SPI-1 (Δ*invC*) or SPI-2 (Δ*ssaV* and Δ*steE*) *m*utants of *S.* Typhimurium. Data is representative of N=3, n=3. Unpaired two tailed Student's t test was performed to obtain the p values. (****p<0.0001,***p < 0.001, ** p<0.01)

infected with MOI=10 of wildtype *S*. Typhimurium and a gentamicin protection assay was performed. Intracellular proliferation of the bacteria was quantified by plating the cell lysate at 2hr and 16hr post-infection. *Salmonella* exhibits compromised intracellular survival in SIRT1 and SIRT3 knock-down RAW264.7 macrophages in comparison to the un-transfected and scrambled controls (**Fig. 2**, A). Further, we have assessed the intracellular proliferation in peritoneal macrophages isolated from thioglycolate-treated adult C57BL/6 mice post SIRT1 (EX-527) and SIRT3 (3TYP) inhibitor treatment. SIRT1 or SIRT3 inhibitor-treated macrophages exhibited attenuated intracellular replication in comparison to the untreated peritoneal macrophages (Fig,2, B). Together, our results depict the role of SIRT1 and SIRT3 in controlling the intracellular proliferation of *S*. Typhimurium.

SIRT1 and SIRT3 inhibition contribute to skewed inflammatory host responses upon *Salmonella* infection

Several reports indicate the role of SIRT1 and SIRT3 in the modulation of host immune responses pertaining to infection scenarios [35][36][37][38]. Therefore, we intend to check whether SIRT1 or SIRT3 regulates immune functions in *Salmonella*-infected macrophages. To delineate the role of SIRT1 and SIRT3 in the modulation of immune responses, we wished to investigate the production of pro-inflammatory and anti-inflammatory cytokines in knockdown (KD) RAW 264.7 macrophages upon *S.* Typhimurium infection. Post 48hr transfection, cells were subjected to wildtype *S.* Typhimurium infection at an MOI of 10. At the indicated time points, cell-free supernatant was harvested and evaluated for pro-inflammatory and anti-inflammatory cytokine production by ELISA. Inhibition of both SIRT1 and SIRT3 increased production of pro-inflammatory cytokine IL-6 significantly at 2hr and 20hr post-infection (Fig.S3, A). Moreover, there was only a significant reduction in anti-inflammatory IL-10 production upon SIRT1 and SIRT3 KD at 2hr and 20hr post-infection (Fig.S3, B). Further, we estimated the production of another pro-inflammatory cytokine, IL-1β at 20hr post-infection under the knockdown condition of SIRT1 and SIRT3 (Fig.S3, C) and we observed heightened IL-1β production under knockdown of SIRT1 and SIRT3 in comparison to the scrambled infected control. In peritoneal macrophages upon SIRT1(EX-527-1μM) or SIRT3(3-TYP-1μM) chemical inhibitor treatment, an increase in IL-6 and IL-1β cytokine levels was observed at 6hr post-infection (Fig.S3, D-E). This indicates the possible role of SIRT1 and SIRT3 in the regulation of cytokine production upon *Salmonella* infection.

Immune functions are an important determinant of macrophage polarization. Since SIRT1 and SIRT3 played an immune-modulatory role in *Salmonella* infection, we investigated whether *Salmonella* infection is associated with a shift in macrophage polarization status. To assess the ability of the pathogen to alter the polarization state of the macrophage, we have undertaken gene expression profiling of various M1 and M2 markers using nanoString nCounter technology along the course of *Salmonella* Typhimurium infection at the indicated time points in RAW 264.7 macrophages. A gradual shift from pro-inflammatory M1 toward the anti-inflammatory M2 state was observed with the progression of *Salmonella* infection. Along the course of infection, there was a reduction in the expression of M1 markers like *NOS2*, *CD40*,*CD86*, *TNF*-α, *Nfkb2*,*IL-6* and a corresponding increase in the expression of the M2 markers such as *Arg-1*, *CCL-17*, *CD 206*, *IL4ra* with an exception of *Tgf*-β (**Fig. 3**, A).In order to validate the polarization potency of the pathogen, FACS was performed using a pro-inflammatory M1 surface marker, CD86 tagged with PE. The data suggests a distinct decrease in CD86 positive population in the infected sets in comparison to the uninfected and the fixed dead bacteria control along the course of *S.* Typhimurium infection (**Fig. 3**, B, Fig. S4, A). Thus, the live pathogen has a propensity to skew the polarization state of the macrophage toward an anti-inflammatory M2 state to subvert the initial acute inflammatory response mounted by the host immune system.

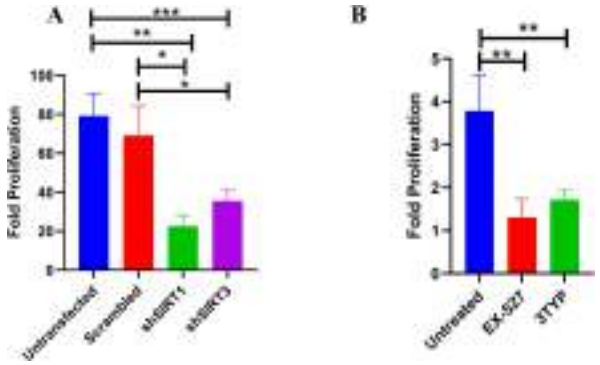

Fig. 2

– Effect of SIRT1 and SIRT3 knockdown in intracellular bacterial proliferation within RAW 264.7 and primary murine macrophages.

A. Fold Proliferation of *Salmonella* Typhimurium within RAW 264.7 macrophages in transfected and un-transfected conditions. Data is representative of N=3, n=3. Unpaired two tailed Student's t test was performed to obtain the p values. (** p<0.01, * p<0.05)

B. Fold Proliferation of *Salmonella* Typhimurium within infected peritoneal macrophages isolated from adult male C57BL/6 mice upon SIRT1 (EX-527) or SIRT3 (3TYP) inhibitor treatment. Unpaired two tailed Student's t test was performed to obtain the p values. (** p<0.01, * p<0.05)

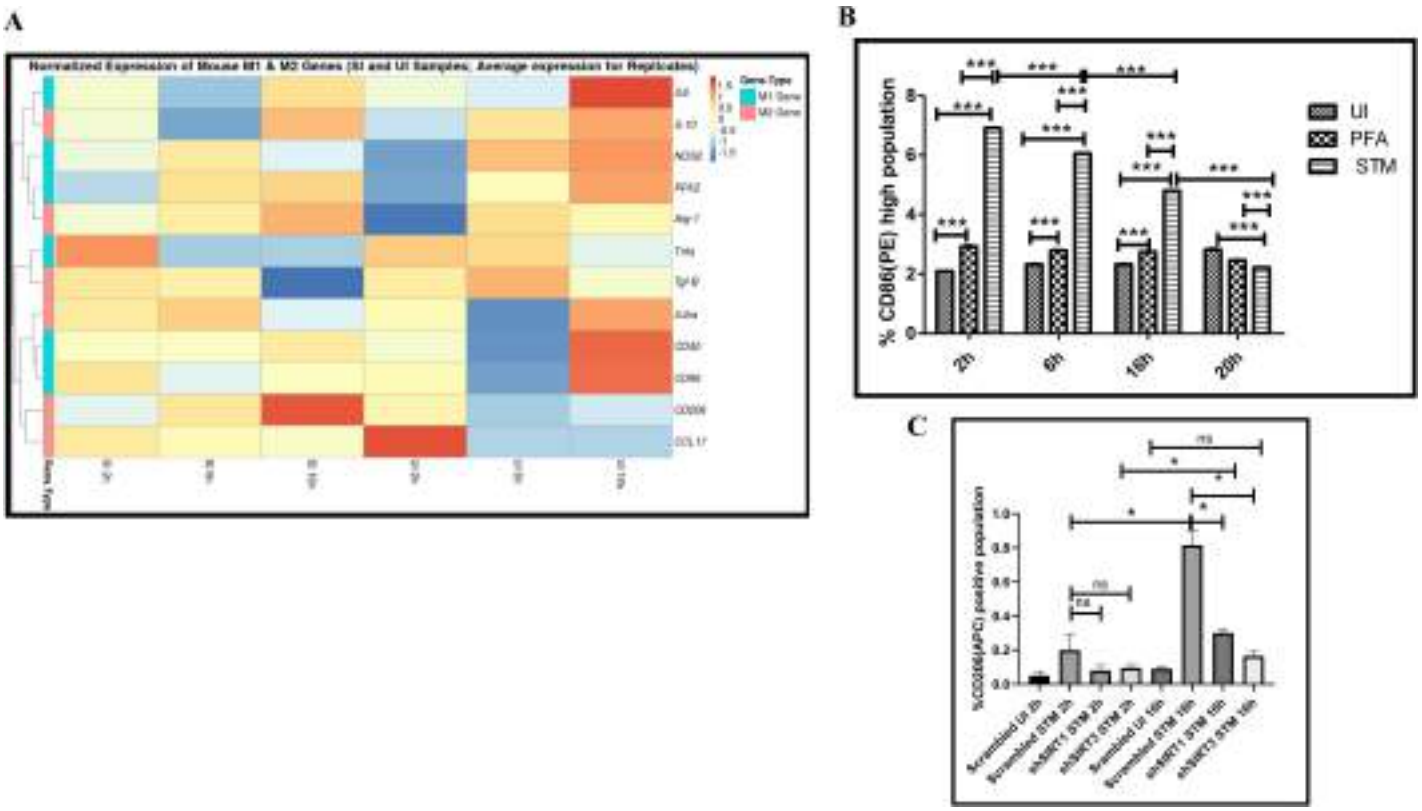

Fig. 3

– Salmonella Typhimurium skews the polarization state of the macrophage toward an immunosuppressive M2 state along the course of infection

A. nanoString gene expression profiling data of *S*. Typhimurium infected RAW 264.7 macrophages versus uninfected control data sets at 2hr, 6hr and 16hr time points of infection. Data is representative of N=2,n=2.
B. Quantitative representation of flow cytometric analysis of alteration in M1 CD86 positive population in *S*. Typhimurium (STM) infected samples in comparison to uninfected (UI) and Paraformaldehyde Fixed (PFA) bacteria at the indicated time post-infection. Data is representative of N=2, n=3. Two-way ANOVA and Bonferroni post-t-test was used to obtain p values. (*** $p < 0.001$)
C. Quantitative representation of flow cytometric analysis of M2 surface marker CD206 in *S*. Typhimurium (STM) infected SIRT1 or SIRT3 knockdown RAW264.7 macrophages in comparison to the scrambled control at the indicated time post-infection. UI-Uninfected sample. Data is representative of N=3, n=3. Two-way ANOVA and Bonferroni post-t-test was used to obtain p values. (*** $p < 0.001$)

To assess the role of SIRT1 and SIRT3 in macrophage polarization, we determined anti-inflammatory CD206 surface marker profiling of the infected macrophages through flow cytometry. Knockdown of SIRT1 or SIRT3 in infected RAW 264.7 macrophages resulted in a reduction in anti-inflammatory CD206 surface marker expression at 16hr post-infection (**Fig. 3**, C, Fig. S4, B). Moreover, SIRT1 or SIRT3 knockdown led to enhanced intracellular ROS generation within the infected macrophages in comparison to the scrambled or the untransfected control (Fig.S5). Further, the Haematoxylin and Eosin staining of the *S*. Typhimurium infected mice liver tissue sections depicted exacerbated signs of inflammation in the SIRT1 (EX-527) or SIRT3 (3TYP) inhibitor-treated cohorts in comparison to the untreated controls with multiple necrotic foci and increased influx of inflammatory cell inflates. Moreover, these acute inflammatory signs of the liver sections get ameliorated in the SIRT1 (SRT1720) activator-treated infected cohort (**Fig. 8**, T-U) (Data described later). Together, these data suggest the role of SIRT1 and SIRT3 in the modulation of host inflammatory response. Previous literature reports have shown that SIRT1 physically interacts with p65 subunit of NF-κB and inhibits transcription by deacetylating p65 at lysine 310 [39]. Moreover, SIRT1-mediated deacetylation of the p65 subunit of the master regulator of the inflammatory response, NF-κB, results in the reduction of the inflammatory responses mediated by this transcription factor [40]. To evaluate the immune regulatory mechanism of SIRT1 in the *S.* Typhimurium (STM) infection scenario, we undertook SIRT1 immunoprecipitation in the infected RAW264.7 macrophages at 16h post-infection alongside the uninfected macrophages and probed for NF-κB p65 interaction. We observed an increased interaction of SIRT1 with NF-κB p65 in the infected macrophages in comparison to the uninfected control (**Fig. 4**, A). Further, the knockdown of SIRT1 resulted in increased acetylation status of the NF-κB p65 upon infection in comparison to the scrambled, infected control (**Fig. 4**, B, C). To understand whether the enzymatic domain of SIRT1 possess any role in mediating this interaction, we carried out NF-κB p65 immunoprecipitation in infected RAW264.7 macrophages in presence or absence of SIRT1 catalytic chemical inhibitor, EX-527(1μM) treatment at 16h post-infection. We observed an increased interaction of NF-κB p65 with SIRT1 in the infected untreated macrophages when compared to the untreated uninfected control (**Fig. 4**, D). However, the interaction of NF-κB p65 with SIRT1 gets abrogated under the EX-527 inhibitor treatment in the infected macrophages thereby implying the function of the catalytic domain in mediating the interaction (**Fig. 4**, D). Moreover, an increased acetylation status of NF-κB p65 was observed in the EX-527 treated infected macrophages in comparison to the untreated infected macrophages (**Fig. 4** E).

SIRT1 and SIRT3 relieve oxidative stress in infected macrophages and alleviation of the intracellular ROS generation restores intracellular survival of *S.* Typhimurium within the SIRT1 or SIRT3 knockdown macrophages

Previous reports have suggested the role of SIRT1 and SIRT3 in oxidative stress conditions. They are known to act in concert as anti-oxidants by reducing ROS production[41][42][43]. Moreover, enhanced ROS production is also a prototype of the classically activated macrophages[44][45]. Here, we examined the effect of SIRT1 and SIRT3 knockdown in intracellular ROS generation in *S.* Typhimurium infected RAW264.7 macrophages through DCFDA staining in FACS. Results depicted significant enhancement in the production of ROS at 16hr post infection upon knockdown of SIRT1 or SIRT3 in comparison to untransfected or scrambled control (Fig.S5, A,B). Upon detection of extracellular ROS generation through Phenol Red Hydrogen Peroxidase assay, we detected higher ROS generation upon SIRT3 KD at 6hr post infection and greater ROS production at 16hr and 20hr time points in SIRT1 knockdown macrophages (Fig.S5,C). Therefore, SIRT1 and SIRT3 play an important role in mitigating the oxidative burst in *Salmonella* infected macrophages. Our previous findings depicted decreased intracellular burden of *S.* Typhimurium within the SIRT1 or SIRT3 knockdown macrophages along with increase in intracellular ROS generation. Therefore, we speculated that the decreased intracellular proliferation within the SIRT1 or SIRT3 knockdown macrophages might be on account of

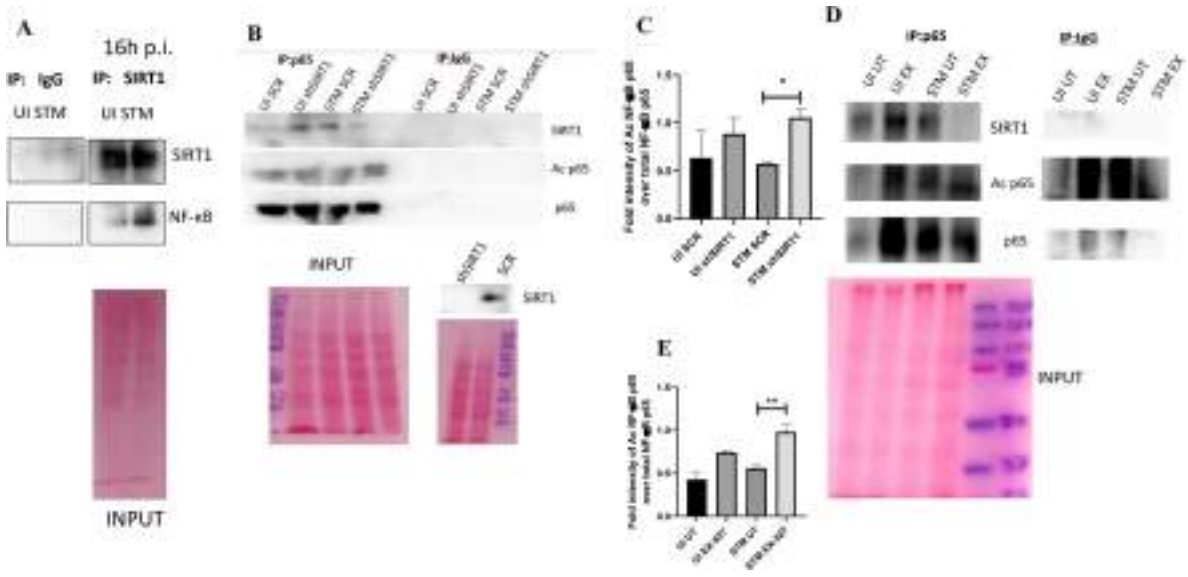

Fig. 4

– SIRT1 mediates modulation of immune functions via deacetylation of p65 subunit of NF-$_{\kappa}$B in *S*.Typhimurium infected macrophages.

A. Immunoblot depicting p65 NF-κB interaction with SIRT1 post immunoprecipitation of SIRT1 in uninfected (UI) or *S.* Typhimurium (STM) infected RAW264.7 macrophages at 16hr post-infection. Data is representative of N=3, n=1
B. An immunoblot depicting p65 NF-κB interaction with SIRT1 as well as the p65 NF-κB acetylation status post immunoprecipitation of p65 (IP: p65) or with control IgG (IP: IgG) in uninfected (UI) or *S.* Typhimurium (STM) infected RAW264.7 macrophages upon knockdown with SIRT1 shRNA or scrambled control.
C. Densitometric plot depicting the band intensities of Acetylated p65 over total p65 in blot B.
D. An immunoblot depicting p65 NF-κB interaction with SIRT1 as well as the p65 NF-κB acetylation status post immunoprecipitation of p65 (IP: p65) or with control IgG (IP: IgG) in uninfected (UI) or *S.* Typhimurium (STM) infected RAW264.7 macrophages upon SIRT1 inhibitor (EX-527, 1μM) treatment at 16hr post-infection. UT-Untreated.
E. Densitometric plot depicting the band intensities of Acetylated p65 subunit of NF-κ B over total p65 NF-κB in blot D.

increased intracellular ROS production which might lead to increased killing of the intracellular bacteria. This hypothesis led us to evaluate the intracellular bacterial burden within the infected SIRT1 or SIRT3 knockdown RAW264.7 macrophages or SIRT1 or SIRT3 inhibitor treated peritoneal macrophages (isolated from C57BL/6 adult mice post 5th day of thioglycolate injection) in presence of a ROS inhibitor named N-Acetyl Cysteine (NAC). NAC acts as a scavenger of ROS by antagonizing the activity of proteasome inhibitors [46]. The attenuated intracellular proliferation of *Salmonella* Typhimurium within the knockdown or the chemical inhibitor treated macrophages got restored upon 1mM treatment of ROS scavenger, NAC (Fig.S6). Therefore, intracellular ROS production within the knockdown murine macrophages is one of the reasons for the attenuated survival of the bacteria.

SIRT1 and SIRT3 play crucial role in mediating metabolic switch in infected macrophages

Macrophage polarization is not only governed by immunological changes but also contributed by metabolic reprogramming[47][24][48]. Since previous data suggested progression of *Salmonella* infection with the shift in polarization state of the macrophage, we decided to investigate alteration of the metabolic state of the macrophages as macrophage polarization is governed by immune-metabolic shift. In pursuit of fulfilling such requirement, we performed gene expression studies of various metabolic genes through nanoString nCounter technology in *S.* Typhimurium infected RAW 264.7 macrophages. Analysis of the gene profile revealed upregulation of genes involved in fatty acid oxidization and tricarboxylic acid cycle and corresponding downregulation of genes involved in glycolysis (**Fig. 5**, A). To validate the findings, we carried out qRTPCR to quantitatively measure the expression of a fatty acid oxidation gene, *PPARδ* in infected RAW 264.7 macrophages. We found that mRNA level was elevated to 2-fold at 2hr and 6hr post-infection. At the late phase of infection, 16hr post infection around 6-fold upregulation in mRNA transcript was noted (**Fig. 5**, B). Lactate estimation assay of *S.* Typhimurium infected RAW264.7 macrophages at the initial time point of 2hr and at the late time point of 16hr post infection revealed decline in lactate (glycolysis end product) production at 16hr in comparison to 2hr post-infection timepoint (**Fig. 5C**). Together, these results suggest the capability of the pathogen to drive a shift in the metabolic status of the infected macrophages toward fatty acid oxidation. Next, we evaluated the function of SIRT1 and SIRT3 in influencing the metabolic switch in the infected macrophages through qRT PCR with several host fatty acid oxidizing genes (*Acox*, *Hadha, Pdha, and AcadL)* and glycolytic gene (*PfkL*) in SIRT1 and SIRT3 knockdown macrophages (Fig. S7, A) and via lactate production assay (**Fig. 5**, D-E). Lactate estimation assay in SIRT1 and SIRT3 knockdown condition revealed enhanced lactate production at 16hr post infection in comparison to the scrambled control which further authenticates the increased host glycolysis upon SIRT1 and SIRT3 knockdown scenario (**Fig. 5**, D-E). SIRT1 and SIRT3 knockdown RAW 264.7 infected macrophages showed decreased expression of fatty acid oxidizing genes and increased expression of glycolytic *PfkL* gene in comparison to the scrambled infected control (Fig. S7, A). Similar results were obtained in the infected peritoneal macrophages under the SIRT1 or SIRT3 catalytic inhibitor treatment (Fig. S7, B-D). Moreover, qRT PCR-mediated metabolic gene profiling of liver and spleen isolated from wildtype *S.* Typhimurium infected macrophages revealed decreased transcript level expression of murine fatty acid oxidation genes upon treatment with SIRT1 (EX-527) or SIRT3 (3TYP) catalytic inhibitors which got reversed upon SIRT1 activator (SRT1720) treatment (Fig. S7, E-F). Moreover, SIRT1 and SIRT3 knockdown or catalytic inhibition in peritoneal macrophages resulted in increased protein expression of host glycolytic genes such as Phosphoglycerate kinase (Pgk), Phosphofructokinase (Pfk) with concomitant reduction in protein expression of TCA cycle gene like Pyruvate dehydrogenase (Pdha1) and fatty acid oxidation genes such as Hadha and Acox1 (**Fig. 5**, F, Fig. S7D). Fatty acid oxidation assay in the RAW264.7 macrophages under SIRT1 or SIRT3 knockdown condition or inhibition treatment revealed significant decrease in fatty acid β oxidation activity of the infected macrophages in comparison to the scrambled or the untreated control (**Fig. 5**, G). To investigate whether the host metabolic switch toward increased fatty acid oxidation is being driven by the

pathogen, we performed fatty acid β oxidation activity assay under wildtype *S*. Typhimurium (STM WT), SPI-1 (Δ*invC*) or SPI-2 (Δ*ssaV* and Δ*steE*) mutants of *S*. Typhimurium infection condition. We found that the wildtype bacteria with its intact SPI-2 effector secretion apparatus could promote increased host fatty acid β oxidation. In the contrary, the SPI-2 (Δ*ssaV* and Δ*steE*) mutants of *S*. Typhimurium failed to drive host metabolic shift towards increased fatty acid oxidation (**Fig. 5**, H).

Collectively, these data suggest the role of SIRT1 and SIRT3 in mediating the *Salmonella* induced host metabolic shift in the infected macrophages.

SIRT1 and SIRT3 concomitantly influences *Salmonella* metabolism

Our previous data indicated a shift in host metabolism toward increased fatty acid oxidation along the course of *Salmonella* Typhimurium infection in murine RAW 264.7 macrophages. *Salmonella* Typhimurium drives the metabolism of the infected macrophage toward fatty acid oxidation. This observation led us to investigate the influence of host metabolic shift on the metabolic status of the pathogen harboring inside the infected macrophages[49]. We were intrigued whether increased glucose availability within the fatty-acid oxidizing macrophages is utilized by the bacteria. Thus, we undertook simultaneous gene expression studies of various *Salmonella* genes involved in their pathogenesis and metabolism through nanoString nCounter technology in *S.* Typhimurium infected RAW 264.7 macrophages. The nanoString gene profile revealed enhanced expression of genes involved in *Salmonella* glycolysis and glucose uptake such as *pfkA* and *ptsG*, respectively (**Fig. 6**, A). This finding indicates the ability of the pathogen to drive the metabolic state of the host toward fatty acid oxidation with corresponding increased glucose utilization by the bacteria favoring their survival inside the host. qRT PCR results with several bacterial fatty acid oxidizing genes (*fadA, fadB,fadL,aceA, aceB*) and glycolytic genes (*ptsG*) in knockdown condition of SIRT1 and SIRT3 in RAW 264.7 macrophages further validated the nanoString gene expression profiles (**Fig. 6**, B). In scrambled control, *Salmonella* infection progresses with increased *Salmonella* glycolysis and reduced bacterial fatty acid oxidation. However, knockdown of SIRT1 and SIRT3 abrogate this bacterial metabolic shift by reducing its glycolysis and by exhibiting enhanced fatty acid oxidation thereby attenuating pathogen intracellular survival. Similar observations were obtained from the qPCR data in the infected mice liver and spleen samples with increased transcript level expression of bacterial fatty acid oxidation genes and decreased expression of bacterial glycolytic genes upon SIRT1 or SIRT3 inhibitor treatment (**Fig. 6** C, D). Therefore, SIRT1 and SIRT3 driven host metabolic switch potentially influence the metabolic profile of the intracellular pathogen.

Mechanism behind SIRT1 or SIRT3 mediated metabolic switch

As per our previous findings, SIRT1 or SIRT3 inhibition led to increased host glycolysis and decline in fatty oxidation in the infected macrophages. HIF1α is a master regulator of glycolysis in host during stress conditions [50]. Previous reports have suggested HIF1α to be a target of deacetylation by SIRT1 at Lys 674 which contribute to metabolic reprogramming in cancer cells. During hypoxia, downregulation of SIRT1 leads to increased acetylation and activation of HIF1α [51]. Additionally, in CD4+ T cells, ectopic expression of SIRT1 inhibited IL-9 production and glycolysis by negatively regulating HIF1α [52]. To delve into the mechanism behind SIRT1 mediated modulation of metabolic responses, we assessed the interaction of SIRT1 with HIF-1α in infected RAW264.7 macrophages. The immunoprecipitation studies of SIRT1 showed increased interaction of the SIRT1 with HIF1α in the *S.* Typhimurium infection scenario with respect to the uninfected control (**Fig. 7**, A). Further, we evaluated the acetylation status of HIF1α in the SIRT1 knockdown status of the infected macrophages. We found that SIRT1 knockdown showed increased acetylation of HIF1α in the infected macrophages in comparison to the scrambled infected control at 16hr post-infection (**Fig. 7**, B,C). Immunoprecipitation studies under SIRT1 (EX-527) inhibitor treatment in RAW264.7 macrophages revealed increased acetylation of HIF1-α

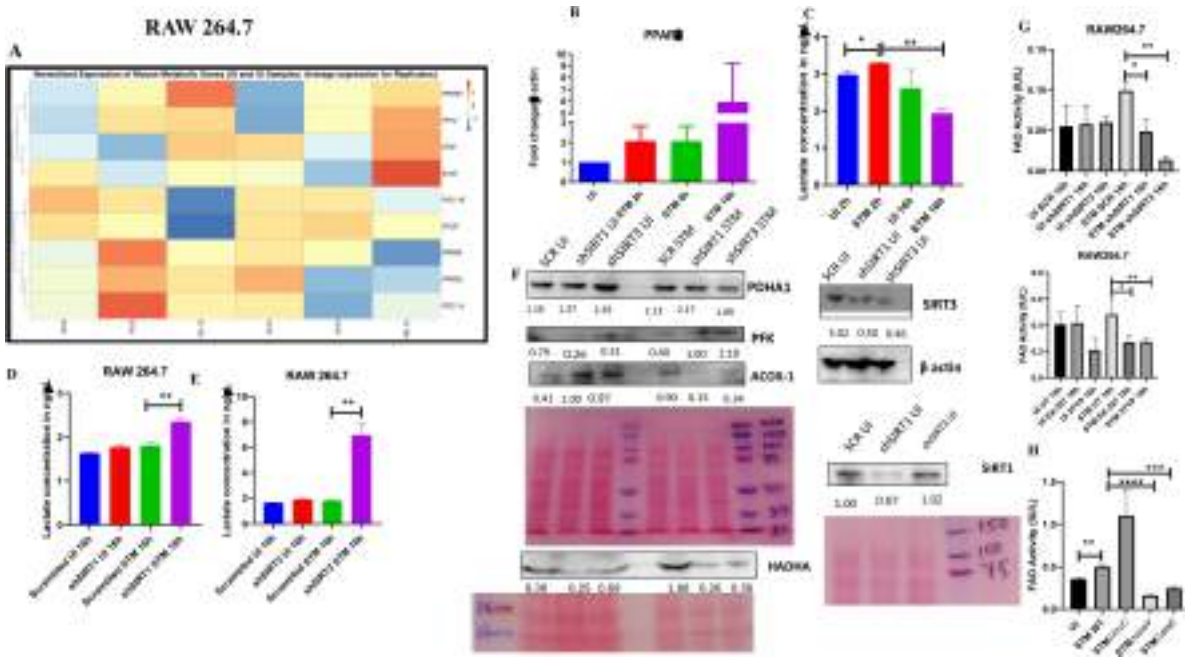

Fig. 5

– *Salmonella* Typhimurium drives the metabolism of the infected macrophage toward fatty acid oxidation

A. Metabolic gene expression data of *S*. Typhimurium infected RAW 264.7 macrophages at 2hr, 6hr and 16hr time points of infection through nanoString. Data is representative of N=2, n=1.
B. *PPARδ* qPCR expression data in *S*. Typhimurium infected RAW 264.7 macrophages at the indicated time points of infection. Data is representative of N=3, n=2.
C. Lactate estimation assay of *S*.Typhimurium infected RAW264.7 macrophages at the initial time point of 2hr and at the late time point of 16hr post infection. Data is representative of N=3, n=3. Unpaired two-tailed Student's t test was performed to obtain the p values. (** p<0.01, * p<0.05)
D-E-Lactate estimation assay of *S*.Typhimurium infected RAW264.7 macrophages upon SIRT1 (D) or SIRT3 (E) knockdown condition at16h post-infection. Data is representative of N=3, n=3. Unpaired two-tailed Student's t test was performed to obtain the p values.
F. Immunoblotting of host glycolytic (PGK), TCA cycle (PDHA1) and fatty acid oxidation (HADHA, ACOX-1) proteins under SIRT1 and SIRT3 knockdown condition of *S*. Typhimurium infected RAW264.7 macrophages at 16h post-infection.
G. Fatty Acid Oxidation (FAO) Assay of uninfected (UI) and infected (STM) RAW264.7 macrophages under SIRT1 or SIRT3 knockdown or inhibitor treatment. N=2, n=2. (** p<0.01, * p<0.05)
H. Fatty Acid Oxidation (FAO) Assay of uninfected (UI) and infected RAW264.7 macrophages under infection with wildtype *S*. Typhimurium (STM WT), SPI-1 (Δ*invC*) or SPI-2 (Δ*ssaV* and Δ*steE*) *m*utants of *S*. Typhimurium. Data is representative of N=2,n=2. (** p<0.01, * p<0.05)

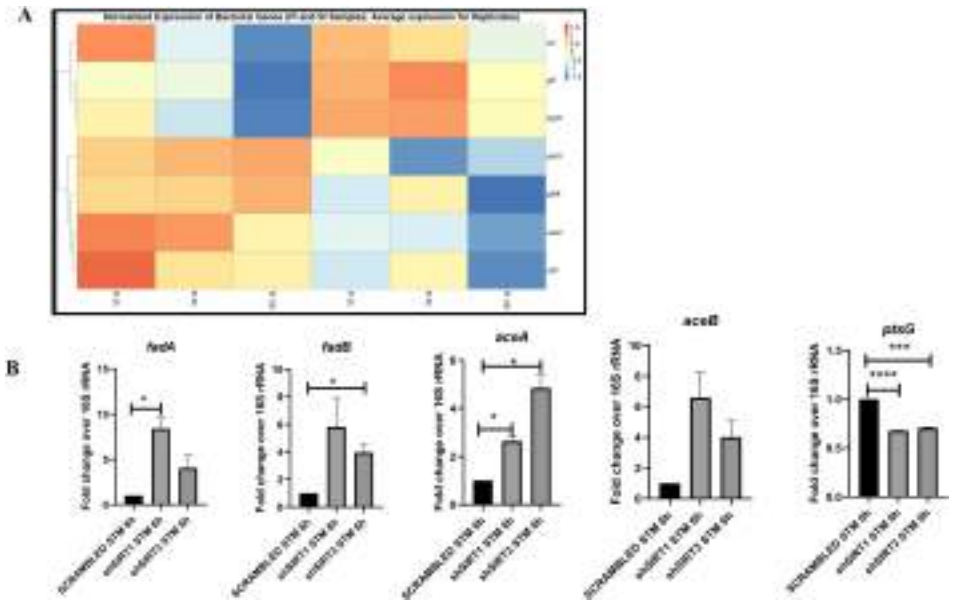

Fig. 6

– *Salmonella* Typhimurium infection proceeds with increased glycolysis and glucose uptake inside the infected RAW 264.7 macrophages

A. *Salmonella* gene expression profiling data of *S*. Typhimurium infected RAW 264.7 macrophages at 2hr, 6hr and 16hr time points of infection through nanoString. SI-*S*. Typhimurium infected, PI-PFA fixed *S*. Typhimurium infected. SPI-1 genes-*Inv, PrgH*, SPI-2 genes-*ssaV,stfF, glk*-glucokinase, *pfkA*-phosphofrucktose kinase A, *ptsG*-Phosphophenolpyruvate-dependent sugar phosphotransferase system (PTS). Data is representative of N=2, n=2.
B. qRT PCR gene expression profiling of *Salmonella* metabolic genes within infected RAW264.7 macrophages in knockdown condition of either SIRT1 or SIRT3 at 6hr post infection. Data is representative of N=3, n=3.
C-D. qRT PCR gene expression profiling of *Salmonella* metabolic genes within infected female C57BL/6 mice spleen (C) and liver (D) under SIRT1 or SIRT3 inhibitor treatment harvested at 5th day post infection of *S.*Typhimurium (10^7 cfu units/animal). Unpaired two-tailed Student's t test was performed to obtain the p values. Data is representative of N=3, n=3. (****p<0.0001, *** p < 0.001, ** p<0.01, * p<0.05)

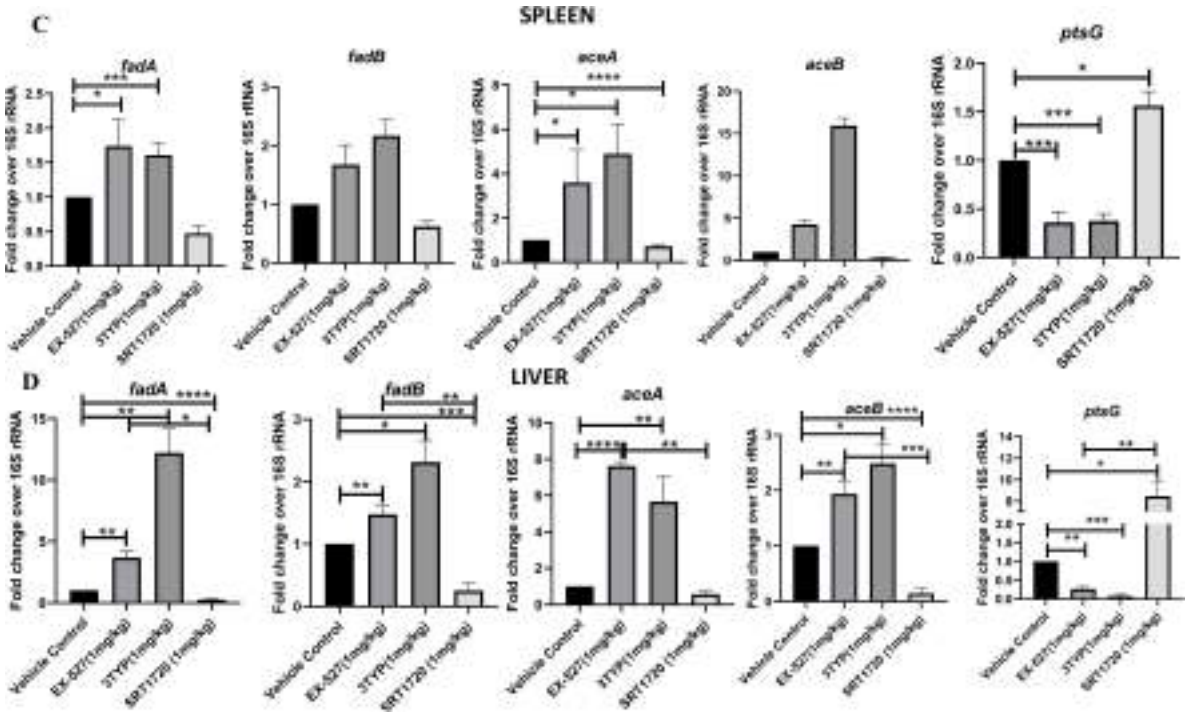

Fig. 6 (continued)

along with reduced interaction of HIF-1α with SIRT1, thereby indicating the probable role of the catalytic domain in influencing the interaction (**Fig. 7** D-F). Further, to ascertain the role of HIF-1α in mediating the glycolytic switch in the infected macrophages, we estimated the lactate production under SIRT1 and SIRT3 knockdown conditions in the presence or absence of HIF-1α inhibitor (chetomin)[53]. Our results depicted a decline in lactate production upon chetomine treatment including under SIRT1 and SIRT3 knockdown conditions (**Fig. 7G**). Together, our results implicate the role of SIRT1 in governing glycolytic shift in the infected macrophages by deacetylating HIF1α. Upon SIRT1 knockdown or inhibition, HIF1α gets hyperacetylated which causes activation of the downstream glycolytic genes. Alternatively, several key literatures suggest the role of SIRT3 in modulating metabolic programming by deacetylating several proteins involved in fatty acid oxidation, the tricarboxylic acid cycle and oxidative phosphorylation [54] [55]. PDHA1 (Pyruvate Dehydrogenase E1 subunit alpha) is a key enzyme linking glycolysis to TCA cycle and oxidative phosphorylation. SIRT3 regulates PDHA1 acetylation by deacetylating PDHA1 at lysine 385 residue, thereby playing a key role in metabolic reprogramming [55]. PDHA1 acetylation coincides with PDH activity and increased PDHA1 phosphorylation [55]. Therefore, we investigated the role of SIRT3 in the modulation of host fatty acid oxidation upon *S.* Typhimurium infection in RAW264.7 macrophages. To do so, we immunoprecipitated PDHA1 and checked for its interaction with SIRT3 or SIRT1 under the knockdown condition of SIRT3 or upon SIRT3 inhibitor treatment (**Fig. 7** I-J). We observed an increased interaction of PDHA1 with SIRT3 in the infection scenario in comparison to the uninfected control which gets eventually abolished under the knockdown condition (**Fig. 7** I-J) and under the chemical inhibitor treatment of SIRT3 (**Fig. 7**, K-L) suggesting the role of the SIRT3 in mediating the interaction with PDHA1. Alongside the decreased interaction of PDHA1 with SIRT3, increased acetylation of PDHA1 was detected upon SIRT3 inhibitor treatment in infected macrophages (**Fig. 7**, K-L).

SIRT1 or SIRT3 inhibition enhances bacterial burden in mice *in vivo*

6-8 weeks old adult male C57BL/6 mice were treated with SIRT1 inhibitor EX-527, SIRT3 inhibitor 3TYP and SIRT1 activator SRT1720 at a dose of 1mg/kg each via intraperitoneal injection (every alternate Day) (**Fig. 8A**). Following the inhibitor treatment, the mice were orally gavaged with 10^7 CFU of *S.* Typhimurium 14028S for organ burden evaluation or with 10^8 CFU of wildtype *S.* Typhimurium for survival studies. On day 5^{th} post-infection, mice were sacrificed, and the liver, spleen and Mesenteric Lymph Node (MLN) were harvested for enumeration of the organ burden. The SIRT1 inhibitor, EX-527 and SIRT3 inhibitor, 3TYP-treated mice cohorts exhibited increased organ loads in liver, spleen and MLN in comparison to the vehicle control. On the contrary, the SRT1720 treated mice group showed organ burden comparable to that of the vehicle control (**Fig. 8**, B). Moreover, the SIRT1 and the SIRT3 inhibitor-treated mice cohorts died earlier than the vehicle-treated control mice group or the SIRT1 activator-treated group (**Fig. 8**, C). Further, the SIRT1 and the SIRT3 inhibitor-treated mice cohorts showed increased splenic length in comparison to the vehicle-treated mice group and the SIRT1 activator-treated mice cohort (**Fig. 8**, D). The increased organ burden in the EX-527 or 3TYP treated group might be due to increased bacterial dissemination in blood. To assess bacterial dissemination, blood was collected from infected mice post-inhibitor treatment at specific days post-infection retro-orbitally and plated onto *Salmonella Shigella* (SS) agar plates for bacterial enumeration. Indeed, increased bacterial dissemination was observed in the blood of mice treated with SIRT1 inhibitor, EX-527 or SIRT3 inhibitor, 3TYP at day 1-, 2-, 3-, 4-post-infection in comparison to the vehicle-treated mice (**Fig. 8**, E). Further, we wanted to examine whether the increased bacterial dissemination was due to increased ROS production or due to the presence of elevated inflammatory cytokine levels like IL-6 and IL-1β. In the wildtype C57BL/6 mice treated with SIRT3 inhibitor 3TYP showed heightened bacterial burden in blood at 5^{th} day post-infection in comparison to the vehicle control. Nevertheless, the *gp91phox-/−* mice group lacking the catalytic subunit of NADPH oxidase did not depict significant variation in the bacterial load among the different mice treatment cohorts (**Fig. 8**, F). Further, the EX-527 (SIRT1 inhibitor) and the 3TYP (SIRT3 inhibitor) treated mice possessed elevated levels of serum IL-6 (**Fig. 8G**), IL-1β (Fig. S3F) and showed increased intracellular ROS burden in

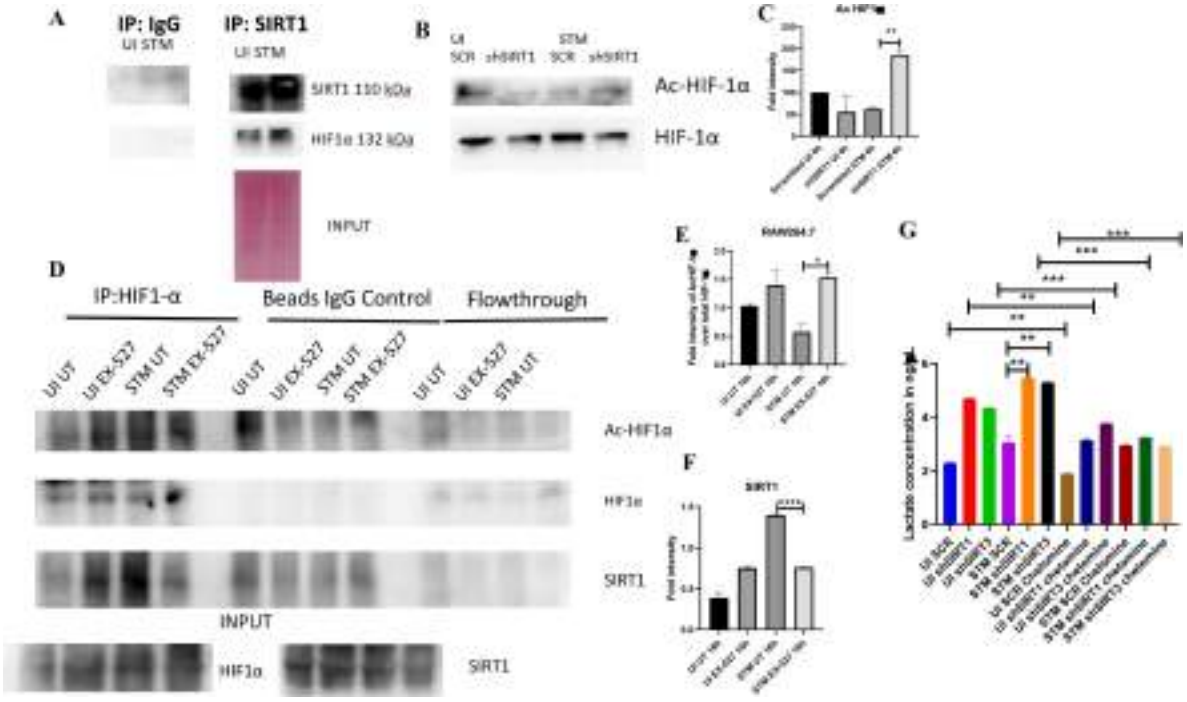

Fig. 7

– SIRT1 inhibition triggers hyperacetylation of glycolytic master regulator HIF-1$_\alpha$ within *S.* Typhimurium infected macrophages while SIRT3 skews metabolism of *S.* Typhimurium-infected macrophages via interaction with PDHA1.

A. An immunoblot depicting HIF-1α interaction with SIRT1 post immunoprecipitation of SIRT1 in uninfected (UI) or *S.* Typhimurium (STM) infected RAW264.7 macrophages at 16hr post-infection. (Derived from same SIRT1 IP blot as in **Fig. 4A**)

B. Immunoblotting of SIRT1 in SIRT1 knockdown uninfected (UI) or *S.* Typhimurium (STM) infected RAW 264.7 cells at 16hr post-infection to assess the acetylation status of HIF-1α.

C. Densitometric plot depicting the band intensities of Acetylated HIF-1α over total HIF-1α in blot B.

D. An immunoblot depicting HIF-1α interaction with SIRT1 as well as the HIF-1α acetylation status post immunoprecipitation of HIF-1$^\alpha$ (IP:HIF-1α or with control IgG (IP:IgG) in uninfected (UI) or *S.* Typhimurium (STM) infected RAW264.7 macrophages upon SIRT1 inhibitor (EX-527, 1μM) treatment at 16hr post-infection. UT-untreated.

E. Densitometric plot depicting the band intensities of Acetylated HIF-1α over total HIF-1α in blot D.

F. Densitometric plot depicting the band intensities of SIRT1 in blot D.

G. Lactate estimation assay of *S.*Typhimurium infected RAW264.7 macrophages upon SIRT1 and SIRT3 knockdown condition in the presence of HIF-1α inhibitor, chetomine (50nM) at16h post-infection. Data is representative of N=3, n=3. Unpaired two-tailed Student's t test was performed to obtain the p values. (****p<0.0001, *** p < 0.001, ** p<0.01, * p<0.05)

H. An immunoblot depicting PDHA1 interaction with SIRT1 or SIRT3 post immunoprecipitation of PDHA1 in uninfected (UI) or *S.* Typhimurium (STM) infected RAW264.7 macrophages in SIRT3 knockdown condition at 16hr post-infection.

I. Densitometric plot depicting the band intensities of SIRT3 interaction over total input in blot

J. An immunoblot depicting PDHA1 interaction with SIRT3 post immunoprecipitation of PDHA1 in uninfected (UI) or *S.* Typhimurium (STM) infected RAW264.7 macrophages at 16hr post-infection under SIRT3 inhibitor (3-TYP, 1μM) treatment at 16hr post-infection. UT-untreated.

K. Densitometric plot depicting the band intensities of Acetylated PDHA1 over total PDHA1 in blot I.

L. Densitometric plot depicting the band intensities of SIRT3 interaction over total input in blot I.

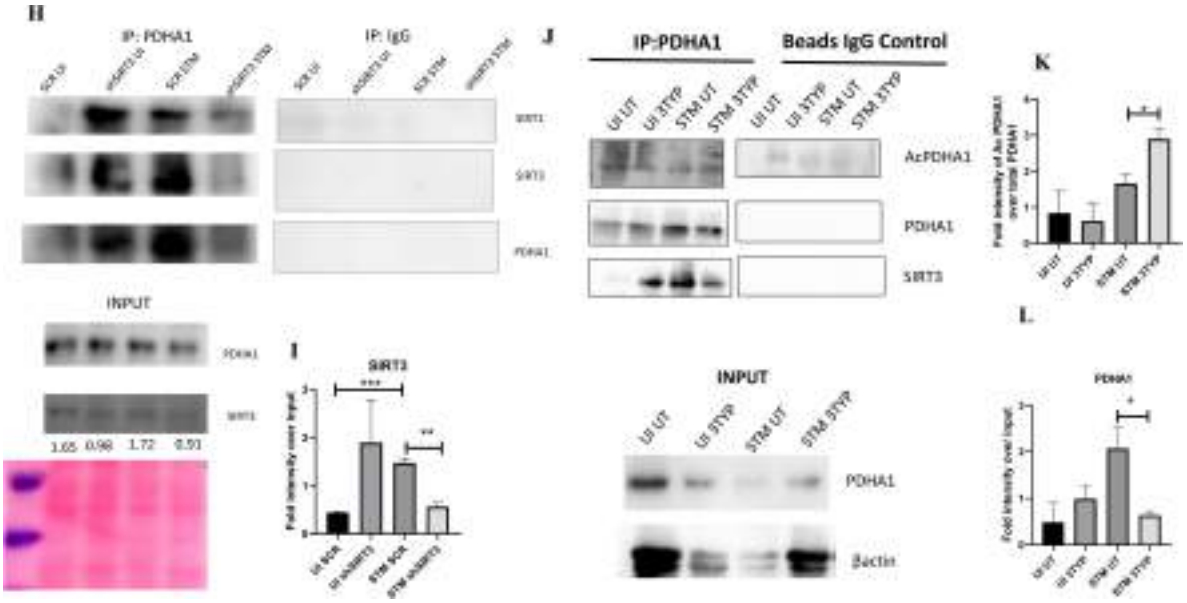

Fig. 7 (continued)

infected liver tissues in comparison to the vehicle-treated control and the SRT1720 (SIRT1 activator) treated mice group (**Fig. 8H**). The increased mouse serum IL-6 and IL-1β production was in a similar line with the increased IL-6 or IL-1β cytokine generation in EX-527 or 3TYP treated peritoneal macrophages under the infection scenario (Fig. S3, D-E). Moreover, estimation of IL-1β within the infected intestinal ileal sections of the mice revealed increased pro-inflammatory IL-1β generation in the SIRT1 and SIRT3 inhibitor-treated mice groups in comparison to the untreated or the SIRT1-activator treated mice cohorts (Fig. S3G). However, contrary to the *in vitro* studies wherein SIRT1 or SIRT3 knockdown or inhibition resulted in attenuated intracellular proliferation, here in *in vivo* mouse model of infection, we observed increased bacterial organ loads owing to increased bacterial dissemination. To delineate this observation further, we evaluated the bacterial load within splenocytes isolated from control or inhibitor-treated C57BL/6 mice infected with GFP expressing *S.* Typhimurium at 5^{th} day post-infection via flow cytometry. We observed heightened bacterial load in the EX-527 or the 3TYP treated mice cohorts (**Fig. 8**, I-J). However, when we enumerated the bacterial count within the F4/80+ macrophage population of the infected splenocytes, we noticed decreased bacterial loads in the EX-527 or 3TYP –treated mice group in comparison to the vehicle-treated control group or the SRT-1720 activator-treated group (**Fig. 8**, K-L). Further, we evaluated additional splenic populations including CD45+, Ly6C+, and CD11c+ populations. Our results show that the CD45+ splenic population depicts increased bacterial loads like that of the total splenic population within the SIRT1 or SIRT3 inhibitor-treated cohorts. However, CD45+ monocytes and Ly6C positive splenic population exhibit compromised burden within the SIRT1 and SIRT3 inhibitor-treated cohorts. Moreover, CD11c+ population, CD45+ granulocytes, or lymphocytes show comparable organ loads to that of the vehicle control or SIRT1 activator-treated mice group (**Fig. 8M-S**, Fig. S8). Overall, our data suggest heterogeneous bacterial burden in diverse splenic populations. This opposing phenotype could be attributed to the increased IL-6 and IL-1β cytokine storm and elevated ROS production upon the SIRT1 or SIRT3 inhibitor treatment which in turn resulted in bacterial dissemination *in vivo* and concomitantly restricted the *in vitro* intracellular proliferation within macrophages. To validate this observation, we estimated the ROS levels within the liver and spleen tissues harvested from *S.* Typhimurium infected C57BL/6 mice, treated with specific catalytic inhibitor, activator or vehicle via DCFDA staining using flow cytometry at 5^{th} day post-infection. We detected escalated levels of ROS within both the infected liver and spleen tissues of the EX-527 or 3TYP-treated mice groups in comparison to the vehicle-treated or the SRT1720 treated mice cohorts (**Fig. 8, H, S9**). Haematoxylin and eosin staining of the liver sections (harvested at 5^{th} day post-infection) revealed increased inflammation with multiple areas of severe acute hepatic necrosis with complete loss of hepatic architecture in the EX-527 and 3-TYP treated liver samples in comparison to the vehicle-treated control and SRT-1720 treated liver samples (**Fig. 8**, T-U). In line with the inhibitor-treated studies, the increased organ loads, and systemic dissemination driven heightened susceptibility of mice toward *S.* Typhimurium infection were replicated in *in vivo* SIRT1 and SIRT3 adeno-associated virus serotype 6 (AAV6) mediated knockdown mice model which showed elevated IL-6 production in comparison to the scrambled control treated mice cohort (**Fig. 8**, V-X, Fig. S10). Simultaneously, the haematoxylin-eosin-stained sections of the liver tissues harvested from the shSIRT1 or shSIRT3 mice cohorts depicted increased pathological scoring with multiple necrotic areas and severely damaged liver tissue architecture in comparison to the scrambled mice control (**Fig. 8**, Y). Altogether, our results implicate the role of SIRT1 and SIRT3 in controlling *S.* Typhimurium infection *in vivo*.

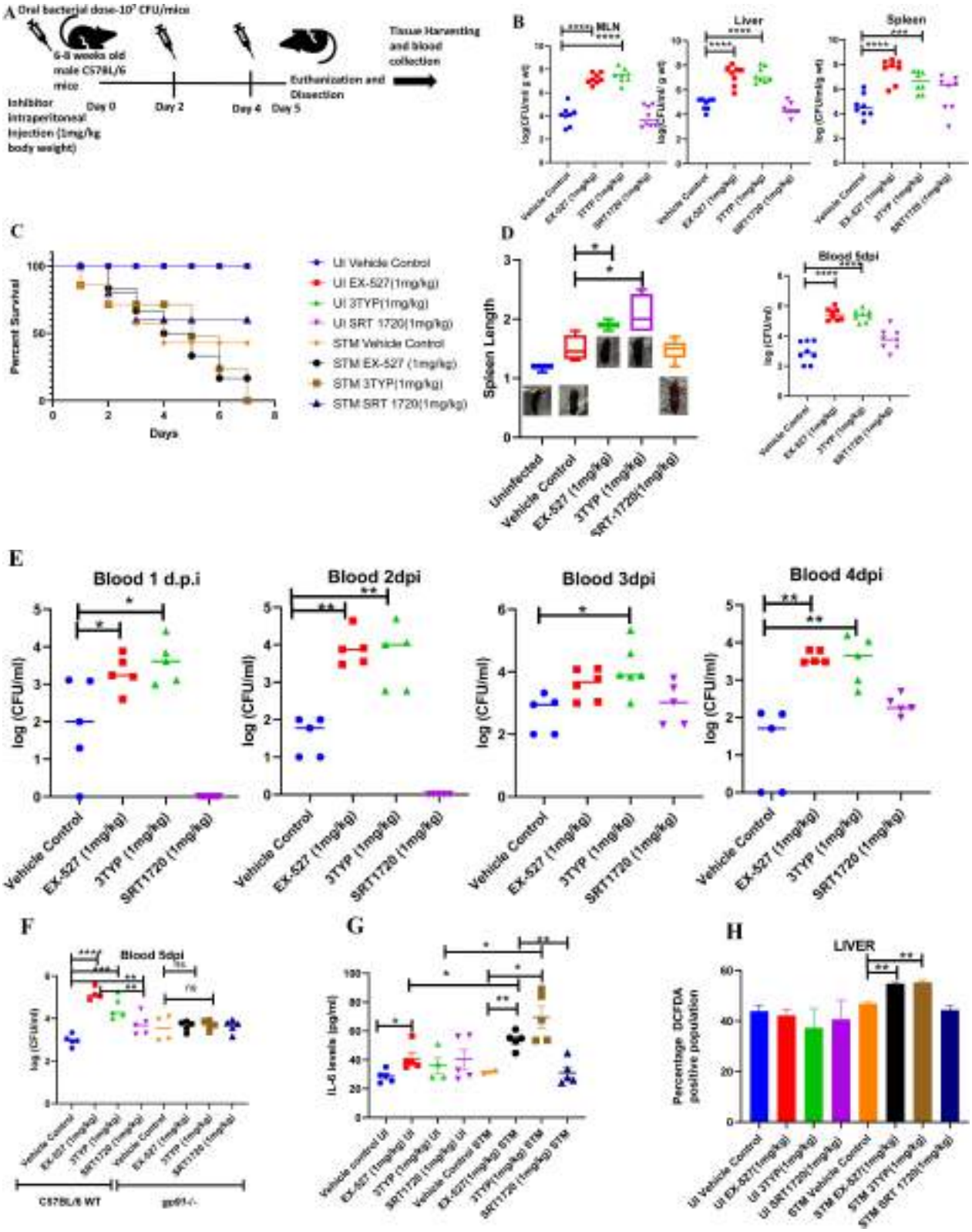
A
Oral bacterial dose-10⁷ CFU/mice
6-8 weeks old male C57BL/6 mice
Inhibitor intraperitoneal injection (1mg/kg body weight)
Day 0
Day 2
Day 4
Day 5
Euthanization and Dissection
Tissue Harvesting and blood collection
B
MLN
Liver
Spleen
Vehicle Control
EX-527 (1mg/kg)
3TYP (1mg/kg)
SRT1720 (1mg/kg)
C
Percent Survival
Days
UI Vehicle Control
UI EX-527(1mg/kg)
UI 3TYP(1mg/kg)
UI SRT 1720(1mg/kg)
STM Vehicle Control
STM EX-527 (1mg/kg)
STM 3TYP(1mg/kg)
STM SRT 1720(1mg/kg)
D
Spleen Length
Uninfected
Vehicle Control
EX-527 (1mg/kg)
3TYP (1mg/kg)
SRT-1720(1mg/kg)
Blood 5dpi
log (CFU/ml)
E
Blood 1 d.p.i
Blood 2dpi
Blood 3dpi
Blood 4dpi
log (CFU/ml)
Vehicle Control
EX-527 (1mg/kg)
3TYP (1mg/kg)
SRT1720 (1mg/kg)
F
Blood 5dpi
log (CFU/ml)
C57BL/6 WT
gp91-/-
G
IL-6 levels (pg/ml)
Vehicle control UI
EX-527 (1mg/kg) UI
3TYP (1mg/kg) UI
SRT1720 (1mg/kg) UI
Vehicle Control STM
EX-527(1mg/kg) STM
3TYP(1mg/kg) STM
SRT1720 (1mg/kg) STM
H
LIVER
Percentage DCFDA positive population
UI Vehicle Control
UI EX-527(1mg/kg)
UI 3TYP(1mg/kg)
UI SRT1720(1mg/kg)
STM Vehicle Control
STM EX-527(1mg/kg)
STM 3TYP(1mg/kg)
STM SRT 1720(1mg/kg)

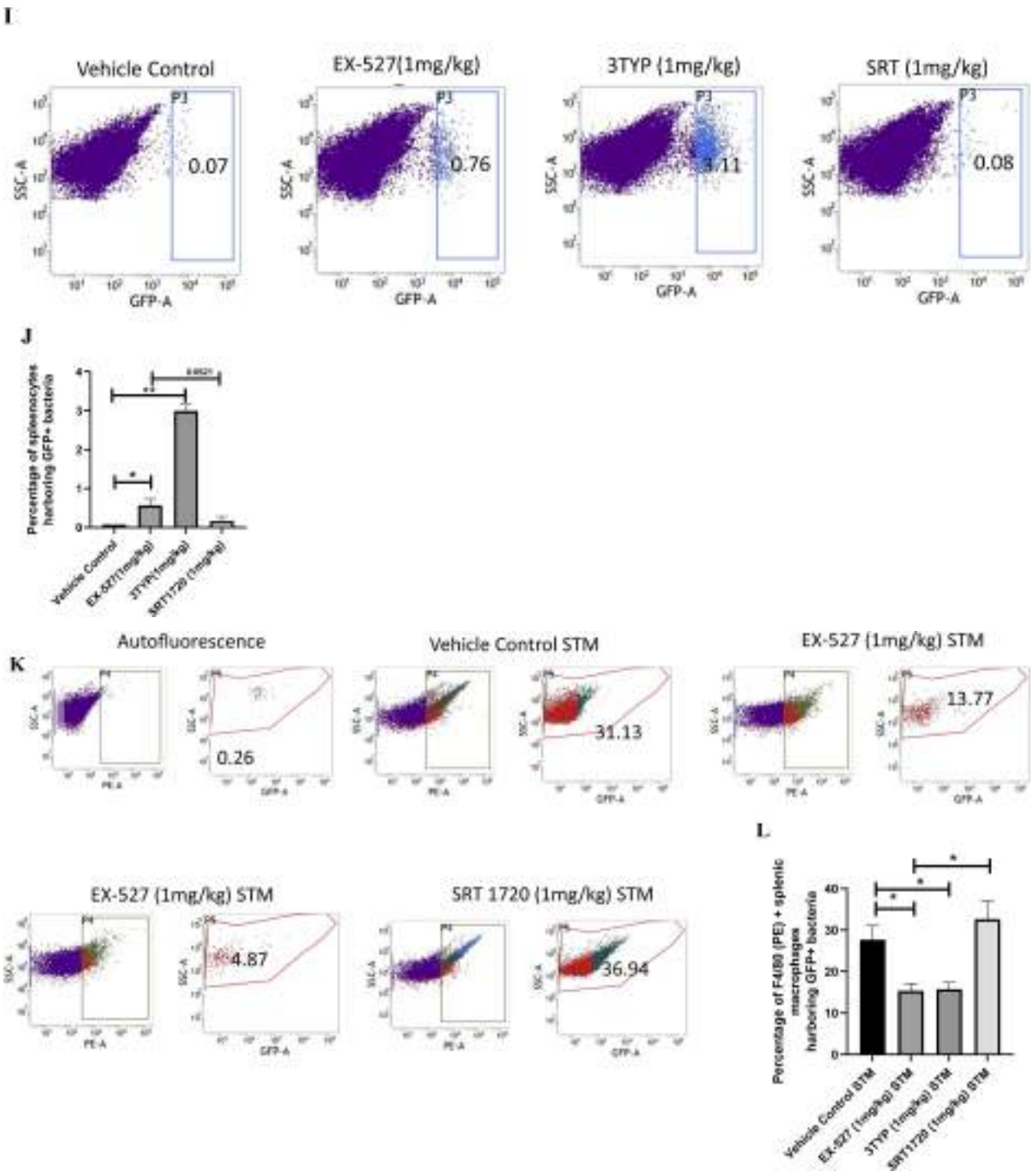
I
Vehicle Control
EX-527(1mg/kg)
3TYP (1mg/kg)
SRT (1mg/kg)
P3
0.07
0.76
3.11
0.08
SSC-A
GFP-A
J
Percentage of spleenocytes harboring GFP+ bacteria
Vehicle Control
EX-527(1mg/kg)
3TYP(1mg/kg)
SRT1720 (1mg/kg)
K
Autofluorescence
Vehicle Control STM
EX-527 (1mg/kg) STM
0.26
31.13
13.77
EX-527 (1mg/kg) STM
SRT 1720 (1mg/kg) STM
4.87
36.94
L
Percentage of F4/80 (PE) + splenic macrophages harboring GFP+ bacteria
Vehicle Control STM
EX-527 (1mg/kg) STM
3TYP (1mg/kg) STM
SRT1720 (1mg/kg) STM

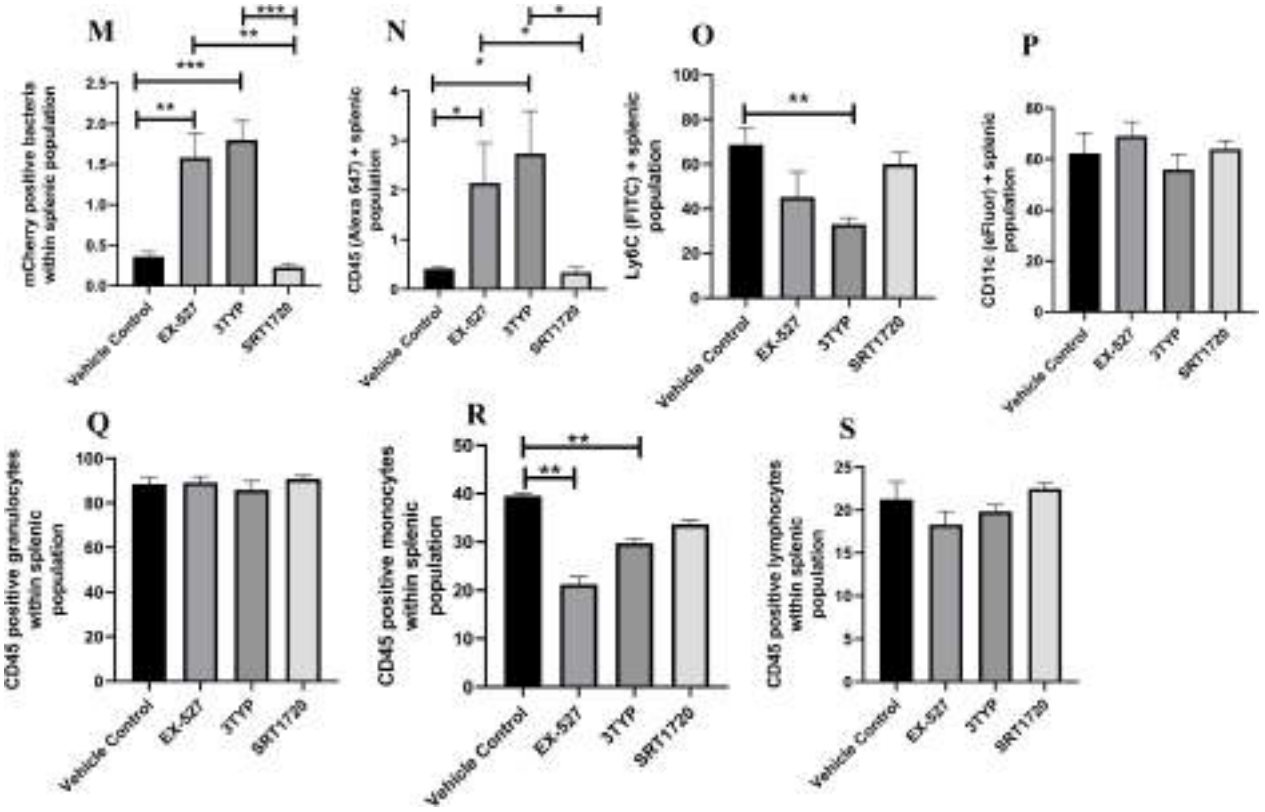
M
mCherry positive bacteria within splenic population
Vehicle Control
EX-527
3TYP
SRT1720
N
CD45 (Alexa 647) + splenic population
O
Ly6C (FITC) + splenic population
P
CD11c (eFluor) + splenic population
Q
CD45 positive granulocytes within splenic population
R
CD45 positive monocytes within splenic population
S
CD45 positive lymphocytes within splenic population

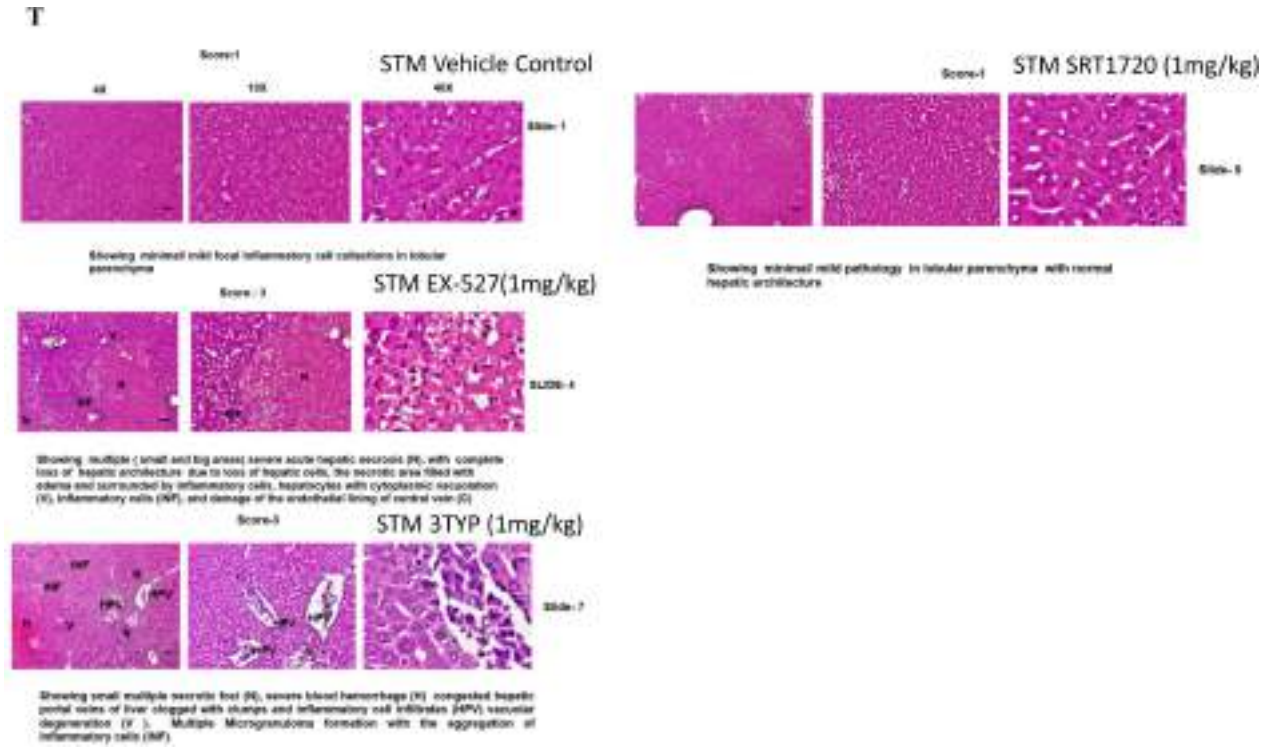
T
STM Vehicle Control
STM SRT1720 (1mg/kg)
STM EX-527(1mg/kg)
STM 3TYP (1mg/kg)

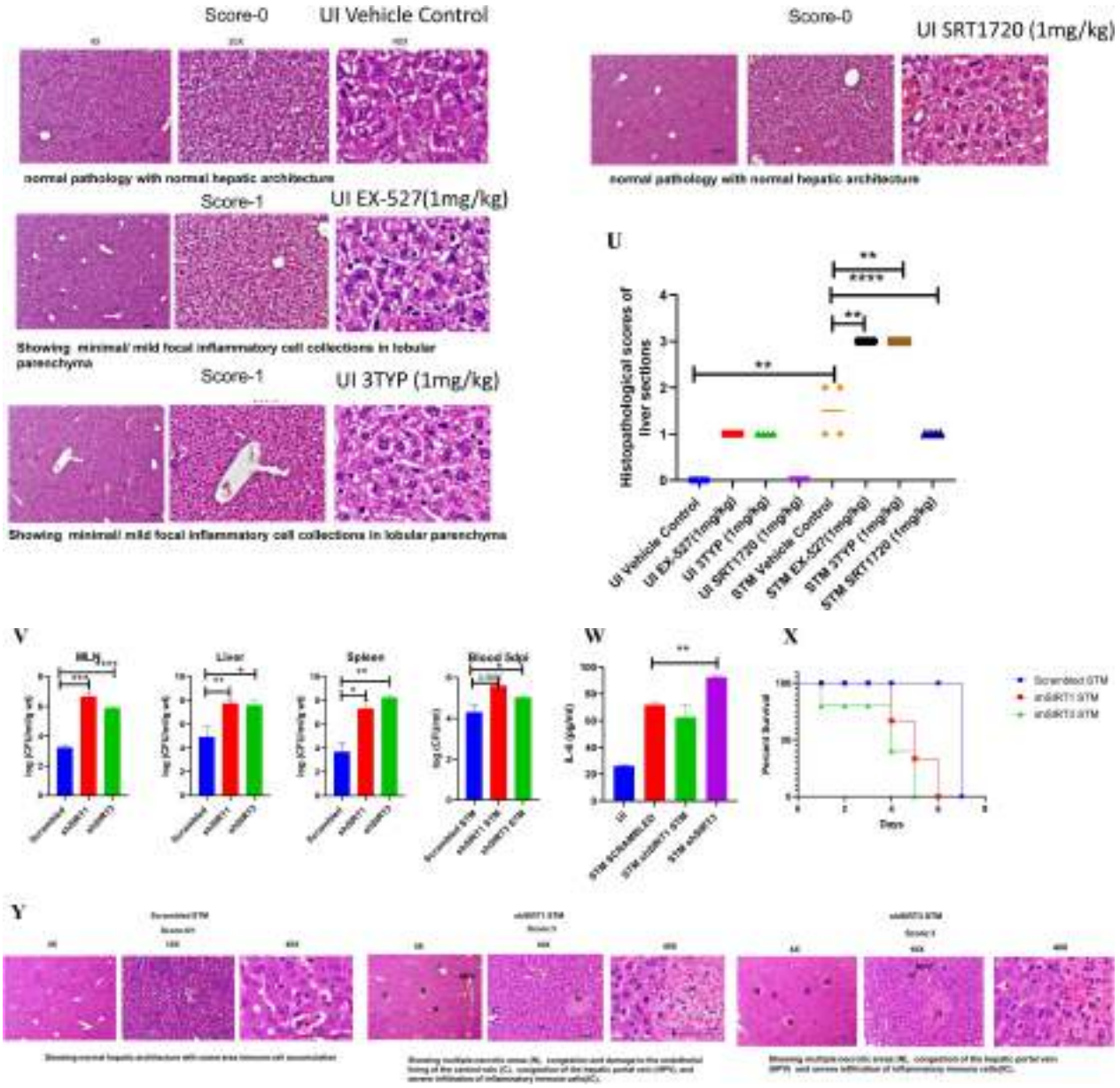
Score-0
UI Vehicle Control
normal pathology with normal hepatic architecture
Score-0
UI SRT1720 (1mg/kg)
normal pathology with normal hepatic architecture
Score-1
UI EX-527(1mg/kg)
Showing minimal/ mild focal inflammatory cell collections in lobular parenchyma
Score-1
UI 3TYP (1mg/kg)
Showing minimal/ mild focal inflammatory cell collections in lobular parenchyma
U
Histopathological scores of liver sections
UI Vehicle Control
UI EX-527(1mg/kg)
UI 3TYP (1mg/kg)
UI SRT1720 (1mg/kg)
STM Vehicle Control
STM EX-527(1mg/kg)
STM 3TYP (1mg/kg)
STM SRT1720 (1mg/kg)
V
Liver
Spleen
Blood Sdpl
W
X
Days
Y

Fig. 8

– Effect of SIRT1 or SIRT3 inhibition on *S.* Typhimurium infected C57BL/6 mice

A. The schematic representation of the experimental strategy for studying the effect of SIRT1 and SIRT3 on the *in vivo* pathogenesis of STM (WT).

B. *In-vivo* organ burden of *S.* Typhimurium upon SIRT1 or SIRT3 inhibition in C57BL/6 mice at day 5 post-infection under specified dosage of inhibitor treatment. Data is representative of N=4, n=8. Mann-Whitney Test was performed to obtain the p values.(****p<0.0001, *** p < 0.001, ** p<0.01, * p<0.05).

C. Percent survival of *S.* Typhimurium infected C57BL/6 mice upon SIRT1 or SIRT3 inhibitor treatment at a specific dose of inhibitor treatment. Data is representative of N=4, n=5.

D. Representation of splenic length of *S.* Typhimurium infected spleen tissue harvested from C57BL/6 mice (males) at day 5 post-infection upon SIRT1 or SIRT3 inhibition at 1mg/kg dosage. Data is representative of N=4, n=8. (** p<0.01, * p<0.05).

E. Bacterial load in blood at different days post-infection upon SIRT1 or SIRT3 inhibition at 1mg/kg dosage in C57BL/6 mice (males). Data is representative of N=3, n>5. (** p<0.01, * p<0.05) Mann-Whitney Test was performed to obtain the p values. (** p<0.01, * p<0.05).

F. Bacterial load in blood at day 5 post-infection upon SIRT1 or SIRT3 inhibition at 1mg/kg dosage in C57BL/6 WT mice (males) and *gp91phox*-/– (males) mice. Data is representative of N=3, n>5. Mann-Whitney Test was performed to obtain the p values. (** p<0.01, * p<0.05).

G. Serum IL-6 levels of *S.* Typhimurium infected C57BL/6 WT mice (males) mice treated with SIRT1(EX-527) or SIRT3 (3TYP) inhibitors or SRT1720 (SIRT1 activator) at 1mg/kg dosage at 5th day post-infection. Data is representative of N=3, n>5. Unpaired two-tailed Student's t test was performed to obtain the p values.(** p<0.01, * p<0.05).

H. Quantitative analysis of percentage population of cells within liver showing DCFDA positive staining shown in Fig. S9, A. Data is representative of N=3, n>5. Unpaired two-tailed Student's t-test was performed to obtain the p values. (** p < 0.01).

I. Enumeration of GFP positive bacterial cells through flow cytometry in splenic tissues homogenate harvested from adult male 6-8 week old C57BL/6 mice (subjected to different chemical treatment-Vehicle treated or SIRT1 (EX-527) or SIRT3 (3-TYP) inhibitor or SIRT1 activator SRT1720 treated at a dose of 1mg/kg) at 5^{th} day post *S.* Typhimurium (expressing GFP) infection (10^{7} CFU orally). Data is representative of N=3, n>5. Unpaired two-tailed Student's t test was performed to obtain the p values. (** p < 0.01).

J. Quantitative analysis of the percentage population of splenic cells harboring GFP+ bacterial cells shown in I. Unpaired two-tailed Student's t test was performed. (** p<0.01, * p<0.05).

K. Enumeration of GFP positive bacterial cells through flow cytometry within F4/80 positive splenic macrophages present within splenic tissues homogenate harvested from adult male 6-8 week old C57BL/6 mice (subjected to different chemical treatment-Vehicle treated or SIRT1 (EX-527) or SIRT3 (3-TYP) inhibitor or SIRT1 activator SRT1720 treated aa t dose of 1mg/kg) at 5^{th} day post *S.* Typhimurium infection. Data is representative of N=3, n>5.

L. Quantitative analysis of percentage population of F4/80 positive macrophage cells harboring GFP+ bacteria shown in K. Unpaired two-tailed Student's t test was performed to obtain the p values. Data is representative of N=3, n>5.(* p < 0.05).

M-S. Quantitative analysis of different mCherry-*S.*Typhimurium-infected splenic populations harboring mCherry+bacteria via flow cytometry depicted in Fig. S8. Unpaired two-tailed Student's t test was performed. (*** p < 0.001,** p<0.01, * p<0.05).

T. Representative image of haematoxylin-eosin-stained liver sections to assess the liver tissue architecture upon *Salmonella* infection at 5th days post-infection in different mice cohorts. (UI-Uninfected, STM-*S.* Typhimurium infected, EX-527-SIRT1 inhibitor, 3TYP-SIRT3 inhibitor, SRT1720-SIRT1 activator, Vehicle Control-(PBS containing 0.1% DMSO). Scale bar-50μm. **Scoring system:-** according to pathological changes the tissue sections are scored as 0 for normal pathology, 1 for mild/ minor pathology, 2 for moderate pathology, and 3 for severe pathological changes.

U. Graph representing the histopathological scoring of the liver sections depicted in L. Unpaired two-tailed Student's t test was performed to obtain the p values. (* p < 0.05)(****p<0.0001, *** p < 0.001, ** p<0.01, * p<0.05).

V. *In-vivo* organ burden of *S.* Typhimurium upon SIRT1 or SIRT3 adenovirus-mediated *in vivo* knockdown in C57BL/6 mice at day 5 post-infection. Data is representative of N=3, n>3. Mann-Whitney Test was performed to obtain the p values. (****p<0.0001, *** p < 0.001, ** p<0.01, * p<0.05).

W. Serum IL-6 levels of *S.* Typhimurium infected C57BL/6 WT mice (males) upon *in vivo* adenovirus-mediated SIRT1 or SIRT3 knockdown. Data is representative of N=3, n>3. Unpaired two-tailed Student's t test was performed to obtain the p values. (** p<0.01, * p<0.05).

X. Percent survival of *S.* Typhimurium infected C57BL/6 mice upon *in vivo* adenovirus-mediated SIRT1 or SIRT3 knockdown. Data is representative of N=3, n>3.

Y. Representative image of haematoxylin-eosin-stained liver sections upon *Salmonella* infection at 5th days post-infection in different mice cohorts. (Scrambled STM, shSIRT1 STM, shSIRT3 STM). Scale bar-50μm. **Scoring system:-** according to pathological changes the tissue sections are scored as 0 for normal pathology, 1 for mild/ minor pathology, 2 for moderate pathology, and 3 for severe pathological changes.

Discussion

Several studies have confirmed the propensity of *Salmonella* to skew the polarization state of the infected macrophages toward an immunosuppressive anti-inflammatory state[56][57][58]. We have validated such findings and further elaborated it by depicting the role of SIRT1 and SIRT3 in the modulation of host immune responses as well as host-bacterial metabolism. *Salmonella* Typhimurium infection modulates the expression profile of both SIRT1 and SIRT3 in the infected macrophages at both mRNA and protein level via its SPI-2 effector. Downregulation of SIRT1 and SIRT3 through shRNA mediated knockdown resulted in heightened pro-inflammatory immune responses with increased production of IL-6 cytokine and decreased surface expression of anti-inflammatory CD206. SIRT1 and SIRT3 downregulation also resulted in increased intracellular ROS production in the infected macrophages. SIRT1 and SIRT3 knockdown macrophages not only show altered host immune status but also depicted shift in the metabolic state with increased glycolytic shift. This altered host metabolism upon SIRT1 and SIRT3 knockdown condition influences the outcome of infection by regulating the intracellular bacterial metabolism which shows reduced bacterial glycolysis and increased fatty acid oxidation. All these outcomes account for attenuated intracellular bacterial proliferation in the SIRT1 and SIRT3 knockdown macrophages. However, in murine model of infection, SIRT1 or SIRT3 inhibitor treatment led to increased organ burden and triggered bacterial dissemination (Fig. S11). Overall, our study highlights the crucial role of SIRT1 and SIRT3 in governing the host immune-metabolic shift during *Salmonella* infection which in turn is vital for maintaining *Salmonella* metabolism.

Previous reports have elucidated the role of SIRT1 and SIRT2 pertaining to *Salmonella* infection. Ganesan et al., have depicted the role of SIRT1 in autophagy in *Salmonella* infection scenario[59]. Gogoi et al., have demonstrated SIRT2 mediated modulation of immune responses in dendritic cells[60]. Till date, there is no report highlighting the role of SIRT3 governing the *Salmonella* pathogenesis. The function of SIRT3 in infection scenario has been explored quite recently. In *Mycobacterium tuberculosis* infection condition, SIRT3 control mitochondrial function and autophagy[38]. SIRT3 downregulation in *Mycobacterium tuberculosis* infected macrophages is associated with dysregulated mitochondrial metabolism and increased cell death[61]. In this study we have explored the role of SIRT1 and SIRT3 in mediating host immune-metabolic switch in *Salmonella* Typhimurium infected macrophages which further govern intracellular bacterial metabolism and pathogenesis.

Our findings suggest the role of SIRT1 and SIRT3 in mediating polarization of the *Salmonella* infected macrophages toward an anti-inflammatory state. Upon knockdown of SIRT1 and SIRT3 in the infected macrophages we detect robust pro-inflammatory response and oxidative burst. This is in line with the findings by S.Elsela et al., wherein SIRT1 knockout RSV(Respiratory Syncytial Virus) – infected BMDCs showed significant increase in *Il1*β, *Il6* and *Il23* expression and ROS generation in comparison to the wild type RSV-infected BMDCs[35]. Also, Kim et al., showed presence of aggravated inflammatory responses in *Mycobacterium tuberculosis* infected SIRT3-/– BMDMs[38]. This heightened pro-inflammatory cytokine and oxidative burst restrict the intracellular survival of the pathogen as detected by the lower intracellular bacterial burden in the SIRT1 and SIRT3 knockdown murine macrophages. *Salmonella* showed enhanced proliferation in the M2 macrophages owing to the reduced arsenals in terms of pro-inflammatory cytokines and ROS production. Moreover, the M2 macrophages are fuelled by increased fatty acid oxidation and reduced glycolysis[62]. This might facilitate enhanced bacterial proliferation as the host un-utilized intracellular glucose can be readily up taken by the pathogen and used to support its own glycolysis. Similarly, M1 or pro-inflammatory macrophages resort to glycolysis to meet their energy demands[63] thereby limiting the glucose availability for the intracellular pathogen[63][64]. In such condition, bacteria show enhanced fatty acid metabolism to sustain their energy demand[65]. In our study, we found that wild type *S.* Typhimurium infection drive host metabolism toward increased fatty acid oxidation via its SPI-2 effector protein with concomitant increase in the bacterial glycolysis. SIRT1 and SIRT3 inhibition abrogates the metabolic switch and triggers increase in host glycolysis which in turn skew the bacterial metabolism from increased glycolysis to enhanced fatty acid oxidation and reduced glycolysis. Together, these findings implicate the role of SIRT1 and SIRT3 in reprograming the host metabolism which in turn affect the intracellular nutrient niche of the pathogen thereby influencing intracellular *Salmonella* proliferation. However, our *in vivo* findings in the murine model of infection show increased bacterial burden upon SIRT1 or SIRT3 inhibition. This increased burden could be attributed to increased dissemination from the macrophages into the bloodstream owing to the increased level of serum IL-6 levels. This is in concert with previous findings in *Klebsiella pneumoniae* infection in mice wherein increased inflammatory response upon HIF-1α activation induces bacterial dissemination [66]. Further correlation analysis of immune responses to *Salmonella* infection revealed that increased innate immune “cassette” opposes the adaptive immune arm leading to increased bacterial load [67]. Future studies might explore the host and bacterial interacting partners of SIRT1 and SIRT3 through mass spectrometry analyses in *Salmonella* infected macrophages which might hint at the underlying mechanism of their action and regulation. Together, this study highlights the complex and multifaceted nature of host-pathogen interactions, and the need for further research to fully understand the role of SIRT1 and SIRT3 in the context of *Salmonella* infection.

Materials and methods

Bacterial Strains, and culture conditions

Salmonella enterica serovar Typhimurium (STM) strain ATCC 14028S or ATCC 14028S constitutively expressing green fluorescent protein (eGFP) or mCherry (RFP) through pFPV plasmid were used. 4% paraformaldehyde fixed STM (PFA) was used as the killed fixed bacteria control. The above-mentioned live bacterial strain was grown overnight in LB broth in 37 ^{0}C at 160 rpm shaking condition in presence or absence of appropriate antibiotic (Ampiciilin-50µg/ml) (**Table-1**) after revival of the bacterial strains from glycerol stock (stored at –80 ^{0}C).

Cell Culture

RAW 264.7 murine macrophages were cultured in DMEM (Lonza) containing 10% FBS (Gibco) at 37 ^{0}C in a humified incubator with 5% CO_2. Prior to each experiment, cells were seeded into 24 well or 6 well plate as per requirement at a confluency of 60%.

For macrophage polarization experiments, the seeded macrophages were subjected to 100ng/ml LPS + 20ng/ml IFN-$_\gamma$ treatment for M1 polarization and 20ng/ml IL-4 treatment for M2 polarization for 24 hrs. Post-polarization, the cell supernatant were collected for validation of polarization status by ELISA and was further subjected to infection protocol.

Peritoneal macrophages were collected in PBS from the peritoneal cavity of C57BL/6 mice aseptically post thioglycolate treatment using 20G needle and 5ml syringe. Following centrifugation, cell pellet was resuspended in RPMI-1640 (Lonza) containing 10% heat-inactivated FBS (Gibco), 100 U/ml penicillin and 100 µg/ml streptomycin and seeded into 6 well-plate. 6hr prior to infection, antibiotic-containing media was replaced with Penicillin-Streptomycin free RPMI-1640 (Lonza) containing 10% heat-inactivated FBS (Gibco).

Transfection

shRNA mediated knockdown was carried out by PEI mediated transfection protocol. Plasmid harbouring shRNA in pLKO.2 vector backbone specific to SIRT1 and SIRT3 were used for transfection. Plasmid harbouring scrambled sequence of shRNA, served as a control, was also used for transfection. Plasmid DNA was used at a concentration of 500ng and 1µg per well of a 24-well plate and 6-well plate respectively. Plasmid and PEI were added in 1:2 ratio in serum free DMEM media and incubated for 20 mins at room temperature. Post incubation, the DNA: PEI cocktail was added to the seeded RAW 264.7 macrophages. After 6-8hrs of incubation, serum-free media was replaced with complete media containing 10% FBS. Post 48hr of transfection, transfected cells were either harvested for knockdown confirmation studies or subjected to infection with STM.

Infection Protocol

Macrophages were infected with stationary-phase bacterial culture with MOI of 10. For synchronization of the infection, tissue culture plates were subjected to centrifugation at 600xg for 5 min and incubated at 37 ^{0}C humified incubator with 5% CO_2 for 25 min. Cells were washed with PBS and were treated with DMEM (Sigma) + 10% FBS (Gibco) containing 100 µg/ml gentamicin for 1 hr. Subsequently, the gentamicin concentration was reduced to 25 µg/ml and maintained until the cells were harvested. For the inhibitor treatment studies, along with 25 µg/ml containing complete media 1µM of SIRT1 (EX-527) inhibitor or SIRT3 (3TYP) or 10mM of N-Acetyl Cysteine (NAC, Sigma) or 50nM of chetomin (Sigma) were added to the cells.

Strains/Plasmids	Characteristics	Source
Salmonella enterica serovar Typhimurium ATCC strain 14028S (STM)	Wild Type (WT)	Gifted by Prof. M. Hensel
pFPV:GFP	Amp^R	Laboratory Stock
pFPV:mCherry	Amp^R	Laboratory Stock
pLKO.2 : shRNA	Amp^R	Gifted by Prof. Subba Rao Gangi Setty
STM Δ *invC*	Kan^R	Laboratory Stock
STM Δ *ssaV*	Chl^R	Laboratory Stock
STM Δ *steE*	Kan^R	Laboratory Stock

Table 1

List of strains and plasmids used in this study

Table 2

List of shRNA used for knockdown

Sirtuins	Construct ID	TRC ID	Sequence (5'---3')
SIRT1	C4	TRCN0000218734	GTACCGGCATGAAGTGCCTCAGATAT TACTCGAGTAATATCTGAGGCACTTC ATGTTTTTTG
SIRT1	C12	TRCN0000018979	CCGGGCAAAGCCTTTCTGAATCTATC TCGAGATAGATTCAGAAAGGCTTTGC TTTTT
SIRT3	E8	TRCN0000038889	CCGGCCCAACGTCACTCACTACTTTC TCGAGAAAGTAGTGAGTGACGTTGG GTTTTTG
SIRT3	E12	TRCN0000038893	CCGGCCACCTGCACAGTCTGCCAAAC
			TCGAGTTTGGCAGACTGTGCAGGTGG TTTTTG

Immunofluorescence confocal microscopic studies

At the specified time points post infection with GFP tagged STM, cells were fixed with 3.5% paraformaldehyde for 15 min. Primary antibody staining was performed with specific primary antibody in the presence of a permeabilizing agent, 0.01% saponin (Sigma) dissolved in 2.5% BSA containing PBS at 4°C for overnight or for 6hr at room temperature (RT). Following this, cells were washed with PBS stained with appropriate secondary antibody tagged with fluorochrome for 1 hr at RT. This was followed by DAPI staining and mounting of the coverslip onto a clean glass slide using the mounting media containing the anti-fade agent. The coverslip sides were sealed with a transparent nail paint. All immunofluorescence images were obtained using Zeiss LSM 710 or Zeiss LSM 880 and were analyzed using ZEN black 2012 software.

Quantitative Real Time PCR

Total RNA was isolated at specific time points post infection by using TRIzol (Takara) as per manufacturer's protocol. Quantification of RNA was performed in Nano Drop (Thermo-Fischer scientific). Quality of isolated RNA was detected by performing 2% agarose gel electrophoresis. 2 µg of RNA was subjected to DNaseI (Thermo Fischer Scientific) treatment at 37°C for 1 hr followed by addition of 0.5M EDTA (final concentration 5mM) and heat inactivation at 65°C for 10 mins. The mRNA was reverse transcribed to cDNA using oligo $(dT)_{18}$ primer, buffer, dNTPs and reverse transcriptase (Takara) as per manufacturer's protocol. The expression profile of target gene was evaluated using specific primers (**Table-3**) by using SYBR green RT-PCR master mix (Takara) in BioRad Real time PCR instrument. β-actin was used as an internal control for mammalian genes and for bacterial genes 16S rRNA was used. All the reaction was setup in 384 well plate with two replicates for each sample.

Intracellular proliferation or gentamicin protection assay

Following infection of the transfected cells with STM at an MOI of 10, cells were treated with DMEM (Sigma) + 10% FBS (Gibco) containing 100 µg/ml gentamicin for 1 hr. Subsequently, the gentamicin concentration was reduced to 25 µg/ml and maintained until the specified time point. Post 2hr and 16hr post-infection, cells were lysed in 0.1% triton-X-100. Lysed cells were serially diluted and plated on *Salmonella-Shigella* (SS) agar to obtain colony-forming units (cfu). Fold proliferation was calculated as cfu at 16hr divided by cfu at 2hr.

Fold Proliferation= [CFU at 16h]/[CFU at 2h]

Western Blotting

Post appropriate time points of infection, the cells were washed in PBS and subsequently harvested in PBS. The cell pellets were obtained after centrifugation at 300g for 7 minutes at 4°C. Cells were lysed in 1X RIPA (10X-0.5M NaCl, 0.5M EDTA pH-8.0, 1M Tris, NP-40, 10% sodium deoxycholate, 10% SDS) buffer containing 10% protease inhibitor cocktail (Roche) for 30 min on ice. Total protein was estimated using Bradford (Bio-Rad) method of protein estimation. Protein samples were subjected to 12 % SDS polyacrylamide gel electrophoresis and then were transferred onto 0.45µm PVDF membrane (18V, 2 hrs). The membrane was blocked using 5% skim milk in TBST (Tris Buffered Saline containing 0.1% Tween-20) for 1hr at RT and subsequently probed with appropriate primary antibody (**Table-4**) for overnight at 4°C. Following wash in TBST, blot was probed with specific HRP conjugated secondary antibody for 1hr at RT. The membrane was developed using ECL (Advansta) and images were captured using ChemiDoc GE healthcare. All densitometric analysis was performed using ImageJ software.

Primer Name	Sequence (5'---3')
SIRT1 FP	ACAAAGTTGACTGTGAAGCTGTAC
SIRT1 RP	GTTCATCAGCTGGGCACCTA
SIRT3 FP	GCTGCTTCTGCGGCTCTATAC
SIRT3 RP	GAAGGACCTTCGACAGACCGT
PPARδ FP	CACAACGCTATCCGCTTTGG
PPARδ RP	ATGCTCCGGGCCTTCTTTTT
βactin FP	CAGCAAGCAGGAGTACGATG
βactin RP	GCAGCTCAGTAACAGTCCG
Acadl FP	CTTGGGAAGAGCAAGCGTACT
Acadl RP	CTGTTCTTTTGTGCCGTAATTCG

Table 3

List of primers

Hadha FP	AGCAACACGAATATCACAGGAAG
Hadha RP	AGGCACACCCACCATTTTGG
Acox1 FP	TCGAAGCCAGCGTTACGAG
Acox1 RP	ATCTCCGTCTGGGCGTAGG
Pdha1 FP	TGTCGGTTCCCAGTCCATCA
Pdha1 RP	CGTTTCCTTTTCACAGCACATGA
Pfkl FP	GAACTACGCACACTTGACCAT
Pfkl RP	CTCCAAAACAAAGGTCCTCTGG
ptsG FP	TATCTGGGCTTCTTTGCGGG
ptsG RP	ACCAGGCAACGCTCGATAAA
fadA FP	TCTGGGATTGATGGAGCAGA
fadA RP	AGACCAATACACATCGTCGC
fadB FP	GTCCCCGAAGAGCAGTTAAG
fadB RP	CCAGTTTAGTTTCCGGCAGA
aceA FP	CGATCTGGTATGGTGCGAAA
aceA RP	TTCTGCCAGTTGAAGGATGG
aceB FP	AGCGTTTCAATCAACAGGGT
aceB RP	CCCGTATTTTTACCTGCCGA
Salmonella 16S rRNA FP	GTGAGGTAACGGCTCACCAA
Salmonella 16S rRNA RP	TAACCGCAACACCTTCCTCC

Table 3 (continued)

Table 4

List of Antibodies

Antibody Name	Catalogue Number
SIRT1 Polyclonal Antibody	Cat #PA5-85921 (ThermoFisher Scientific)
SIRT3 Polyclonal Antibody	**Cat#** PA5-13222(ThermoFisher Scientific)
CD 86	**Cat#**12-086282PE(ThermoFisherScientific)
CD 206	**Catalog#** 17-2069-42 (ThermoFisherScientific)
F4/80 Antibody	BD Horizon, Cat-565411
HIF-1α	**sc-13515 SCBT**
NF-κβ p65	CST(D14E12)XP® RabbitmAb #8242
Acetylated-Lysine Antibody	**Cat #9441(Cell Signaling Technology)**
PDHA1	**Catalog No. A13687 (ABclonal)**
HADHA	**Catalog No. A5346 (ABclonal)**
ACOX1	**Catalog No. A8091 (ABclonal)**
PGK	**Catalog No. A12686 (ABclonal)**
PFK	**Catalog No. A5477 (ABclonal)**
β actin	A3854 (Sigma)

Immunoprecipitation

For co-immunoprecipitation, cells were washed with PBS and were lysed in native lysis buffer containing 1% Nonidet P-40, 20 mM Tris (pH 8), 2 mM EDTA, 150 mM NaCl and protease inhibitors mixture (Roche Diagnostics) for 30 min at 4°C. Cell debris was removed by centrifugation at 10,000 rpm for 10 min and the supernatant was treated with the specific antibody against the protein to be precipitated. Antibody-lysate complexes were immunoprecipitated using Protein A/G-linked magnetic beads (MagGenome) according to the manufacturer's protocol. Beads were extensively washed with washing buffer and denatured at 95 °C for 10 min. Denatured precipitates were subjected to SDS-PAGE (12% gel) followed by transfer to 0.45 µ PVDF membrane. The membrane was blocked using 5% skimmed milk in TBST (Tris Buffered Saline containing 0.1% Tween-20) for 1h at room temperature and eventually probed for the target primary antibodies or Anti-acetylated Lysine (Ac-K) primary antibody overnight at 4°C. The blot was probed with a specific HRP-conjugated secondary antibody for 1hr at RT after rigorous washing in TTBS. ECL (BioRad) was used for detection and images were captured using ChemiDoc GE healthcare.

ELISA

Estimation of cytokines in cell-free supernatant or in mice serum was performed according to the manufacturer's instructions. Briefly, 96-well ELISA plates (BD Bioscience) were coated overnight with capture antibody at 4°C. Following day, plates were washed with 0.1% Tween-20 containing PBS and blocked with 10% FBS for 1 h. Following blocking, wells were washed and incubated with 100 µL of test samples for 2 h at room temperature. Subsequently, plates were washed and incubated with detection antibody and enzyme reagent for 1 h at room temperature (BD Bioscience). TMB (Sigma) was used as a substrate and reactions were stopped with 2 N H_2SO_4. For the estimation of IL-1β, pre-coated ELISA (SARD Biosciences) plates were used, and ELISA was performed as per manufacturer's protocol. Absorbance was measured at 450 nm wavelength in Tecan Plate reader and the concentration of cytokines were interpolated from a standard curve.

Flow cytometry

After specific time points post infection, cells were washed and harvested in PBS. Following centrifugation, cell pellet was resuspended in FACS buffer comprised of 1% BSA in PBS. Blocking was performed with Fc blocker (purified Anti-mouse CD16/CD32, eBioscience) dissolved in FACS blocking buffer for 30 min on ice. Following a washing step with PBS, antibody staining was performed with PE-conjugated CD86 antibody or APC-conjugated CD206 (Thermo Scientific) for 45 min on ice. After washing in PBS, the cell pellet was resuspended in 1% PFA in PBS. Subsequently, PFA was removed, and cells were resuspended in FACS buffer and reading was taken in BD FACSVerse instrument. For flow cytometry studies in mice tissues, the harvested liver or spleen was homogenized into single-cell suspension post RBC lysis (RBC lysis Buffer, Sigma). The homogenized cell suspension was washed and resuspended in FACS buffer containing the PE-conjugated Rat anti-mouse F4/80 antibody (BD Horizon, Cat-565411) or eFluor450-conjugated anti-mouse CD11c antibody (eBioscience), or FITC-conjugated anti-mouse Ly6C antibody (BD Pharmingen) or Alexa647-conjugated anti-mouse CD45 antibody (BioLegend). Following staining protocol, the cells were washed in PBS and the cells were resuspended in FACS buffer and the FACS protocol was performed either in BD FACSVerse or CytoFLEX flow cytometer (Beckman).

For DCFDA staining, one hour before the indicated time point of infection, cells were incubated with 10µM DCFDA containing DMEM media at 37°C humidified incubator with 5% $CO_2$for 45 min. Post incubation, cells were washed and harvested in PBS. Readings were measured in BD FACSVerse instrument.

All analysis was done using BD FACSuite software.

Phenol Red-Hydrogen Peroxidase Assay

Post 48hr of transfection, cells were infected with STM culture at an MOI of 10. Cells were incubated with Phenol Red solution containing hydrogen peroxidase enzyme (8.5U/ml). At, the designated time points post-infection, the supernatant was collected, and the absorbance was taken at 610 nm in Tecan Plate reader. The exogenously produced H2O2 was quantified using a standard curve of known concentration of H_2O_2.

Gene expression studies by nanoString nCounter technology

Total RNA was isolated at specific time points post infection by using TRIzol (Takara) as per manufacturer's protocol. Quantification of RNA was performed in Nano Drop (Thermo-Fischer scientific) and Qubit Bioanalyzer (Agilent 2100 Bioanalyzer). Quality of isolated RNA was detected by performing 2% agarose gel electrophoresis. Post quality check, samples were subjected to nanoString nCounter technology (theraCUES). This technology allows multi-plex, spatially resolved RNA expression quantification with appropriate probes designed against the target gene.

Lactate Estimation Assay

Cell-supernatant was harvested at the specific time-points post-infection and the lactate content of the sample was estimated using the Lactate Assay Kit (Sigma, Catalog Number-MAK064) as per manufacturer's protocol. Briefly, 50µl of the sample was added to each 96 well-plate and each of the well 50µl of the master reaction mix containing 46µl of lactate assay buffer, 2µl of lactate enzyme mix, and 2µl of lactate probe was added. After the addition of the master reaction mix to the sample, they were mixed by horizontal shaker or via pipetting. The plate was incubated for 30 minutes in dark at room temperature. Post incubation, absorbance was measured at 570nm. The lactate content of the sample was estimated from the lactate standard curve ranging from 0-10 nmole/µl.

Fatty Acid Oxidation Assay

At 16h post-infection, cell pellets were harvested and stored at-80°C. The fatty acid oxidation assay protocol was followed as per manufacturer's instructions (AssayGenie Fatty Acid Oxidation (FAO) Assay Kit, Catalogue Code-BR00001). Briefly, cell pellets were lysed using 1X Cell lysis buffer (provided in the kit) and the cell supernatant were obtained post centrifugation of the cell lysate in a cold microfuge at 14,000rpm for 5min. The protein content of the cell supernatants was estimated using Bradford (Bio-Rad) method. 20µl of the protein sample was added to each 96-well plate in duplicate on ice. Each sample was treated with 50µl of control solution and 50µl of reaction solution by swiftly adding one 50µl of control solution to one set of wells and 50µl of reaction solution to the other set of wells. The contents were gently mixed for 10s. The plate is covered and incubated in a 37°C incubator for 30-60 min (without CO_2). After incubation cherry red colour appears in the wells. The O.D. is measured at 492nm using a plate reader at 30 min,60 min or 120 min. The control well reading was subtracted from the reaction well reading for each sample for each time point. The subtracted reading is used for enzyme activity calculation by considering the incubation time.

Animal Experiment

For all experiments, 6–8 weeks old C57BL/6 or *gp91phox*-/− mice were used. For organ burden analysis, 6 weeks old C57BL/6 or *gp91phox*-/− mice were infected with 10^7 CFU bacteria via oral gavaging. For bacterial enumeration via flow cytometry, mice were infected with 10^7 GFP-expressing bacteria orally. Infected mice were intraperitoneally injected on every other day with either 1 mg/kg body weight of SIRT1 inhibitor EX-527 (Sigma-Aldrich) [32], or SIRT3 inhibitor 3TYP (Selleck Chemical) [33] or SIRT1 activator SRT1720 (Calbiochem, Sigma-Aldrich) [34] or treated with vehicle alone. 5 days post infection, mice were sacrificed, and bacterial organ load

was estimated by plating the tissue homogenates on SS agar plates. For calculating percentage survival, 6 weeks old C57BL/6 mice were infected with 10^8 bacteria orally and monitored till fatality. For flow cytometry studies, the harvested liver or spleen were homogenized into single cell suspension and were subjected to flow cytometry. The animal experiments were carried out in accordance with the approved guidelines of the institutional animal ethics committee at the Indian Institute of Science, Bangalore, India (Registration No: 48/1999/CPCSEA). All procedures involving the use of animals were performed according to the Institutional Animal Ethics Committee (IAEC)-approved protocol.

In vivo knockdown

For in vivo knockdown adeno-associated virus serotype 6 (AAV6) was used. AAV6 viruses were produced in HEK293T cells. Briefly, HEK293T cells were transfected with AAV plasmid encoding shRNAs targeting SIRT1, SIRT3 and scramble control under U6 promoter together with helper plasmid using PEI Max 40000 (Polysciences USA). Next day transfection medium was removed, and fresh culture medium was added. Forty-eight hours later, medium was collected, and fresh culture medium was added and incubated for next forty-eight hours. Again, culture medium was collected and cells were harvested by trypsinization. Collected medium containing secreted AAV viral particles was incubated with 40% PEG 8000 overnight. Precipitated viral particles were then collected by centrifugation and re-suspended in PBS. Cells containing AAV viral particles were then lysed with citrate buffer and incubated with 40% PEG 8000 and processed similarly to medium for viral particle precipitation. Precipitated viral particles were then cleaned with chloroform and loaded on iodixanol gradient for further cleaning using ultracentrifugation. Cleaned viral particles were collected from the forty percent gradient and loaded on Amicon 100K cut-off columns. Purified AAV particles were then titrated by real-time PCR. For infection of AAV6, the mice were intravenously injected with a volume of 200 µl containing approximately 10^{12} viral particles harbouring the respective scrambled or shRNA constructs. The mice were infected at 7^{th} day after injection of the virus with 10^6 cfu units of *S*. Typhimurium orally. Fifth day post-infection, mice were euthanized, and dissected out for organ harvesting and blood collection. The knockdown was validated by performing western blotting and qPCR of the harvested liver tissue (Fig. S10).

Haematoxylin and Eosin Staining

6-8 weeks old C57BL/6 mice were infected with 10^7 bacteria orally. Infected mice were intraperitoneally injected every alternate with either 1 mg/kg body weight of SIRT1 inhibitor EX-527, or SIRT3 inhibitor 3TYP or SIRT1 activator SRT1720 or treated with vehicle alone. 5 days post infection, mice were euthanized, and livers were collected and fixed using 3.5% paraformaldehyde. The fixed liver was then dehydrated using a gradually increasing concentration of ethanol and embedded in paraffin. 5µm sections were collected on coated plates. Sections were further rehydrated and then stained with hematoxylin and eosin. Images were collected in a Leica microscope. **Scoring system:-** according to pathological changes the tissue sections are scored as 0 for normal pathology, 1 for mild/ minor pathology, 2 for moderate pathology, and 3 for severe pathological changes.

Statistical analysis

Data were analyzed and graphed using the GraphPad Prism 8 software (San Diego, CA). Statistical significance was determined by Student's t-test or Two-way ANOVA and Bonferroni post-t-test to obtain p values. Adjusted p-values below 0.05 are considered statistically significant. The results are expressed as mean ± SD or SEM of three independent experiments.

Acknowledgements

We duly thank Prof. Subba Rao Gangi Setty and Prof. Michael Hensel for providing us with the shRNA knockdown constructs and the *S*. Typhimurium 14028S strain, respectively.

Funding

This work was supported by the DAE SRC fellowship (DAE00195) and DBT-IISc partnership umbrella program for advanced research in biological sciences and Bioengineering to DC. Infrastructure support from ICMR (Centre for Advanced Study in Molecular Medicine), DST (FIST), and UGC (special assistance) is highly acknowledged. DH sincerely acknowledges the CSIR-SPM fellowship for her financial support. SKG is supported by Ramalingaswami Re-entry Fellowship BT/RLF/re-entry/14/2019 from DBT, Government of India. The funders had no role in study design, data collection and analysis, decision to publish, or preparation of the manuscript.

Author contribution

DH and DC have conceptualized the study. DH has contributed to the experiment designing, visualization, methodology, investigation, formal analysis, literature survey, validation, writing (original draft), reviewing, and editing of the manuscript. RSR has performed the histopathological scoring of the liver sections and the retro-orbital injection of the adenoviral constructs in mice. ADC and SKG have prepared and provided AAV6, for *in vivo* mice knockdown experiments. DC has contributed to the funding acquisition, project administration, and overall supervision of the work. All authors approved the final version of the manuscript.

Declaration of interest

The authors are unaware of any conflicting interests and thereby declare no conflict of interest.

References

1. Landry J, Sutton A, Tafrov ST, Heller RC, Stebbins J, Pillus L, et al. (2000) **The silencing protein SIR2 and its homologs are NAD-dependent protein deacetylases** *Proc Natl Acad Sci U S A* **97**:5807–11

2. Jackson MD, Denu JM (2002) **Structural identification of 2'– and 3'-O-acetyl-ADP-ribose as novel metabolites derived from the Sir2 family of beta –NAD+-dependent histone/protein deacetylases** *J Biol Chem* **277**:18535–18544 https://doi.org/10.1074/jbc.M200671200

3. Sauve AA, Celic I, Avalos J, Deng H, Boeke JD, Schramm VL (2001) **Chemistry of gene silencing: The mechanism of NAD+-dependent deacetylation reactions** *Biochemistry* **40**:15456–63

4. Bitterman KJ, Anderson RM, Cohen HY, Latorre-Esteves M, Sinclair DA (2002) **Inhibition of silencing and accelerated aging by nicotinamide, a putative negative regulator of yeast Sir2 and human SIRT1** *J Biol Chem* **277**:45099–107

5. Sanders BD, Jackson B, Marmorstein R (2010) **Structural basis for sirtuin function: What we know and what we don't** *Biochim Biophys Acta – Proteins Proteomics* **1804**:1604–16 https://doi.org/10.1016/j.bbapap.2009.09.009

6. Lin Z, Fang D (2013) **The Roles of SIRT1 in Cancer** *Genes and Cancer* **4**:97–104

7. Guarente L (2007) **Sirtuins in aging and disease** *Cold Spring Harb Symp Quant Biol* **72**:483–8

8. Martínez-Redondo P, Vaquero A (2013) **The Diversity of Histone Versus Nonhistone Sirtuin Substrates** *Genes and Cancer* **4**:148–63

9. Liu TF, Yoza BK, El Gazzar M, Vachharajani VT, McCall CE (2011) **NAD+-dependent SIRT1 deacetylase participates in epigenetic reprogramming during endotoxin tolerance** *J Biol Chem* **286**:9856–64

10. Gazzar M El, Yoza BK, Hu JYQ, Cousart SL, McCall CE (2007) **Epigenetic silencing of tumor necrosis factor α during endotoxin tolerance** *J Biol Chem* **282**:26857–64

11. Liu TF, Vachharajani V, Millet P, Bharadwaj MS, Molina AJ, McCall CE (2015) **Sequential actions of SIRT1-RELB-SIRT3 coordinate nuclear-mitochondrial communication during immunometabolic adaptation to acute inflammation and sepsis** *J Biol Chem* **290**:396–408

12. Kong X, Wang R, Xue Y, et al. (2010) **Sirtuin 3, a new target of PGC-1alpha, plays an important role in the suppression of ROS and mitochondrial biogenesis** *PLoS One* **5**

13. van de Ven RAH, Santos D, Haigis MC (2017) **Mitochondrial Sirtuins and Molecular Mechanisms of Aging** *Trends Mol Med* **23**:320–31

14. Garai P., Gnanadhas D.P., Chakravortty D. (2012) **Salmonella enterica serovars Typhimurium and Typhi as model organisms: revealing paradigm of host-pathogen interactions** *Virulence* **3**:377–88

15. Bhutta ZA, Threlfall J (2009) **Addressing the global disease burden of typhoid fever** *JAMA* **302**:898–899 https://doi.org/10.1001/jama.2009.1259

16. Majowicz SE, Musto J, Scallan E, et al. (2010) **The global burden of nontyphoidal Salmonella gastroenteritis** *Clin Infect Dis* **50**:882–889 https://doi.org/10.1086/650733

17. Haraga A., Ohlson M.B., Miller S.I. (2008) **Salmonellae interplay with host cells** *Nat Rev Microbiol* **6**:53–66

18. Hajra D., Nair A.V., Chakravortty D. (2021) **An elegant nano-injection machinery for sabotaging the host: Role of Type III secretion system in virulence of different human and animal pathogenic bacteria** *Phys Life Rev* **38**:25–54

19. Lawrence T, Natoli G (2011) **Transcriptional regulation of macrophage polarization: Enabling diversity with identity** *Nat Rev Immunol* **11**:750–61

20. Martinez FO, Helming L, Gordon S (2009) **Alternative Activation of Macrophages: An Immunologic Functional Perspective** *Annu Rev Immunol* **27**:451–83

21. Namgaladze D, Brüne B (2014) **Fatty acid oxidation is dispensable for human macrophage IL-4-induced polarization** *Biochim Biophys Acta – Mol Cell Biol Lipids* **1841**:1329–35

22. Hui X, Zhang M, Gu P, Li K, Gao Y, Wu D. (2017) **Adipocyte SIRT 1 controls systemic insulin sensitivity by modulating macrophages in adipose tissue** *EMBO Rep* **18**:645–57

23. Jia Y, Han S, Li J, et al. (2017) **IRF8 is the target of SIRT1 for the inflammation response in macrophages** *Innate Immun* **23**:188–195 https://doi.org/10.1177/1753425916683751

24. Kratz M, Coats BR, Hisert KB, Hagman D, Mutskov V, Peris E, et al. (2014) **Metabolic dysfunction drives a mechanistically distinct proinflammatory phenotype in adipose tissue macrophages** *Cell Metab* **20**:614–25 https://doi.org/10.1016/j.cmet.2014.08.010

25. Cimen H, Han MJ, Yang Y, Tong Q, Koc H, Koc EC (2010) **Regulation of succinate dehydrogenase activity by SIRT3 in mammalian mitochondria** *Biochemistry* **49**:304–11

26. Vazquez-Torres A, Xu Y, Jones-Carson J, Holden DW, Lucia SM, Dinauer MC, et al. (2000) **Salmonella pathogenicity island 2-dependent evasion of the phagocyte NADPH oxidase** *Science* **287**:1655–8

27. Miller BH, Fratti RA, Poschet JF, Timmins GS, Master SS, Burgos M, et al. (2004) **Mycobacteria Inhibit Nitric Oxide Synthase Recruitment to Phagosomes during Macrophage Infection** *Infect Immun* **72**:2872–8

28. Bost KL, Clements JD (1997) **Intracellular Salmonella dublin induces substantial secretion of the 40-kilodalton subunit of interleukin-12 (IL-12) but minimal secretion of IL-12 as a 70-kilodalton protein in murine macrophages** *Infect Immun* **65**:3186–92

29. Pathak SK, Basu S, Basu KK, Banerjee A, Pathak S, Bhattacharyya A, et al. (2007) **Direct extracellular interaction between the early secreted antigen ESAT-6 of Mycobacterium tuberculosis and TLR2 inhibits TLR signaling in macrophages** *Nat Immunol* **8**:610–8

30. Tumitan ARP, Monnazzi LGS, Ghiraldi FR, Cilli EM, De Medeiros BMM (2007) **Pattern of macrophage activation in yersinia-resistant and yersinia-susceptible strains of mice** *Microbiol Immunol* **51**:1021–8

31. Brubaker RR (2003) **Interleukin-10 and inhibition of innate immunity to Yersiniae: Roles of Yops and LcrV (V antigen)** *Infect Immun* **71**:3673–81

32. Morató L, Astori S, Zalachoras I, et al. (2022) **eNAMPT actions through nucleus accumbens NAD+/SIRT1 link increased adiposity with sociability deficits programmed by peripuberty stress** *Sci Adv* **8** https://doi.org/10.1126/sciadv.abj9109

33. Hu B, Wang P, Zhang S, et al. (2022) **HSP70 attenuates compression-induced apoptosis of nucleus pulposus cells by suppressing mitochondrial fission via upregulating the expression of SIRT3** *Exp Mol Med* **54**:309–323 https://doi.org/10.1038/s12276-022-00745-9

34. Tan P, Wang M, Zhong A, et al. (2021) **SRT1720 inhibits the growth of bladder cancer in organoids and murine models through the SIRT1-HIF axis** *Oncogene* **40**:6081–6092 https://doi.org/10.1038/s41388-021-01999-9

35. Elesela S, Morris SB, Narayanan S, Kumar S, Lombard DB, Lukacs NW (2020) **Sirtuin 1 regulates mitochondrial function and immune homeostasis in respiratory syncytial virus infected dendritic cells** *PLoS Pathog* **16**

36. Liu G, Bi Y, Xue L, et al. (2015) **Dendritic cell SIRT1-HIF1α axis programs the differentiation of CD4+ T cells through IL-12 and TGF-β1** *Proc Natl Acad Sci U S A* **112**:E957–E965 https://doi.org/10.1073/pnas.1420419112

37. Yang H, Hu J, Chen Y (Jason), Ge B (2019) **Role of Sirt1 in innate immune mechanisms against Mycobacterium tuberculosis via the inhibition of TAK1 activation** *Arch Biochem Biophys* **667**:49–58 https://doi.org/10.1016/j.abb.2019.04.006

38. Kim TS, Jin YB, Kim YS, Kim S, Kim JK, Lee HM, et al. (2019) **SIRT3 promotes antimycobacterial defenses by coordinating mitochondrial and autophagic functions** *Autophagy* :1356–1375 https://doi.org/10.1080/15548627.2019.1582743

39. Yeung F, Hoberg JE, Ramsey CS, et al. (2004) **Modulation of NF-kappaB-dependent transcription and cell survival by the SIRT1 deacetylase** *EMBO J* **23**:2369–2380 https://doi.org/10.1038/sj.emboj.7600244

40. Yang H, Zhang W, Pan H, et al. (2012) **SIRT1 activators suppress inflammatory responses through promotion of p65 deacetylation and inhibition of NF-κB activity** *PLoS One* **7** https://doi.org/10.1371/journal.pone.0046364

41. Singh CK, Chhabra G, Ndiaye MA, Garcia-peterson LM, Mack NJ, Ahmad N (2018) **The Role of Sirtuins in Antioxidant and Redox Signaling** *Antioxid Redox Signal* **28**:643–61

42. Kitada M, Ogura Y, Monno I, Koya D (2019) **Sirtuins and Type 2 Diabetes: Role in Inflammation, Oxidative Stress, and Mitochondrial Function** *Front Endocrinol (Lausanne* **10**

43. Merksamer PI, Liu Y, He W, Hirschey MD, Chen D, Verdin E (2013) **The sirtuins, oxidative stress and aging: an emerging link** *Aging (Albany NY* **5**:144–150 https://doi.org/10.18632/aging.100544

44. Rendra E, Riabov V, Mossel DM, Sevastyanova T, Harmsen MC, Kzhyshkowska J (2019) **Immunobiology Reactive oxygen species (ROS) in macrophage activation and function in diabetes** *Immunobiology* **224**:242–53 https://doi.org/10.1016/j.imbio.2018.11.010

45. Zhou Y, Que KT, Zhang Z, et al. (2018) **Iron overloaded polarizes macrophage to proinflammation phenotype through ROS/acetyl-p53 pathway** *Cancer Med* **7**:4012–4022 https://doi.org/10.1002/cam4.1670

46. Halasi M, Wang M, Chavan TS, Gaponenko V, Hay N, Gartel AL (2013) **ROS inhibitor Nacetyl-L-cysteine antagonizes the activity of proteasome inhibitors** *Biochem J* **454**:201–8

47. De Santa F, Vitiello L, Torcinaro A, Ferraro E (2019) **The Role of Metabolic Remodeling in Macrophage Polarization and Its Effect on Skeletal Muscle Regeneration** *Antioxid Redox Signal* **30**:1553–1598 https://doi.org/10.1089/ars.2017.7420

48. Galván-Peña S, O'Neill LAJ (2014) **Metabolic reprogramming in macrophage polarization** *Front Immunol* **5**:1–6

49. Taylor SJ, Winter SE (2020) **Salmonella finds a way: Metabolic versatility of Salmonella enterica serovar Typhimurium in diverse host environments** *PLoS Pathog* **16**:10–5 https://doi.org/10.1371/journal.ppat.1008540

50. Kierans SJ, Taylor CT (2021) **Regulation of glycolysis by the hypoxia-inducible factor (HIF): implications for cellular physiology** *J Physiol* **599**:23–37 https://doi.org/10.1113/JP280572

51. Lim JH, Lee YM, Chun YS, Chen J, Kim JE, Park JW (2010) **Sirtuin 1 modulates cellular responses to hypoxia by deacetylating hypoxia-inducible factor 1alpha** *Mol Cell* **38**:864–878 https://doi.org/10.1016/j.molcel.2010.05.023

52. Wang Y, Bi Y, Chen X, et al. (2016) **Histone Deacetylase SIRT1 Negatively Regulates the Differentiation of Interleukin-9-Producing CD4(+) T Cells** *Immunity* **44**:1337–1349 https://doi.org/10.1016/j.immuni.2016.05.009

53. Viziteu E, Grandmougin C, Goldschmidt H, et al. (2016) **Chetomin, targeting HIF-1α/p300 complex, exhibits antitumour activity in multiple myeloma** *Br J Cancer* **114**:519–523 https://doi.org/10.1038/bjc.2016.20

54. Hirschey MD, Shimazu T, Goetzman E, et al. (2010) **SIRT3 regulates mitochondrial fatty-acid oxidation by reversible enzyme deacetylation** *Nature* :464–7285 https://doi.org/10.1038/nature08778

55. Zhang Y, Wen P, Luo J, et al. (2021) **Sirtuin 3 regulates mitochondrial protein acetylation and metabolism in tubular epithelial cells during renal fibrosis** *Cell Death Dis* **12**

56. Panagi I, Jennings E, Zeng J, Günster RA, Stones CD, Mak H, et al. (2020) **Salmonella Effector SteE Converts the Mammalian Serine/Threonine Kinase GSK3 into a Tyrosine Kinase to Direct Macrophage Polarization** *Cell Host Microbe* **27**:41–53

57. Stapels DAC, Hill PWS, Westermann AJ, Fisher RA, Thurston TL, Saliba AE, et al. (2018) **Salmonella persisters undermine host immune defenses during antibiotic treatment** *Science* **362**:1156–60

58. Pham THM, Brewer SM, Thurston T, Massis LM, Honeycutt J, Lugo K, et al. (2020) **Salmonella-Driven Polarization of Granuloma Macrophages Antagonizes TNFMediated Pathogen Restriction during Persistent Infection** *Cell Host Microbe* **27**:54–67 https://doi.org/10.1016/j.chom.2019.11.011

59. Ganesan R, Hos NJ, Gutierrez S, Fischer J, Stepek JM, Daglidu E, et al. (2017) **Salmonella Typhimurium disrupts Sirt1/AMPK checkpoint control of mTOR to impair autophagy** *PLoS Pathog* **13**:1–22

60. Gogoi M, Chandra K, Sarikhani M, Ramani R, Sundaresan NR, Chakravortty D (2018) **Salmonella escapes adaptive immune response via SIRT2 mediated modulation of innate immune response in dendritic cells** *PLoS Pathog* **14**:1–22

61. Smulan LJ, Martinez N, Kiritsy MC, Kativhu C, Cavallo K, Sassetti CM, et al. (2021) **Sirtuin 3 downregulation in mycobacterium tuberculosis-infected macrophages reprograms mitochondrial metabolism and promotes cell death** *MBio* **12**:1–15

62. Eisele NA, Ruby T, Jacobson A, Manzanillo PS, Cox JS, Lam L, et al. (2013) **Salmonella require the fatty acid regulator PPARδ for the establishment of a metabolic environment essential for long-term persistence** *Cell Host Microbe* **14**:171–82 https://doi.org/10.1016/j.chom.2013.07.010

63. Cramer T, Yamanishi Y, Clausen BE, et al. (2003) **HIF-1alpha is essential for myeloid cell mediated inflammation** *Cell* **112**:645–657 https://doi.org/10.1016/s0092-8674(03)00154-5

64. Merrill GF, Kurth EJ, Hardie DG, Winder WW (1997) **AICA riboside increases AMP activated protein kinase, fatty acid oxidation, and glucose uptake in rat muscle** *Am J Physiol* **273**:E1107–E1112 https://doi.org/10.1152/ajpendo.1997.273.6.E1107

65. Reens AL, Nagy TA, Detweiler CS (2019) **Salmonella enterica Requires Lipid Metabolism Genes To Replicate in Proinflammatory Macrophages and Mice** *Infect Immun* **88**:e00776–19

66. Holden VI, Breen P, Houle S, Dozois CM, Bachman MA (2016) **Klebsiella pneumoniae Siderophores Induce Inflammation, Bacterial Dissemination, and HIF-1α Stabilization during Pneumonia** *mBio* **7**:e01397–16 https://doi.org/10.1128/mBio.01397-16

67. Hotson AN, Gopinath S, Nicolau M, et al. (2016) **Coordinate actions of innate immune responses oppose those of the adaptive immune system during Salmonella infection of mice** *Sci Signal* **9** https://doi.org/10.1126/scisignal.aaa9303

Editors

Reviewer #2 (Public Review):

Dipasree Hajra et al demonstrated that Salmonella was able to modulate the expression of Sirtuins (Sirt1 and Sirt3) and regulate the metabolic switch in both host and Salmonella, promoting its pathogenesis. The authors found Salmonella infection induced high levels of Sirt1 and Sirt3 in macrophages, which were skewed toward the M2 phenotype allowing Salmonella to hyper-proliferate. Mechanistically, Sirt1 and Sirt3 regulated the acetylation of

HIF-1alpha and PDHA1, therefore mediating Salmonella-induced host metabolic shift in the infected macrophages. Interestingly, Sirt1 and Sirt3-driven host metabolic switch also had an effect on the metabolic profile of Salmonella. Counterintuitively, inhibition of Sirt1/3 led to increased pathogen burdens in an in vivo mouse model. Overall, this is a well-designed study.

Comments on revised version:

The authors have performed additional experiments to address the discrepancy between in vitro and in vivo data. While this offers some potential insights into the in vivo role of Sirt1/3 in different cell types and how this affects bacterial growth/dissemination, I still believe that Sirt1/3 inhibitors could have some effect on the gut microbiota contributing to increased pathogen counts. This possibility can be discussed briefly to give a better scenario of how Sirt1/3 inhibitors work in vivo. Additionally, the manuscript would improve significantly if some of the flow cytometry analysis and WB data could be better analyzed.

https://doi.org/10.7554/eLife.93125.2.sa2

Reviewer #3 (Public Review):

Summary:

In this paper Hajra et al have attempted to identify the role of Sirt1 and Sirt3 in regulating metabolic reprogramming and macrophage host defense. They have performed gene knock down experiments in RAW macrophage cell line to show that depletion of Sirt1 or Sirt3 enhances the ability of macrophages to eliminate Salmonella Typhimurium. However, in mice inhibition of Sirt1 resulted in dissemination of the bacteria but the bacterial burden was still reduced in macrophages. They suggest that the effect they have observed is due to increased inflammation and ROS production by macrophages. They also try to establish a weak link with metabolism. They present data to show that the switch in metabolism from glycolysis to fatty acid oxidation is regulated by acetylation of Hif1a, and PDHA1.

Strengths:

The strength of the manuscript is that the role of Sirtuins in host-pathogen interactions has not been previously explored in-depth making the study interesting. It is also interesting to see that depletion of either Sirt1 or Sirt3 results in a similar outcome.

Weaknesses:

The major weakness of the paper is the low quality of data, making it harder to substantiate the claims. Also, there are too many pathways and mechanisms being investigated. It would have been better if the authors had focussed on either Sirt1 or Sirt3 and elucidated how it reprograms metabolism to eventually modulate host response against Salmonella Typhimurium. Experimental evidence is also lacking to prove the proposed mechanisms. For instance they show correlative data that knock down of Sirt1 mediated shift in metabolism is due to HIF1a acetylation but this needs to be proven with further experiments.

https://doi.org/10.7554/eLife.93125.2.sa1

Author response:

The following is the authors' response to the original reviews.

Reviewer #1 (Public Review):

Summary:

The current manuscript by Hajra et al deals with the role of the prominent Sirtuins SIRT1 and -3 during infection of macrophages with Salmonella Typhimurium (ST). Apparently, ST infection induces upregulation of host cell SRTs to aid its own metabolism during the intracellular lifestyle and to help reprogramming macrophage polarization. The manuscript has two parts, namely one part that deals with Salmonella infection in cells, where RAW 264.7 murine macrophage-like cells, sharing some features with primary macrophages, were employed. Infected RAW cells displayed a tendency to polarize towards wound-healing M2 and not inflammatory M1 macrophages, which was dependent on SRT. Consequently, the inflammatory response in RAW was more robust in the absence of SRT. Moreover, loss of SRTs leads to impaired bacterial proliferation in these cells, which was attributed to defects in metabolic adaption of the bacteria in the absence of SRT-activity and to the increased M1 inflammatory response.

Unfortunately, the line of argumentation remains incomplete because corresponding assays in mice showed the opposite result as compared to the experiments using RAW 264.7 cells. i.e. loss of SRTs leads to increased bacterial load in animals (versus impaired proliferation in RAW 264.7 cells). The authors cannot explain this discrepancy.

Strengths:

Extensive analysis of Salmonella infection in RAW macrophage-like cells and mice in the context of SRT1/3 function.

Weaknesses:

Lack of connection between the cell-based and organismic data, which are not supportive of each other.

We are highly grateful for your valuable and insightful comments. Thank you for appreciating the merit of our manuscript. We agree with the opposing phenotypes among the RAW264.7 cell line (Fig. 2A), primary peritoneal macrophages (ex vivo) (Fig.2B), and in vivo mouse model (Fig.8) findings. Both RAW264.7 macrophage and peritoneal macrophage infection show attenuated intracellular bacterial proliferation owing to the heightened proinflammatory burst. This is in sharp contrast to our in vivo mouse model of infection which shows increased organ burden and bacterial dissemination. The higher bacterial load in the organs including the spleen (Fig.8B) is attributed to increased pro-inflammatory cytokine burst and ROS production (Fig.8F-H, Fig.S9) triggering bacterial dissemination. The pro-inflammatory arsenals like IL-6, IL-1β and ROS that limit bacterial proliferation within the macrophages (F4/80+ macrophages within the spleen or in RAW264.7 macrophages or primary peritoneal macrophages) are facilitating bacterial dissemination in blood and to the other organs (Fig. 8I-L, Fig.S3F-G). This is in line with the following previous findings-

Klebsiella pneumoniae infection triggers an inflammatory response via secretion of IL-6 upon HIF-1α activation that induces bacterial dissemination (Holden VI, Breen P, Houle S, Dozois CM, Bachman MA. Klebsiella pneumoniae Siderophores Induce Inflammation, Bacterial Dissemination, and HIF-1α Stabilization during Pneumonia. mBio. 2016 Sep 13;7(5):e01397-16. doi: 10.1128/mBio.01397-16. PMID: 27624128; PMCID: PMC5021805.).

Correlation analysis of immune responses to *Salmonella* infection revealed that increased innate immune “cassette” opposes the adaptive immune arm leading to increased bacterial load in mice (Hotson AN, Gopinath S, Nicolau M, Khasanova A, Finck R, Monack D, et al.

Coordinate actions of innate immune responses oppose those of the adaptive immune system during Salmonella infection of mice. Science signaling. 2016;9(410):ra4).

In our revised manuscript, we have assessed additional splenic populations including CD45+, Ly6C+, and CD11c+ populations. Our results show that the CD45+ splenic population depicts increased bacterial loads like that of the total splenic population within the SIRT1/3 inhibited cohorts. However, CD45+ monocytes and Ly6C positive splenic population exhibit compromised burden within the SIRT1/3 inhibited cohorts. Moreover, within the CD11c+ population, CD45+ granulocytes or lymphocytes show comparable organ loads to that of the vehicle control or SIRT1 activator-treated mice group (Fig. M-S, Fig.S8). Overall, our data suggest heterogeneous bacterial burden in diverse splenic populations.

> ***Reviewer #2 (Public Review):***
>
> *Dipasree Hajra et al demonstrated that Salmonella was able to modulate the expression of Sirtuins (Sirt1 and Sirt3) and regulate the metabolic switch in both host and Salmonella, promoting its pathogenesis. The authors found Salmonella infection induced high levels of Sirt1 and Sirt3 in macrophages, which were skewed toward the M2 phenotype allowing Salmonella to hyper-proliferate. Mechanistically, Sirt1 and Sirt3 regulated the acetylation of HIF-1alpha and PDHA1, therefore mediating Salmonella-induced host metabolic shift in the infected macrophages. Interestingly, Sirt1 and Sirt3-driven host metabolic switch also had an effect on the metabolic profile of Salmonella. Counterintuitively, inhibition of Sirt1/3 led to increased pathogen burdens in an in vivo mouse model. Overall, this is a well-designed study. There are a few comments below that would further strengthen the current study.*
>
> *Major comments:*
>
> *In the in vivo study (lines 436-446) - the authors noticed increased pathogen burden in the EX-527 or the 3TYP-treated mice cohorts but decreased pathogen burden within the F4/80+ macrophage population. What are the other cell types that have increased pathogen burden in splenocytes from EX-527 or the 3TYP treated? Can this be further explored and explained?*
>
> *While the authors indicated that IL-6 cytokine storm and elevated ROS production could result in bacterial dissemination in vivo, one could also argue that Sirt1/3 inhibitors might have an impact on gut function and/or gut microbiota (PMID: 22115311). Did Sirt1/3 inhibitors also lead to increased pathogen burdens in the gut? If so, the potential effect of these in vivo treatments on gut microbiota/colonization resistance should be discussed.*
>
> *Minor comment:*
>
> *Sirt1 has been shown to be degraded during Salmonella infection (PMID: 28192515), which is different from the current study. An explanation should be provided for this.*

We thank you for your encouraging and gracious comments. We deeply appreciate your time and efforts in providing constructive feedback for the betterment of our work. As per your precious suggestions, we have assessed additional splenic populations including CD45+, Ly6C+, and CD11c+ populations apart from F4/80+ macrophage populations. Our analysis suggests that the CD45+ splenic population show increased bacterial loads similar to the total splenic population within the SIRT1/3 inhibited cohorts. However, CD45+ monocytes and Ly6C positive splenic population exhibit compromised burden within the SIRT1/3 inhibited cohorts. Moreover, CD11c+ population, CD45+ granulocytes or lymphocytes show comparable organ loads to that of the vehicle control or SIRT1 activator treated mice group (Fig. 8M-S). Overall, our data suggest heterogeneous bacterial burden in diverse splenic populations.

We immensely appreciate the reviewer for this insightful question about the effect of SIRT1/3 on the gut per se. To answer your question, we observed increased pathogen loads within the mesenteric lymph nodes of the gut in the SIRT1/3 inhibitor-treated mice groups (Fig.8B). In our revised manuscript, we evaluated gut inflammation via IL1-β estimation in the mice's ileal tissues and have observed heightened IL-1β production in the inhibitor-treated mice cohorts in comparison to the vehicle control (Fig. S3G). We have also examined gut epithelial pathology via Haematoxylin-Eosin (H&E) staining of the ileal sections to address the effect of in vivo treatment on gut microbiota and colonization resistance which is appended here. However, the gut microbiota crosstalk and their effect on colonization resistance is a part of another current study and it is being examined in detail there. Therefore, this appended H&E has not been incorporated in the revised manuscript.

Author response image 1.

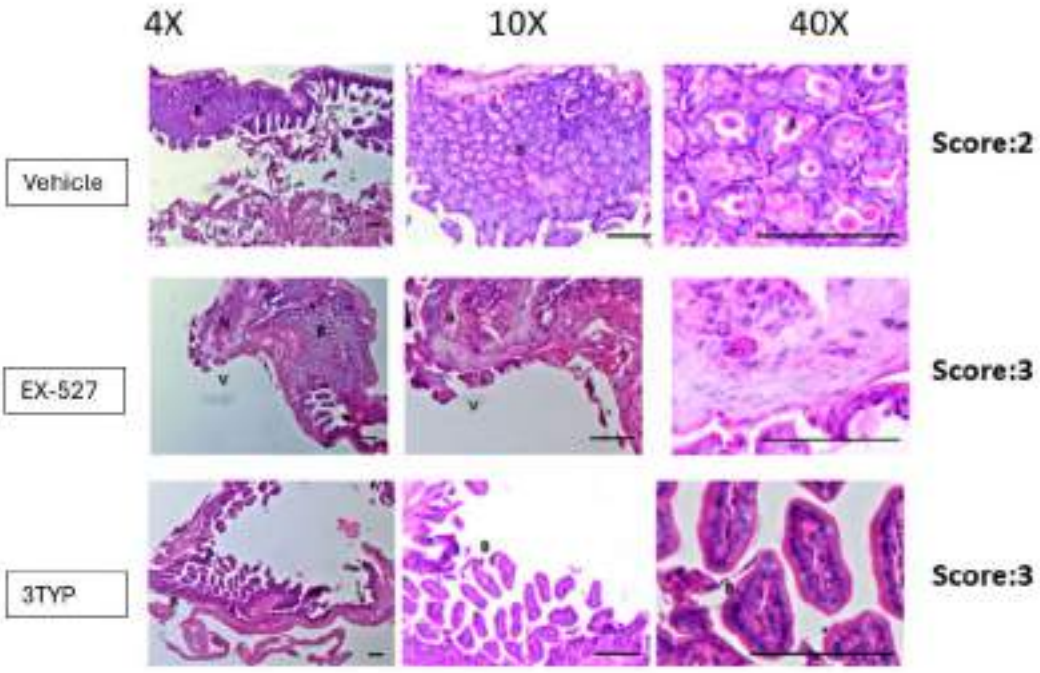

In line with the reference PMID: 28192515, where Sirt1 has been shown to be degraded during *Salmonella* infection at later time points of infection, our study also has shown that both SIRT1 mRNA (Fig. 1A) and protein levels (Fig. S1A) show an elevated expression at 2h and 6h post-infection and show a downregulation at 16h in comparison to the 6h time point. However, SIRT3 expression levels remain elevated even at later time points of infection. Therefore, we speculate that there is a shared role between SIRT1 and SIRT3 that facilitates the phenotypes reported in our study.

> ***Reviewer #3 (Public Review):***
>
> *Summary:*
>
> *In this paper, Hajra et al have attempted to identify the role of Sirt1 and Sirt3 in regulating metabolic reprogramming and macrophage host defense. They have performed gene knockdown experiments in RAW macrophage cell lines to show that depletion of Sirt1 or Sirt3 enhances the ability of macrophages to eliminate Salmonella Typhimurium. However, in mice, inhibition of Sirt1 resulted in dissemination of the*

> *bacteria but the bacterial burden was still reduced in macrophages. They suggest that the effect they have observed is due to increased inflammation and ROS production by macrophages. They also try to establish a weak link with metabolism. They present data to show that the switch in metabolism from glycolysis to fatty acid oxidation is regulated by acetylation of Hif1a, and PDHA1.*
>
> *Strengths:*
>
> *The strength of the manuscript is that the role of Sirtuins in host-pathogen interactions has not been previously explored in-depth making the study interesting. It is also interesting to see that depletion of either Sirt1 or Sirt3 results in a similar outcome.*
>
> *Weaknesses:*
>
> *The major weakness of the paper is the low quality of data, making it harder to substantiate the claims. Also, there are too many pathways and mechanisms being investigated. It would have been better if the authors had focussed on either Sirt1 or Sirt3 and elucidated how it reprograms metabolism to eventually modulate host response against Salmonella Typhimurium. Experimental evidence is also lacking to prove the proposed mechanisms. For instance, they show correlative data that the knockdown of Sirt1-mediated shift in metabolism is due to HIF1a acetylation but this needs to be proven with further experiments.*

We appreciate the reviewer's critical analysis of our work. In the revised manuscript, we aimed to eliminate the low-quality data sets and have tried to substantiate them with better and conclusive ones, as directed in the recommendations for the author section. We agree with the reviewer that the inclusion of both Sirtuins 1 and 3 has resulted in too many pathways and mechanisms and focusing on one SIRT and its mechanism of metabolic reprogramming and immune modulation would have been a less complicated alternative approach. However, as rightly pointed out, our work demonstrated the shared and few overlapping roles of the two sirtuins, SIRT1 and SIRT3, together mediating the immune-metabolic switch upon *Salmonella* infection. As per the reviewer's suggestion, we have performed additional experiments with HIF-1α inhibitor treatment in our revised manuscript to substantiate our correlative findings on SIRT1-mediated regulation of host glycolysis (Fig.7G).

> ***Reviewer #1 (Recommendations For The Authors):***
>
> *The authors state "SIRT1 and SIRT3 inhibition resulted in increased pathogen loads in organs and triggered enhanced bacterial dissemination, together leading to increased susceptibility of the mice to S. Typhimurium infection owing to increased ROS and IL-6 production." How can this be reconciled? To the reviewer, this is not a convincing explanation. The reviewer is not a mouse pathologist, so maybe did not understand the argument in full.*
>
> *However, in order to clarify whether these phenomena can be brought into context and explained by for instance cell-autonomous (in (RAW) macrophages) versus non-autonomous (in mice) mechanisms, it would be required to bring in context the organismic phenotype with a cellular phenotype, using more physiologic primary macrophages.*
>
> *(1) The authors show in Figure 8 that in general SRT inhibition leads to increased infection whereas SRT activation results in decreased infection. This is even true for e the spleen (e.g. Figure 8B), which should be full of macrophages upon infection.*
>
> *(2) Only Figure 8L implies that endogenous primary, splenic macrophages show a higher infection rate upon pharmacologic SRT activation, which would potentially mirror the*

> *RAW results. This is however not supportive of their own explanation: Who would now produce more ROS and IL6 if these macrophages are more supportive of intracellular ST? Is there a difference in the roles or SRTs between different types of macrophages and/or neutrophils? And between macrophages and somatic cells concerning ST infection? The reviewer tends to believe that RAW cells display a defective killing response (such as ROS production) as they are highly transformed cells. Therefore, the authors should use cultured peritoneal macrophages or BMDMs in addition to RAW264.7 cells.*
>
> *The literature cited by the authors also implies that the inflammatory response in mice is higher in the absence of SRTs. This is in line with a role for SRTs in (negatively) regulating M1 inflammatory polarization but probably not with increased bacterial burden in mice. If it was, then increased dissemination could be explained by increased tissue damage. However, the flow cytometry experiments from infected organs then do not confirm that, as the infection of individual cells is higher upon SRT inhibition. Thus there seems a broad gap between the role of SRTs in ST infection in RAW264.7 cells versus non-transformed cells.*
>
> *I would not discard the RAW results, as I am convinced that they contain valuable data. However, it needs to be clarified what aspect of the host response RAW 264.7 cells represent. Primary macrophages might likely be more aggressive towards the bacteria. Finally, the question arises: what is the role of the metabolic switch in the in vivo setting?*
>
> *The reviewer recommends repeating some key experiments by in-vitro-infecting BMDMs or isolated peritoneal macrophages (after some days of culturing) to bridge between the present RAW-derived data and the mouse data. How is the bacterial load with and without SRT inhibitor/activator in primary macrophages, when infected outside of the body? Can ex-vivo infection also affect polarization of e.g. peritoneal macrophages or the metabolic switch? If it is possible to find a conclusive explanation for their data, then this story might really add to our understanding of another aspect of how ST manipulates the host to survive.*
>
> *In case the reviewer understands the mouse experiments correctly, all assays on peritoneal cells were performed after in-vivo-infection and/or treatment.*
>
> *Together, RAW 264.7 murine macrophage-like cells might not be the right model to understand the phenotypes in full. As far as the reviewer knows, these cells are not capable of killing bacteria as effectively as activated primary macrophages or neutrophils.*

A few of the key findings of RAW264.7 macrophages have been replicated in primary peritoneal macrophages (Fig. 2B, S3E-F, S6B, S7B-D). We wanted to clarify that the peritoneal macrophage experiments were performed ex vivo, wherein peritoneal macrophages were isolated from mice were then subjected to SIRT1/3 inhibitor treatments and *Salmonella* infection and not after in vivo treatment or infection. In ex vivo setting, we have examined the effect of SIRTs on the metabolic switch during *Salmonella* infection (Fig. S7B-D) which resembled our RAW264.7 macrophage data. Additionally, in *in vivo* setting, we have analyzed the transcript level expression of host metabolic genes and corresponding bacterial metabolic genes in infected mice liver and spleen tissue under SIRT1/3 inhibitor treatment (Fig.S7E-F, Fig.6C-D). Our primary peritoneal macrophage data exactly mirrors the RAW264.7 macrophage findings showing attenuated intracellular bacterial proliferation owing to the heightened proinflammatory burst upon SIRT1/3 knockdown or inhibition (Fig.2A-B). This is opposite to our in vivo mouse model of infection which shows increased organ burden and bacterial dissemination (Fig.8A-H). The pro-inflammatory arsenals that limit bacterial proliferation within the macrophages (F4/80+ macrophages within the spleen or in RAW264.7 macrophages or primary peritoneal macrophages) are facilitating bacterial dissemination in

blood and to the other organs owing to tissue damage (Fig.8E-L). This is in line with the following previous findings-

Klebsiella pneumoniae infection triggers an inflammatory response via secretion of IL-6 upon HIF-1α activation that induces bacterial dissemination (Holden VI, Breen P, Houle S, Dozois CM, Bachman MA. Klebsiella pneumoniae Siderophores Induce Inflammation, Bacterial Dissemination, and HIF-1α Stabilization during Pneumonia. mBio. 2016 Sep 13;7(5):e01397-16. doi: 10.1128/mBio.01397-16. PMID: 27624128; PMCID: PMC5021805.).

Correlation analysis of immune responses to *Salmonella* infection revealed that increased innate immune "cassette" opposes the adaptive immune arm leading to increased bacterial load in mice (Hotson AN, Gopinath S, Nicolau M, Khasanova A, Finck R, Monack D, et al. Coordinate actions of innate immune responses oppose those of the adaptive immune system during Salmonella infection of mice. Science Signaling. 2016;9(410):ra4).

As per the reviewer's suggestions, we have analyzed other populations apart from F4/80+ macrophages and have observed that the CD45+ splenic population depicts increased bacterial loads like that of the total splenic population within the SIRT1/3 inhibited cohorts. However, CD45+ monocytes and Ly6C positive splenic population exhibit compromised burden within the SIRT1/3 inhibited cohorts. Moreover, the CD1c+ population, CD45+ granulocytes, or lymphocytes show comparable organ loads to that of the vehicle control or SIRT1 activator-treated mice group (Fig.8M-S, Fig.S8). Overall, our data suggest heterogeneous bacterial burden in diverse splenic populations.

> ***Reviewer #3 (Recommendations For The Authors):***
>
> *Abstract*
>
> *The authors state that perturbing Sirt1 and Sirt3 results in a shift in Salmonella's metabolism. On the contrary, the data reflects the metabolism in the host cell and not the bacteria. This statement is wrong. They only show increased expression of some of the glycolytic genes in Salmonella, which is not sufficient to make the claim that the switch to fatty acid oxidation in macrophages is due to utilisation of glucose by the bacteria.*

We value the reviewer's response and have accordingly reframed our sentence in the abstract (Line 24-25).

> *Fig 1: Expression of Sirt1 - The data needs to be supported with a western blot for Sirt1 and Sirt3 but the Western blots shown in the supplementary figure are of very poor quality and do not support the authors' claim.*

We have repeated the western blot and have supplemented the previous blot with an alternate blot in Fig. S1A as per your precious input.

> *Why haven't the authors shown any representative blots for Sirt1 and Sirt3 upon infection with Salmonella mutants? They need to italicize the genes when they describe mRNA expression.*

Previously we had only performed transcript-level expression of *Sirt1* and *Sirt3* upon infection with *Salmonella* mutants and therefore representative blot image was absent. The gene names have been duly italicized while describing mRNA expression (Line 126-154). We regret the inconvenience caused. We have performed the western blotting to assess the protein expression profile upon infection with *Salmonella* mutants as per the reviewer's suggestion and the representative blot image has been duly appended in the revised manuscript (Fig. S1B).

> *What is the rationale for examining Sirt1 and Sirt3 mRNA in M1 and M2 macrophages? Salmonella infection on its own will polarise the macrophages towards M1. How long were these macrophages infected? The time points are missing.*

The rationale behind the examination of Sirt1 and Sirt3 mRNA in M1 and M2 polarized was to ascertain whether indeed M1 polarized macrophages exhibit decreased expression of Sirt1 or Sirt3 and polarization of macrophages toward M2 state show upregulation of Sirt1 and Sirt3 upon *Salmonella* infection. After confirming these above-mentioned findings through this preliminary experiment, we then hypothesized whether *Salmonella* infection on its own will polarise the macrophages toward an immunosuppressive M2 state at a later time course of infection as infection drives the induction of SIRT expression and whether this is mediated by Sirt1 and Sirt3 (Fig. 3). We are extremely apologetic for not mentioning the 16h time-point in the figure and the missing time point has been duly documented in the revised manuscript (Line 155).

> *Fig S2 knockdown of Sirt1 and Sirt3 are not convincing.*

We are extremely sorry for the inconclusive knockdown blot. An alternative blot has been substantiated in the revised manuscript (Fig. S2,C-D).

> *Fig 2A and 2B the time point post infection has not been mentioned. Although it is stated that 2h and 16h post-infection samples were analysed. Only one time point has been shown.*

We are sorry for the confusion. We wanted to clarify that Fig.2A and Fig. 2B show the fold proliferation where fold proliferation was calculated as CFU at 16hr divided by CFU at 2hr as mentioned in the materials and methods section under the heading of Intracellular proliferation or gentamicin protection assay.

Fold Proliferation= [CFU at 16h]/[CFU at 2h]

> *The cytokines data are intriguing in that the increase in IL-6 relative to control is seen only at 2h and 20h but not at 6h. Il-6 at 20h in untransfected cells is comparable to uninfected cells. Did the authors investigate cell death? Salmonella induces various forms of cell death which could account for the decreased cytokine production at later time points.*

We have investigated the cell death upon *Salmonella* infection via MTT assay. At later time points of infection, we indeed observed around 16 percent decrease in cell survival compared to the initial time point of 2h. The results have been appended here and it supports our eminent reviewer's reasoning for the decreased cytokine production at later time points.

Author response image 2.

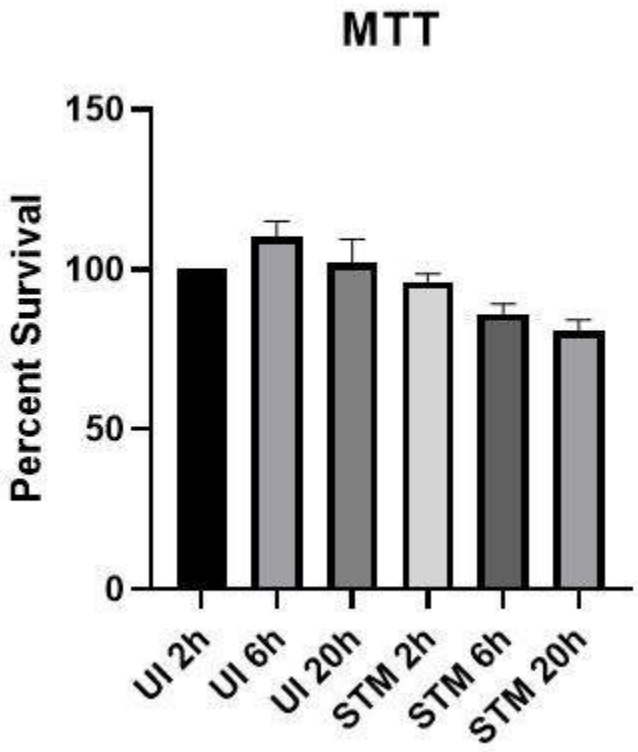

> *Additional cytokines such as IL-1b would be helpful. Also, not sure how uninfected macrophages produce nearly 200pg of IL-10.*

As per the author's critical suggestion, we have assessed the IL-1b cytokine production at 16h post-infection in RAW264.7 macrophages and peritoneal macrophages and mice serum samples at 5th day post-infection (Fig.S3C, S3E-F). Our results indicate increased production of IL-b in the infected SIRT1/3 knockdown RAW264.7 macrophages, SIRT1/3 inhibitor-treated peritoneal macrophages and in mice serum samples under SIRT1/3 inhibitor treatment in comparison to the vehicle control. Additionally, we have quantified IL-1b in mice ileal tissues under SIRT1/3 inhibitor treatment (Fig.S3G) and have obtained heightened intestinal IL-1b production in the inhibitor-treated cohorts. We thank the reviewer for raising the concern for 200pg of IL-10 in the uninfected macrophages. We have repeated the experiment and have provided an alternative representative graph for the experiment wherein the IL-10 levels in the uninfected cohorts range between 20-40pg/ml (Fig. S3B).

> *It is surprising that the authors have found increased Sirt1 binding to NFkB, however there is no change in acetylated NFkB upon infection (Fig 4B). Acetylated p65 is equally high in uninfected Scrambled siRNA, UI shSirt1, STM Scr, and STM shSirt1. Furthermore, increased binding of Sirt1 with NFkb would mean decreased acetylation hence decreased inflammation. However, Salmonella induces profound inflammation.*

We thank the reviewers for their insightful and critical questioning. We truly acknowledge that due to oversaturation there was no apparent change in the acetylated p65 among the different sample sets. Therefore, in the revised manuscript we have provided an image at lower exposure where the changes in the acetylation of the p65 subunit are apparent.

Salmonella induces inflammation upon challenge similar to any other pathogens and induces acute inflammatory responses. This heightened acute inflammation at the initial phases of infection subsides at a later phase of infection. Here, we have performed the Sirt1 interaction with NFκB at 16hr post-infection where increased binding of Sirt1 with NFκB facilitates the resolution of the _Salmonella-_induced acute inflammation. This is in line with previous reports that suggest SIRT1 suppresses acute inflammation through the promotion of p65 acetylation and inhibition of NFκB activity. (Yang H, Zhang W, Pan H, et al. SIRT1 activators suppress inflammatory responses through promotion of p65 deacetylation and inhibition of NF-κB activity. *PLoS One*. 2012;7(9):e46364. doi:10.1371/journal.pone.0046364, Liu TF, Yoza BK, El Gazzar M, Vachharajani VT, McCall CE. NAD+-dependent SIRT1 deacetylase participates in epigenetic reprogramming during endotoxin tolerance. J Biol Chem. 2011;286(11):9856–64., Liu TF, Vachharajani V, Millet P, Bharadwaj MS, Molina AJ, McCall CE. Sequential actions of SIRT1-RELB-SIRT3 coordinate nuclear-mitochondrial communication during immunometabolic adaptation to acute inflammation and sepsis. J Biol Chem. 2015;290(1):396–408.)

> *Please explain how the acetylated p65 was analysed.*

Total endogenous p65 subunit was immunoprecipitated using Anti-NFκB p65 antibody and the immunoprecipitated fraction was probed with Anti-Acetylated Lysine antibody to assess acetylated p65.

> *An increase in ROS production is seen in a relatively small percentage of cells- not more than 4% of cells. How does this contribute to such a significant difference in intracellular bacterial burden? Also, it is not clear how the authors calculated the fold change in proliferation. It is better to show the actual bacterial burden logarithmically.*

We strongly agree with the reviewer's concerns, and we have reanalyzed the flow cytometric data set. The revised data have been presented in Fig. S5 which shows a considerable increase in DCFDA positive population. For instance, the infected scrambled control shows around 2.44% of ROS-producing cells, however knockdown of SIRT1 and SIRT3 increases the ROS-producing cells to 27.34% and 28.64% respectively.

Fold proliferation was calculated as CFU at 16hr divided by CFU at 2hr as mentioned in the materials and methods section under the heading of Intracellular proliferation or gentamicin protection assay. Fold proliferation has been calculated as opposed to absolute CFU values to nullify the differential phagocytosis of bacteria to the macrophages among the samples.

Fold Proliferation= [CFU at 16h]/[CFU at 2h]

> *An increase in metabolic genes is not sufficient to show that the macrophages are metabolically reprogrammed.*

We thank the reviewer for the valuable comment. We agree that an increase in metabolic gene profile is not sufficient to claim metabolic reprogramming. Therefore, in addition to the metabolic gene profile, we have estimated lactate production (end-product of glycolysis) as an indicator of glycolysis (Fig. 5 C-E) and have performed the fatty acid β oxidation activity (Fig. 5G-H) to support our claims.

> *Figure 5F the band intensities do not visually match the bands shown for PFK. For instance, shSIRT1 STM (1.00) and shSIRT3 STM (0.81).*

We are extremely sorry for the erroneous band intensity for shSIRT3. Upon reanalysis of the band intensities, we have corrected the band intensity for shSIRT3 to 2.28 (Fig.5F).

> *It is surprising that HADHA is not expressed in uninfected samples.*

We are extremely apologetic for the inappropriate representative blot. We feel that the discrepancy might have arisen due to the usage of old antibodies. We have provided an alternate blot for the HADHA gene where fresh antibody staining solution was used for probing which shows expression even in the uninfected samples (Fig.5F).

> *Figure 6A - What is the significance of PFA fixed samples (PI) compared to SI samples? This has not been discussed.*

PFA-fixed samples are paraformaldehyde-treated bacterial samples that harbor the immune signals or Pattern Associated Molecular Patterns (PAMPs). The rationale for using PI in addition to SI samples was to show whether the phenomena is driven by live metabolically active pathogens or is mediated by PAMPs.

> *I understand that the hypothesis is that during the later phase of infection, there is an increase in fatty acid oxidation which correlates with a decrease in inflammation. However, at 6h there is no increase in genes regulating fatty acid oxidation. Why did the authors choose 6h when the previous experiments have been done at 16h?*

We indeed agree with the reviewer's understanding of our hypothesis that there is an increase in fatty acid oxidation along the progression of infection which correlates with a decrease in inflammation. The *Salmonella* intracellular replication has been reported to commence at 6h post-internalization when SPI-2 effector expression is fully established (Helaine S, Thompson JA, Watson KG, Liu M, Boyle C, Holden DW. Dynamics of intracellular bacterial replication at the single cell level. *Proc Natl Acad Sci U S A*. 2010;107(8):3746-3751. doi:10.1073/pnas.1000041107). Therefore, we have assessed the 6h timepoint post-infection in addition to the initial and later timepoints of 2h and 16h respectively. Additionally, the nanostring gene profiling data of both host and bacterial genes indicate the onset of both metabolic (Fig. 5A, 6A) and immune genes (Fig. 3A) modulation at 6h post-infection. We have validated these results via qPCR studies and have observed an upregulation in the transcript level of fatty acid oxidation genes as depicted in Fig. S7A in RAW264.7 macrophages.

> *Line 355 it is mentioned that Sirt1 and Sirt3 abrogate metabolic shift by reducing glycolytic flux. This is incorrect as experiments such as carbon chase assays have not been performed to investigate glycolytic flux.*

As per the reviewer's valuable suggestion, we have removed the word 'flux' from the above-mentioned statement(Line 351, Line 353).

> *Lines 392-393: "We immunoprecipitated PDHA1 and checked for its interaction with SIRT3 or SIRT1 under knockdown condition of SIRT3 or upon SIRT3 inhibitor treatment (Fig.7 G-H)"*
>
> *What is the rationale for checking PDHA1 interaction with Sirt under Sirt knockdown conditions?*

We are thankful to the reviewer for the critical comments. The rationale for checking PDHA1 interaction with Sirt was to ascertain that indeed Sirt interacted with PDHA1 under *S.* Typhimurium infection and abrogation of either protein expression (knockdown) or their enzymatic activity (inhibitor treatment) diminished the interaction.

> *Moreover, the blots are very confusing and do not represent the authors' claims.*

> *(1) In the input blot I do not see Sirt3 depletion in shSirt3 knockdown sample.*

The knockdown has been quantified in the input blot as per your suggestion. A knockdown of 40% has been obtained in the uninfected dataset whereas a knockdown of 47.1% has been obtained in the infected data set at 16h post-infection (Fig.7H).

> *(2) Why does Sirt1 interact with PDHA1 similar to Sirt3. Do both the proteins bind to PDHA1 at the same time/ competitively? If so do they both deacetylate?*

In literature, Sirt3 has been shown to interact with PDHA1 and deacetylate PDHA1. However, the interaction of Sirt1 with PDHA1 has not been reported previously and therefore we are unable to comment on the exact dynamics of the interaction. Future studies need to be performed to explore these phenomena in depth. However, SIRT1 agonist SRT1720 has been shown to impact PDH phosphorylation and its activity (Han Y, Sun W, Ren D, Zhang J, He Z, Fedorova J, Sun X, Han F, Li J. SIRT1 agonism modulates cardiac NLRP3 inflammasome through pyruvate dehydrogenase during ischemia and reperfusion. Redox Biol. 2020 Jul;34:101538).

> *(3) Figure 7I in the IP: IgG samples Sirt3 seem to bind to IgG non-specifically, which questions the specificity of Sirt3 binding to PDHA1.*

We appreciate the reviewer for pointing out this concern. The immunoprecipitation experiment has been repeated and the same has been appended in the revised manuscript and we observe no non-specific binding of Sirt3 antibody to IgG.

> *(4) In Figure 7I all the bands Ac PDHA1, PDHA1, and Sirt3 look similar with double bands, which has not been seen in other blots. How is this possible?*
>
> *This cannot explain the increase in beta-oxidation observed.*

We thank the reviewer for raising this concern. We have repeated the experiment and provided the alternative blot as per the reviewer's suggestion.

The rationale for performing this experiment was to show that SIRT plays an important role in the activation of downstream TCA cycle pathways via PDHA1 deacetylation during *Salmonella* infection. The deacetylation of PDHA1 has been previously reported to cause transcriptional activation of the downstream TCA cycle and oxidative phosphorylation (Zhang Y, Wen P, Luo J, et al., Cell Death Dis.,2021). Additionally, PDHA1 hyperacetylation has been reported to cause lactate overproduction (An, S., Yao, Y., Hu, H. *et al.* PDHA1 hyperacetylation-mediated lactate overproduction promotes sepsis-induced acute kidney injury via Fis1 lactylation. *Cell Death Dis* 14, 457 (2023)). In our study, increased lactate production and PDHA1 hyperacetylation have been observed during SIRT3 inhibition conditions upon *Salmonella* infection.

https://doi.org/10.7554/eLife.93125.2.sa0

THE JOURNAL OF INFECTIOUS DISEASES

MAJOR ARTICLE

Functional ompa of *Salmonella* Typhimurium provides protection from lysosomal degradation and inhibits autophagic processes in macrophages

Atish Roy Chowdhury[1#], Dipasree Hajra[1#], Debapriya Mukherjee[1#], Abhilash Vijay Nair[1], and Dipshikha Chakravortty[1, 2,*]

[1]Department of Microbiology and Cell Biology, Indian Institute of Science, Bangalore, Karnataka, India-560012; [2]School of Biology, Indian Institute of Science Education and Research, Thiruvananthapuram, Kerala 695551, India

Our previous study showed that OmpA-deficient *Salmonella* Typhimurium (STM) failed to retain LAMP-1, quit *Salmonella*-containing vacuole (SCV) and escaped to the host cytosol. Here we show that the cytosolic population of STM *ΔompA* sequestered autophagic markers, syntaxin17 and LC3B in a *sseL*-dependent manner and initiated lysosomal fusion. Moreover, inhibition of autophagy using bafilomycinA1 restored its intracellular proliferation. Ectopic overexpression of OmpA in STM *ΔsifA* restored its vacuolar niche and increased interaction of LAMP-1, suggesting a *sifA*-independent role of OmpA in maintaining an intact SCV. The OmpA extracellular loops impaired the LAMP-1 recruitment to SCV and caused bacterial release into the cytosol of macrophages, but unlike STM *ΔompA*, they retained their outer membrane stability and didn't

[*]*Corresponding author*: Dipshikha Chakravortty, Email: dipa@iisc.ac.in, Tel: 0091 80 2293 2842, Fax: 0091 80 2360 2697

#These authors contributed equally

Current address: Department of Microbiology and Cell Biology, Indian Institute of Science, Bangalore, Karnataka, India-560012

DOI: 10.1093/infdis/jiae376

activate the lysosomal degradation pathway aiding in their intra-macrophage survival. Finally, OmpA extracellular loop mutations protected the cytosolic STM Δ*sifA* from the lysosomal surveillance, revealing a unique OmpA-dependent strategy of STM for its intracellular survival.

Keywords: *Salmonella*-containing vacuole (SCV), outer membrane protein A (OmpA), OmpA extracellular loops, syntaxin 17, LC3B, lysosomes, LAMP-1, EEA-1

INTRODUCTION

Salmonella Typhimurium (STM) causes self-limiting diarrhea and gastroenteritis, seriously threatening human health worldwide [1-3]. The Global Burden of Diseases, Injuries, and Risk Factors Study (GBD) estimated 5,35,000 cases of invasive non-typhoidal *Salmonella* infection worldwide, with approximately 77500 deaths in 2017 [4, 5]. After entering the host cells, *Salmonella* Typhimurium resides within a modified membrane-bound acidic compartment called *Salmonella*-containing vacuole (SCV) [6, 7]. The successful intracellular proliferation of the bacteria depends upon the formation and maintenance of an intact SCV within the host cells [8]. The disruption of SCV and subsequent release of the bacteria into the cytosol of macrophages abrogates its proliferation [9]. In contrast, the cytosol of the epithelial cells promotes bacterial proliferation [10]. The SPI-1 and SPI-2 encoded virulent effectors, together with host proteins maintain the stability of SCV [11, 12].

Outer membrane protein A (OmpA) is a barrel-shaped porin protein found on the outer membrane of STM that protects itself from oxidative and nitrosative stress [13, 14]. The deficiency of OmpA makes the bacteria susceptible to the β-lactam antibiotics and hampers its ability to form a biofilm [15, 16]. A previous study from our group showed that deleting *ompA* reduced the expression of SPI-2 effector *sifA* in STM and compromised its intravacuolar inhabitation. The OmpA-deficient STM showed impaired pH and redox homeostasis and could not cause systemic infection [14]. However, the SPI-2 independent role of OmpA in maintaining the stability of SCV has been poorly understood.

In the current study, we established a *sifA*-independent additional role of OmpA in maintaining the stability of SCV. Expressing OmpA in STM *ΔsifA* restored its vacuolar niche and improved its intracellular survival. The introduction of mutations in the extracellular loops of OmpA completely abolished the recruitment of LAMP-1 to the SCV and facilitated bacterial escape into macrophage cytosol. Unlike the OmpA-deficient STM, the loop mutants retained their outer membrane stability, pH homeostasis, and *sifA* expression. This cytosolic pool of the OmpA loop mutants aggravated the accumulation of autophagic adaptor proteins such as LC3B and p62/SQSTM in the infected cells. But quite surprisingly, they escaped lysosomal surveillance and successfully survived in the cytosol of macrophages. Moreover, the escape of STM *ΔsifA* expressing wild-type and extracellular loop mutants of OmpA from the host lysosomal degradation pathway strongly highlighted a novel role of OmpA used by STM for its intracellular proliferation.

MATERIALS AND METHODS

Bacterial strains, eukaryotic cell lines, media, and culture conditions

The bacterial strains were revived from the glycerol stock (stored at -80^{0}C) and plated on LB agar with or without appropriate antibiotics **(Table-S1)**. Dead bacteria were produced by treating the wild-type bacteria with 3.5% paraformaldehyde for 30 minutes. The RAW264.7 cells were maintained in DMEM supplemented with 10% FCS at 37^{0}C temperature in the presence of 5% CO_2. U937 cells were maintained in RPMI 1640 media supplemented with 10% FCS. The U937 cells were treated with phorbol myristate acetate (PMA) (20 ng/ mL) for 24 hours at 37^{0}C temperature in the presence of 5% CO_2, followed by supplementation with fresh RPMI (10% FCS) media and further incubated for 24 hours before infection.

Additional information related to **'Materials and Methods'** has been incorporated in the Supplementary Materials.

RESULTS

The cytosolic population of STM *δompa* activates host autophagy machinery during the late phase of infection in macrophages.

STM (WT) recruits focal adhesion kinase (FAK) on the surface of the intact SCV in a SPI-2 T3SS (T3SS2)-dependent manner, which can suppress the host autophagy machinery by activating the Akt-mTOR signaling pathway [17]. Earlier, we showed that intracellular STM *ΔompA* that forms a malfunctioning T3SS2 and quits the SCV during the late phase of infection is cured from macrophages by nitrosative stress [14]. Hence, we hypothesized that *ompA*-deficient STM can activate the host autophagy machinery. The reduced percent colocalization of STM *ΔompA* with LAMP-1 validated our previous findings **(Figure 1A).** The activation of host autophagy was confirmed by studying the recruitment of autophagy markers, syntaxin 17 **(Figure 1A)** and LC3B **(Figure S1A)** [18-21], on the intracellular STM. The co-staining of LAMP-1 and syntaxin 17 in infected macrophages (**Figure 1A**) showed that the wild-type STM residing inside the SCV (**Figure 1A.1**) could restrict the recruitment of syntaxin 17 (**Figure 1A.3 and 1A.5**). On the contrary STM *ΔompA*, that rarely colocalizes with LAMP-1 (**Figure 1A.2**) profoundly sequestered syntaxin 17 (**Figure 1A.4 and 1A.6**). Altogether, we concluded the formation of syntaxin 17$^+$ LC3B$^+$ autophagosome around the *ompA* deficient bacteria in the cytosol of macrophages. We further observed that the intracellular proliferation of STM *ΔompA* was attenuated compared to STM (WT) in macrophages, which was recovered upon bafilomycin A1 [22] treatment **(Figure 1B)**. In the presence of bafilomycin A1, the reduced recruitment of syntaxin 17 and LC3B around STM *ΔompA* strongly demonstrated the role of autophagy in clearing STM *ΔompA* from macrophages **(Figure S1B and S1C)**. Wild-type STM uses SPI-2 effector SseL for protection from autophagy [23]. In our study, STM *ΔompA*, *ΔsseL*, and *ΔompAΔsseL* showed significant defects

in replication compared to the wild-type bacteria in macrophages **(Figure 1C)**. The comparable intracellular proliferation of STM *ΔompA*, *ΔsseL*, and *ΔompAΔsseL* suggested that the induction of autophagy by STM *ΔompA* occurs in a *sseL*-dependent manner. To determine whether the autophagy machinery could target the mutant bacteria to the lysosomes, we studied the activation and subsequent fusion of the lysosomes with wild-type and *ompA*-deficient STM. Unlike STM (WT), the enhanced co-localization of STM *ΔompA* with the lysosomes (labeled with Texas red ovalbumin) suggested a heightened lysosomal activity of infected macrophages (**Figure 1D**). *Listeria monocytogenes* uses listeriolysin O (LLO) to degrade phagosomal compartments and escape lysosomal fusion [24]. Expressing LLO in wild-type STM releases the bacteria from the SCV into the cytosol of the host cells [14]. The reduced fusion of lysosomes with STM (WT): *LLO*, strongly suggested that the targeting of STM *ΔompA* to the lysosomes is particularly due to the absence of OmpA and not because of its cytosolic localization (**Figure 1D**). Moreover, compared to the wild-type STM (**Figure 1E.1, 1E.3, and 1E.5**), the higher co-localization of STM *ΔompA* with syntaxin 17 (**Figure 1E.2**) and lysosomes (**Figure 1E.4 and 1E.6**) proved that the activation of autophagy directs the mutant bacteria to the lysosomal degradation. This observation was further supported by measuring the enhanced activity of lysosomal enzymes upon STM *ΔompA* infection [25, 26]. The higher acid phosphatase activity of STM *ΔompA*-infected macrophages compared to the wild-type and *ompA*-complemented strains strongly suggested the presence of functionally active lysosomes (**Figure S2A**). Altogether, our data revealed that during the late phase of infection in macrophages, STM *ΔompA* reaches the cytosol and activates host autophagy machinery. As a result, the mutant bacteria trapped inside syntaxin 17^+, $LC3B^+$ autophagosome is targeted to the lysosomes, facilitating their clearance from the macrophages.

STM *δompa* escapes the SCV during the immediate early stage of infection in macrophages.

To determine the LAMP-1 recruitment dynamics around the SCV, RAW264.7, and U937 cells were infected with wild-type, OmpA-mutant, and complemented strains of STM, and the vacuolar niche of the pathogen was investigated at 2- and 6-hours post-infection. Compared to the wild-type and complemented strains, the reduced co-localization of STM *ΔompA* with LAMP-1 at 2- and 6 hours post-infection in RAW 264.7 cells (**Figure S3A and S3B**) indicated that the knockout bacteria quit the SCV and come to the cytosol even before the early stage of infection. To inspect whether this phenotype is cell type-specific, the SCV niche of bacteria was investigated in U937 cells. In accordance with our previous observation, we observed that compared to STM (WT), STM *ΔompA* has a higher propensity to escape the SCV before the early stage of infection (**Figure S4A – S4C**). The formation of SCV is a dynamic process, requiring the recruitments of EEA-1, Rab5, and transferrin receptors, which are replaced by late endosome membrane markers like-LAMP-1/2/3, Rab7, and V-ATPase during the later stage of infection [8, 27]. Compared to STM (WT), the higher recruitment of EEA-1 around STM *ΔompA* at 15 minutes post-infection in U937 cells (**Figure 2A**) suggested that both the bacteria reside within the $EEA\text{-}1^+$ vacuoles during the immediate early stage of infection. Simultaneously, the co-localization of wild-type and mutant

bacteria with LAMP-1 was studied at 15-, 30-, and 120 minutes post-infection in macrophages (**Figure 2B and 2C**). At 15- and 30-minutes post-infection, STM *ΔompA* recruited more LAMP-1 compared to STM (WT) in U937 (**Figure 2B**) and RAW264.7 (**Figure 2C**) cells. However, with an increase in time (at 120 minutes post-infection), the wild-type STM acquired more LAMP-1 than the *ompA*-deficient bacteria in both cells (**Figure 2B and 2C**). The inability of STM *ΔompA* to retain the acquired LAMP-1 suggested an interruption in the SCV maturation. Overall, our findings revealed that STM *ΔompA* quits the SCV at the immediate early stage of infection in macrophages.

Salmonella Typhimurium utilizes ompa to interact with host LAMP-1 (SCV) during infection in macrophages.

Earlier, we have seen that in the absence of OmpA, STM could not retain LAMP-1 and eventually quit the SCV. Hence, we hypothesized a probable direct interaction between OmpA and LAMP-1, which could stabilize the SCV. To show the interaction between STM OmpA and host LAMP-1, macrophages infected with wild-type STM were co-stained with anti-STM-OmpA and host-LAMP-1 specific antibodies. The co-localization of STM-OmpA with mouse-LAMP-1 at 2- and 6 hours post-infection suggested a stable interaction between these two proteins in RAW264.7 cells (**Figure 3A**). This interaction increased at 16 hours after infection (**Figure 3A**). We also found that the interaction of STM-OmpA with LAMP-1 significantly increased with time in activated U937 cells (**Figure S5B**). To support this observation, *Salmonella* Typhimurium OmpA was immunoprecipitated from infected RAW264.7 cells at 2-, 6-, and 16 hours post-infection and probed for LAMP-1 to determine their probable association **(Figure 3B)**. Consistent with our previous findings, the co-immunoprecipitation experiment established a stable interaction between STM-OmpA and mouse LAMP-1 at 6- and 16-hour post-infection **(Figure 3B)**. Studies showed that deleting SPI-2 effector SifA impairs the vacuolar niche of STM in host cells [9]. To determine the SPI-2 dependence of OmpA in maintaining the integrity of SCV, we infected RAW264.7 cells with STM (WT), *ΔompA*, *ΔsifA*, and *ΔsifA*:*ompA*. Co-immunoprecipitation study showed that in *sifA*-deficient STM, OmpA does interact with LAMP-1, while the overexpression of OmpA in *sifA*-deficient STM enhanced its interaction with LAMP-1 **(Figure 3C)**. In immunofluorescence imaging, it was found that unlike STM (WT), the OmpA-deficient *Salmonella* Typhimurium rarely colocalizes with LAMP-1, which confirmed their cytosolic localization **(Figure 3D)**. In addition, we observed reduced recruitment of LAMP-1 around STM *ΔsifA* compared to STM (WT), indicating their impaired vacuolar life within the macrophages **(Figure 3D)**. However, the increased colocalization of STM *ΔsifA*:*ompA* with LAMP-1 strongly suggested an improvement in the vacuolar localization of STM *ΔsifA* upon overexpression of OmpA **(Figure 3D)**. In addition, we found that STM *ΔsifA*:*ompA* proliferates better than *ΔsifA* in macrophages **(Figure 3E),** suggesting a *sifA*-independent role of OmpA in maintaining the stability of SCV by bridging the interaction between the bacteria and LAMP-1.

Introducing mutation in the extracellular loops does not alter the function of ompa in *Salmonella* Typhimurium.

OmpA is embedded into the outer membrane of STM with the help of its cylindrical structure consisting of eight anti-parallel β-sheets connected with four periplasmic turns and four extracellular loops (**Figure 4A**). We hypothesized that bacteria use these extracellular loops to interact with LAMP-1 while staying within the SCV. We compared the STM OmpA extracellular loop sequences with pathogenic *Escherichia coli* K1 (**Figure 4A**) [28, 29]. Without hampering the structure of OmpA, the conserved and unique domains of the loops were altered by site-directed mutagenesis (**Figure 4A**), and six different variants (such as L1-1, L1-2, L2-1, L2-2, L3-1, L4-1) were generated. Functionally active OmpA regulates the permeability of the bacterial outer membrane [13, 14]. The proper folding and functional characterization of OmpA with mutations in the extracellular loops were tested by measuring the outer membrane permeability of STM (WT), *ΔompA*, *ΔompA*: pQE60-*ompA*, *ΔompA*: pQE60-*ompA*-L1-1, *ΔompA*: pQE60-*ompA*-L1-2, *ΔompA*: pQE60-*ompA*-L2-1, *ΔompA*: pQE60-*ompA*-L2-2, *ΔompA*: pQE60-*ompA*-L3-1 and *ΔompA*: pQE60-*ompA*-L4-1 by $DiBAC_4$ staining (**Figure 4B**). Outer membrane porins can regulate the pH homeostasis in bacteria [30, 31]. We incubated the bacterial strains in phosphate buffer (pH=5) and stained them with an acidotropic dye BCECF-AM. The higher 488/405 ratio corresponding to STM *ΔompA* suggested an interruption in the pH sensing ability of STM in the absence of OmpA, which validated our previous study [14] **(Figure 4C)**. Here, we observe lower 488/405 values for the OmpA-loop mutants. This suggested an uninterrupted pH sensing ability of the bacteria due to the retained functionality of loop mutant variants **(Figure 4C)**. The expression of SPI-2 effector *sifA* requires the acidification of the bacterial cytosol [32]. Unlike STM *ΔompA*, the unaltered expression of *sifA* in the OmpA loop mutants growing in SPI-2-inducing acidic F media proved the proper pH sensing abilities of these mutants **(Figure 4D)**. Altogether, this led us to conclude that introducing mutations in the extracellular loops of OmpA does not alter their canonical function in STM.

Mutation in the extracellular loops of ompa releases the bacteria into the cytosol of macrophages but is insufficient for lysosomal activation.

To decipher the role of the extracellular loops in the intracellular pathogenesis of STM, the OmpA-loop mutants were used for infecting macrophages. Unlike the wild-type and complemented strains, the reduced co-localization of OmpA-loop mutants with LAMP-1 suggested their escape from the SCV at 6 hours post-infection **(Figure S6A)** and their localization in the cytosol until 16 hours of infection in macrophages (**Figure 5A**). The enhanced cytosolic localization of the loop mutants was further confirmed by chloroquine resistance assay (**Figure 5B**). Like STM *ΔompA*, the higher cytosolic abundance of the OmpA loop mutants suggested that the extracellular loops of OmpA execute an essential function in maintaining the stability of the SCV by retaining the LAMP-1 pool **(Figure 5B)**. We further pulled down the OmpA loop mutants from the infected macrophages and probed for LAMP-1 to show the direct interaction of the OmpA extracellular loops with LAMP-1 **(Figure S6B)**. Unlike the wild-type strain, immunoprecipitation of the

OmpA-loop mutants did not show a considerable interaction with LAMP-1 **(Figure S6B)**. The disruption of SCV by OmpA-loop mutants was further confirmed by the induction of autophagy (P62/ SQSTM1 and LC3B) in the infected macrophages **(Figure S6C)**. However, unlike STM *ΔompA*, the reduced co-localization of the OmpA-loop mutants with lysosomes (Texas red) suggested that the autophagy adaptor proteins are insufficient to target them to the lysosomal degradation pathway **(Figure 5C)**. Even after harboring mutations in the externally exposed loops, the stable outer membrane in these mutants could be responsible for their escape from host lysosomal fusion. To ascertain that this de-novo anti-lysosomal function of OmpA is independent of *sifA*, we expressed the wild-type and multiple loop mutants of OmpA in *ompA* and *sifA* double-negative bacteria. Compared to the single knockouts of *ompA* and *sifA*, the greater colocalization of STM *ΔompAΔsifA* with Texas red showed a SPI-2 independent anti-lysosomal function of OmpA **(Figure 5D)**. However, the loss of Texas red signal from the surroundings of STM *ΔsifA* expressing wild-type and loop mutants of OmpA revealed a protective role of OmpA against the lysosomal degradation pathway **(Figure 5D)**. Consistent with this observation, we found that the mutations in the extracellular loops of OmpA did not hamper the intracellular proliferation of the bacteria **(Figure 5E)**. All the loop mutants survived better than STM *ΔompA* while staying in the cytosol of macrophages (**Figure 5E**). Altogether, we concluded that despite the induction of autophagy, the presence of OmpA in the bacterial outer membrane protects the cytosolic population of STM from lysosomal degradation and provides them with fitness benefits for intracellular proliferation.

DISCUSSION

While infecting the host cell, *Salmonella* Typhimurium stays inside a modified vesicle called SCV [33-35]. The low pH of the SCV upregulates the expression of SPI-2 genes [36, 37]. With the help of SPI-2 encoded T3SS (T3SS2) and virulent factors, STM inhibits phagolysosomal maturation and suppresses lysosomal biogenesis [26, 38]. The formation of SCV is a dynamic and complex process that employs a wide array of host and bacterial proteins [33, 39]. STM majorly uses SPI-1 and SPI-2 encoded virulent factors to regulate the biogenesis and maintain the stability of SCV [12, 38, 40-42]. Introducing point mutation in host Rab7 or deleting *sifA* from STM, led to the bacterial escape into the host cytosol from SCV [10, 43]. On the contrary, the deletion of *sseJ* in the *sifA* null background restored the vacuolar niche of STM [44].

STM lacking an active T3SS2 can damage the SCV and activate host autophagy machinery [17, 45]. In line with these findings, we observed that the cytosolic population of STM *ΔompA* colocalizes more with autophagy markers syntaxin 17 and LC3B. STM uses T3SS2-encoded deubiquitinase SseL to escape host autophagy machinery [23]. The comparable attenuated intracellular proliferation of STM *ΔompA*, *ΔsseL*, and *ΔompAΔsseL* suggested that the induction of autophagy by STM *ΔompA* happens in a *sseL*-dependent manner. The autophagy machinery targeted the cytosolic STM *ΔompA* to the lysosomes. However, the reduced co-localization of

STM (WT): *LLO* (residing in the cytosol with intact OmpA on its outer membrane) with lysosomes indicated a previously undiscussed role of OmpA in protecting the cytosolic STM from being targeted to the host lysosomes.

Our study revealed that, unlike wild-type bacteria, STM *ΔompA* could not retain the acquired LAMP-1 pool and gradually escape from the SCV during infection. In addition, the lack of difference in recruiting EEA1 between wild-type and *ompA* mutants suggests that without altering the biogenesis of SCV, the absence of OmpA in STM only hampers the integrity of the SCV membrane by restricting the recruitment of LAMP-1. The co-immunoprecipitation and confocal imaging showed that the interaction of *Salmonella* Typhimurium OmpA with host LAMP-1 was stable during the early and middle stages of infection and further increased during the later stage. The ectopic expression of OmpA in the *sifA* null background restored its vacuolar niche and intracellular survival. This strongly proved an additional *sifA*-independent role of OmpA in maintaining the SCV stability by directly interacting with host LAMP-1.

We assumed that the externally exposed extracellular loops of OmpA maintain the stability of SCV by directly interacting with host LAMP-1. The unique and conserved sequences of the extracellular loops of STM OmpA were replaced with nonpolar amino acids by site-directed mutagenesis. We observed that altering the loops of OmpA did not confer any change in its ability to maintain the outer membrane stability of bacteria when transformed into STM *ΔompA*. Moreover, the impaired pH homeostasis of STM *ΔompA* was recovered in the OmpA-loop mutants. We observed that each of these individual loops plays a crucial role in bridging the interaction of bacteria with LAMP-1 during infection in murine macrophages. Unlike STM *ΔompA*, even after expressing *sifA* [9], the release of the OmpA-loop mutants into the cytosol of macrophages strongly supported a *sifA*-independent role of OmpA in maintaining the stability of SCV.

Interestingly without being targeted to the lysosomes, the OmpA loop mutants attracted the autophagic adaptor proteins such as LC3B and p62/SQSTM in the cytosol of macrophages. STM uses SPI-2 effector protein SifA to escape lysosomal fusion [42]. Our study revealed that OmpA loop mutants can express *sifA* like wild-type STM. To assess the involvement of *sifA* in OmpA-dependent lysosomal escape, we infected macrophages with *sifA*-deficient bacteria expressing wild-type and different loop mutants of OmpA. Compared to the *ompA* and *sifA* single and double knockout bacterial strains, the lower recruitment of Texas red around STM *ΔompAΔsifA* expressing wild-type and mutated OmpA showed a *sifA*-independent de-novo function of OmpA against host lysosomal surveillance. Even after harbouring mutations in the extracellular loops, the stable function of OmpA in the bacterial outer membrane played a significant role in avoiding lysosomal fusion. This OmpA-dependent subterfuge of lysosomal check-point further rendered the cytosolic pool of bacteria with a specific fitness advantage during their intracellular growth.

Altogether, our study provides an OmpA-dependent novel mechanism used by *Salmonella* Typhimurium to maintain the stability of SCV and escape lysosome-mediated clearance, thereby improving their life inside the host cell. STM uses the extracellular loops of OmpA to bridge the

interaction between host LAMP-1 and the bacterial membrane. Without OmpA, the bacteria fail to retain the LAMP-1 pool on the SCV, and due to disruption of SCV, they enter the cytosol. The cytosolic bacteria lacking OmpA and deficient in SPI-2 effector *sifA* activate the host autophagy machinery, which further leads to the clearance of the bacteria by the lysosomal degradation pathway. However, cytosolic bacteria with intact OmpA (loop mutants) could efficiently bypass the lysosomal fusion in a *sifA*-independent manner **(Figure 6)**.

Abbreviations

STM: *Salmonella* Typhimurium

OmpA: Outer membrane protein A

LC3B: Microtubule-associated protein 1A/ 1B-light chain 3

Stx17: Syntaxin 17

BafA: Bafilomycin A

LLO: Listeriolysin O

SCV: *Salmonella* containing vacuole

T3SS: Type 3 secretion system

LAMP-1: Lysosome-associated membrane protein-1

EEA-1: Early endosome antigen-1

RFP: Red fluorescent protein

GFP: Green fluorescent protein

SifA: *Salmonella*-induced filament A

BCECF-AM: 2',7'-Bis-(2-Carboxyethyl)-5-(and-6)-Carboxyfluorescein

$DiBAC_4$: bis-(1,3-dibutyl barbituric acid)-tri methylene oxonol

Author Contributions: ARC and DC conceived the study and designed the experiments. ARC performed all the experiments, analyzed the data, constructed the figures, and wrote the original manuscript draft. DH performed the western blots, co-immunoprecipitations, and Texas red ovalbumin assay with *sifA* mutants with OmpA variants. DM and AVN performed the experiments with ARC. ARC, DH, DM, and AVN proofread and edited the manuscript. DC supervised the study. All the authors read and approved the manuscript.

Acknowledgments: We sincerely thank the departmental confocal facility, departmental real-time PCR facility, central bioimaging facility, and central flow cytometry facility at IISc. Mr. Puneeth and Ms. Navya from the departmental confocal facility are acknowledged for their assistance in image acquisition. Ms. Leepika and Ms. Sharon from the central flow cytometry facility are duly acknowledged for their help in flow cytometry data acquisition. Dr. Shivjee Sah from Professor Umesh Varshney's lab MCB, IISc, is duly thanked for constructing the *ompA*-pQE60 recombinant plasmid.

Funding: This work was funded by the DAE SRC fellowship (DAE00195) and the DBT-IISc partnership umbrella program for advanced research in biological sciences and Bioengineering. Infrastructure support from ICMR (Centre for Advanced Study in Molecular Medicine), DST (FIST), and UGC is sincerely acknowledged. DC acknowledges the ASTRA Chair professorship grant from IISc and the TATA innovation fellowship grant. ARC sincerely thanks IISc, MHRD, Govt. of India, and the late Dr. Krishna S. Kaikini estate for the Shamrao M. Kaikini and Krishna S. Kaikini scholarship. DH acknowledges CSIR, Govt. of India, for the SPM fellowship. DM and AVN thanks IISc and MHRD, Govt. of India, for the fellowship.

Availability of data and materials: All data generated in this study are within the manuscript and its supporting information files.

Declarations

Ethics statement

Not applicable.

Consent for publication

Not applicable.

Competing interests

The authors declare to have no conflict of interest.

References

1. Galan, J.E., Salmonella Typhimurium and inflammation: a pathogen-centric affair. Nat Rev Microbiol, 2021.
2. Chaudhuri, D., et al., Salmonella Typhimurium Infection Leads to Colonization of the Mouse Brain and Is Not Completely Cured With Antibiotics. Front Microbiol, 2018. **9**: p. 1632.
3. Hariharan, V., et al., phoP maintains the environmental persistence and virulence of pathogenic bacteria in mechanically stressed desiccated droplets. iScience, 2023. **26**(5): p. 106580.
4. Collaborators, G.B.D.N.-T.S.I.D., The global burden of non-typhoidal salmonella invasive disease: a systematic analysis for the Global Burden of Disease Study 2017. Lancet Infect Dis, 2019. **19**(12): p. 1312-1324.

5. Chowdhury, A.R., et al., Defying the odds: Determinants of the antimicrobial response of Salmonella Typhi and their interplay. Mol Microbiol, 2023.
6. Chatterjee, R., et al., From Eberthella typhi to Salmonella Typhi: The Fascinating Journey of the Virulence and Pathogenicity of Salmonella Typhi. ACS Omega, 2023. **8**(29): p. 25674-25697.
7. Chatterjee, R., et al., Salmonella Typhimurium PgtE is an essential arsenal to defend against the host resident antimicrobial peptides. Microbiol Res, 2023. **271**: p. 127351.
8. Meresse, S., et al., The rab7 GTPase controls the maturation of Salmonella typhimurium-containing vacuoles in HeLa cells. EMBO J, 1999. **18**(16): p. 4394-403.
9. Beuzon, C.R., et al., Salmonella maintains the integrity of its intracellular vacuole through the action of SifA. EMBO J, 2000. **19**(13): p. 3235-49.
10. Brumell, J.H., et al., Disruption of the Salmonella-containing vacuole leads to increased replication of Salmonella enterica serovar typhimurium in the cytosol of epithelial cells. Infect Immun, 2002. **70**(6): p. 3264-70.
11. Jackson, L.K., et al., The Salmonella virulence protein SifA is a G protein antagonist. Proc Natl Acad Sci U S A, 2008. **105**(37): p. 14141-6.
12. Bakowski, M.A., et al., The phosphoinositide phosphatase SopB manipulates membrane surface charge and trafficking of the Salmonella-containing vacuole. Cell Host Microbe, 2010. **7**(6): p. 453-62.
13. van der Heijden, J., et al., Salmonella Rapidly Regulates Membrane Permeability To Survive Oxidative Stress. mBio, 2016. **7**(4).
14. Roy Chowdhury, A., et al., Salmonella Typhimurium outer membrane protein A (OmpA) renders protection from nitrosative stress of macrophages by maintaining the stability of bacterial outer membrane. PLoS Pathog, 2022. **18**(8): p. e1010708.
15. Tsai, M.H., et al., Characterization of Salmonella resistance to bile during biofilm formation. J Microbiol Immunol Infect, 2020. **53**(4): p. 518-524.
16. Chowdhury, A.R., et al., Loss of outer membrane protein A (OmpA) impairs the survival of Salmonella Typhimurium by inducing membrane damage in the presence of ceftazidime and meropenem. J Antimicrob Chemother, 2022.
17. Owen, K.A., et al., Activation of focal adhesion kinase by Salmonella suppresses autophagy via an Akt/mTOR signaling pathway and promotes bacterial survival in macrophages. PLoS Pathog, 2014. **10**(6): p. e1004159.
18. Itakura, E., C. Kishi-Itakura, and N. Mizushima, The hairpin-type tail-anchored SNARE syntaxin 17 targets to autophagosomes for fusion with endosomes/lysosomes. Cell, 2012. **151**(6): p. 1256-69.
19. Itakura, E. and N. Mizushima, Syntaxin 17: the autophagosomal SNARE. Autophagy, 2013. **9**(6): p. 917-9.
20. Ren, H., et al., The Autophagosomal SNARE Protein Syntaxin 17 Is an Essential Factor for the Hepatitis C Virus Life Cycle. J Virol, 2016. **90**(13): p. 5989-6000.
21. Miller, C. and J. Celli, Avoidance and Subversion of Eukaryotic Homeostatic Autophagy Mechanisms by Bacterial Pathogens. J Mol Biol, 2016. **428**(17): p. 3387-98.
22. Redmann, M., et al., Inhibition of autophagy with bafilomycin and chloroquine decreases mitochondrial quality and bioenergetic function in primary neurons. Redox Biol, 2017. **11**: p. 73-81.

23. Mesquita, F.S., et al., The Salmonella deubiquitinase SseL inhibits selective autophagy of cytosolic aggregates. PLoS Pathog, 2012. **8**(6): p. e1002743.
24. Ruan, Y., et al., Listeriolysin O Membrane Damaging Activity Involves Arc Formation and Lineaction -- Implication for Listeria monocytogenes Escape from Phagocytic Vacuole. PLoS Pathog, 2016. **12**(4): p. e1005597.
25. Honsi, T.G. and J. Stenersen, Activity and localisation of the lysosomal marker enzymes acid phosphatase, N-acetyl-beta-D-glucosaminidase, and beta-galactosidase in the earthworms Eisenia fetida and E. veneta. Comp Biochem Physiol B Biochem Mol Biol, 2000. **125**(3): p. 429-37.
26. Eswarappa, S.M., et al., Division of the Salmonella-containing vacuole and depletion of acidic lysosomes in Salmonella-infected host cells are novel strategies of Salmonella enterica to avoid lysosomes. Infect Immun, 2010. **78**(1): p. 68-79.
27. Steele-Mortimer, O., et al., Biogenesis of Salmonella typhimurium-containing vacuoles in epithelial cells involves interactions with the early endocytic pathway. Cell Microbiol, 1999. **1**(1): p. 33-49.
28. Maruvada, R. and K.S. Kim, Extracellular loops of the Escherichia coli outer membrane protein A contribute to the pathogenesis of meningitis. J Infect Dis, 2011. **203**(1): p. 131-40.
29. Kim, K.S., Human Meningitis-Associated Escherichia coli. EcoSal Plus, 2016. **7**(1).
30. Sato, M., et al., Expression of outer membrane proteins in Escherichia coli growing at acid pH. Appl Environ Microbiol, 2000. **66**(3): p. 943-7.
31. Bekhit, A., et al., The role of OmpC and OmpF in acidic resistance in Escherichia coli. Biol Pharm Bull, 2011. **34**(3): p. 330-4.
32. Kenney, L.J., The role of acid stress in Salmonella pathogenesis. Curr Opin Microbiol, 2019. **47**: p. 45-51.
33. Steele-Mortimer, O., The Salmonella-containing vacuole: moving with the times. Curr Opin Microbiol, 2008. **11**(1): p. 38-45.
34. Majee, S., et al., Spatiotemporal evaporating droplet dynamics on fomites enhances long term bacterial pathogenesis. Commun Biol, 2021. **4**(1): p. 1173.
35. Hajra, D., et al., Salmonella Typhimurium U32 peptidase, YdcP, promotes bacterial survival by conferring protection against in vitro and in vivo oxidative stress. Microb Pathog, 2022. **173**(Pt B): p. 105862.
36. Yu, X.J., et al., pH sensing by intracellular Salmonella induces effector translocation. Science, 2010. **328**(5981): p. 1040-3.
37. Martin-Orozco, N., et al., Visualization of vacuolar acidification-induced transcription of genes of pathogens inside macrophages. Mol Biol Cell, 2006. **17**(1): p. 498-510.
38. Shotland, Y., H. Kramer, and E.A. Groisman, The Salmonella SpiC protein targets the mammalian Hook3 protein function to alter cellular trafficking. Mol Microbiol, 2003. **49**(6): p. 1565-76.
39. Chandra, K., et al., GH18 family glycoside hydrolase Chitinase A of Salmonella enhances virulence by facilitating invasion and modulating host immune responses. PLoS Pathog, 2022. **18**(4): p. e1010407.
40. Dumont, A., et al., SKIP, the host target of the Salmonella virulence factor SifA, promotes kinesin-1-dependent vacuolar membrane exchanges. Traffic, 2010. **11**(7): p. 899-911.
41. Alberdi, L., et al., Regulation of kinesin-1 activity by the Salmonella enterica effectors PipB2 and SifA. J Cell Sci, 2020. **133**(9).

42. McGourty, K., et al., Salmonella inhibits retrograde trafficking of mannose-6-phosphate receptors and lysosome function. Science, 2012. **338**(6109): p. 963-7.
43. Beuzon, C.R., S.P. Salcedo, and D.W. Holden, Growth and killing of a Salmonella enterica serovar Typhimurium sifA mutant strain in the cytosol of different host cell lines. Microbiology (Reading), 2002. **148**(Pt 9): p. 2705-2715.
44. Ruiz-Albert, J., et al., Complementary activities of SseJ and SifA regulate dynamics of the Salmonella typhimurium vacuolar membrane. Mol Microbiol, 2002. **44**(3): p. 645-61.
45. Birmingham, C.L., et al., Autophagy controls Salmonella infection in response to damage to the Salmonella-containing vacuole. J Biol Chem, 2006. **281**(16): p. 11374-83.

Figure 1. STM *ΔompA* quits the SCV during the late phase of infection in macrophages and activates host autophagy machinery.

(A) Images representing the recruitment of LAMP-1 (SCV marker) and Syntaxin 17 (autophagy marker) around STM (WT): RFP and *ΔompA*: RFP (MOI=20) in RAW264.7 cells at 16 hours post-infection. The percent co-localization (in $\log_2$ scale) of bacteria with LAMP-1 and syntaxin 17 have been represented as a vertical bar graph. Scale bar = 5μm, (n≥150, N=2, Unpaired student's t-test (Two-tailed)). (B) Intracellular survival of STM (WT) and *ΔompA* (MOI=10) in RAW264.7 cells in the presence and absence of autophagy inhibitor bafilomycin A (50 nM) (n=3, N=2, One-way ANOVA with Tukey's multiple comparison test). (C) Intracellular survival of STM (WT), *ΔompA*, *ΔsseL*, and *ΔompAΔsseL* (MOI=10) in RAW264.7 cells (n=3, N=2, One-way ANOVA with Tukey's multiple comparison test). (D) Representative image of lysosomal fusion (Texas red ovalbumin) with STM (WT): *GFP*, *ΔompA*: *GFP*, and STM (WT): *LLO* (MOI=20) in RAW264.7 cells at 16 hours post-infection. PFA-fixed dead bacteria were used as a control (MOI=25). The colocalization coefficient of bacteria with the lysosomes has been represented as a vertical bar graph. Scale bar = 5μm, (n=50, N=2, One-way ANOVA with Tukey's multiple comparison test). (E) Confocal images representing the fusion of STM (WT): *GFP* and *ΔompA*: *GFP* (MOI=20) with syntaxin 17 and lysosomes (Texas red ovalbumin) in RAW264.7 cells at 16 hours post-infection. The co-localization coefficient of bacteria with lysosomes and syntaxin 17 has been represented as a vertical bar graph. Scale bar = 5μm, (n≥ 50, N=2, Unpaired student's t-test (Two-tailed)).

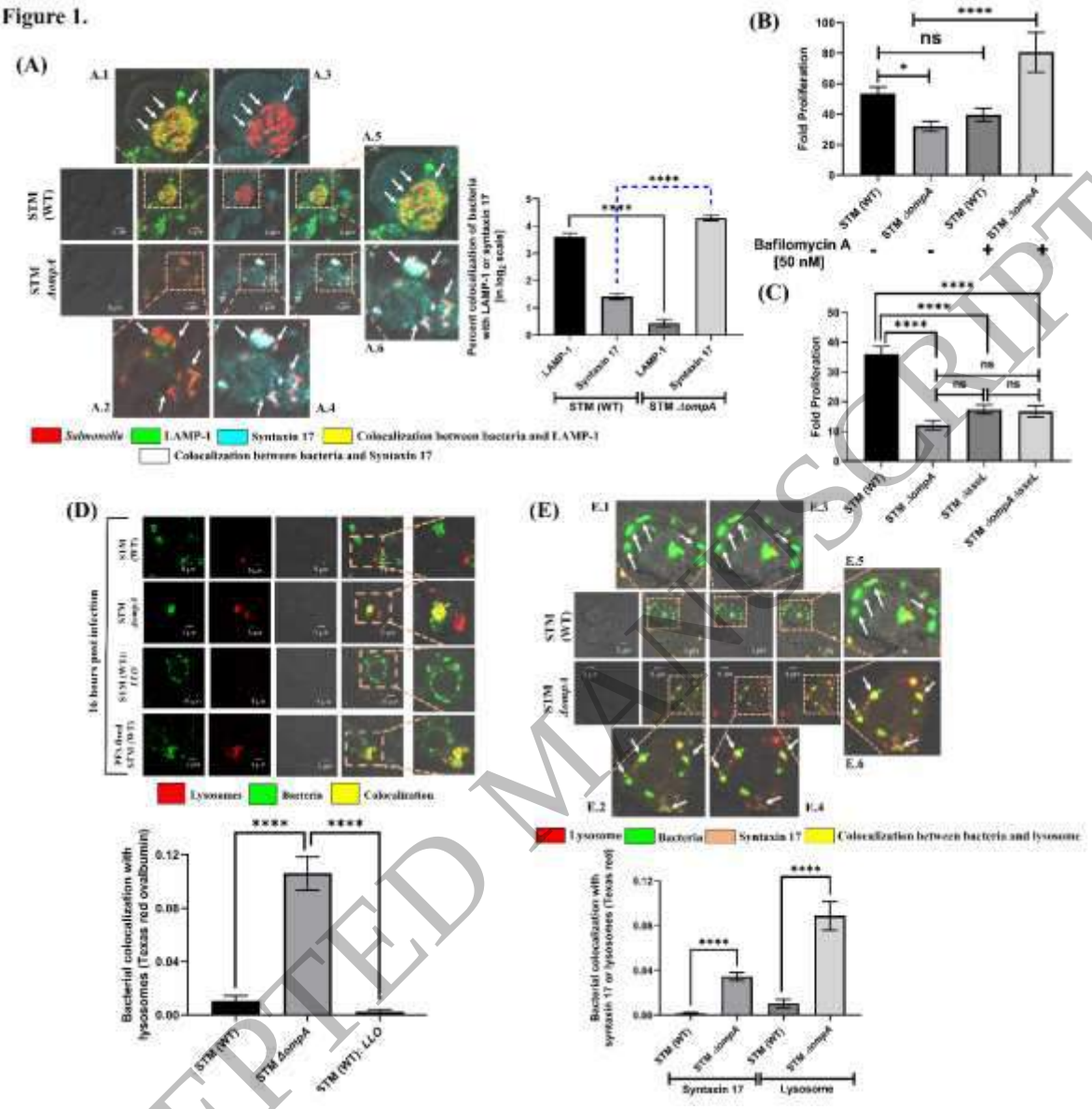

*(p) **< 0.005, (p) ***< 0.0005, (p) ****< 0.0001*. (Unpaired student's t-test (Two-tailed) or One-way ANOVA with Tukey's multiple comparison test)

Figure 2. STM *ΔompA* quits the SCV during the immediate early stage of infection in macrophages.

(A) Image representing the recruitment of EEA-1 around STM (WT), *ΔompA*, and PFA fixed dead bacteria (MOI=25) in the activated U937 cells at 15 minutes post-infection. The percent co-localization (in $\log_2$ scale) of bacteria with EEA-1 has been represented as a vertical bar graph. Scale bar = 5µm, (n≥30, N=2, Unpaired student's t-test (Two-tailed)). (B) Representative image of the recruitment of human LAMP-1 on STM (WT): RFP, and *ΔompA*: RFP (MOI=20) in activated U937 cells at 15-, 30-, and 120-minutes post-infection. The percent co-localization (in $\log_2$ scale) between the bacteria and human LAMP-1 has been represented as a vertical bar graph.

Scale bar = 5µm, (n≥50, N=2, Unpaired student's t-test (Two-tailed)). (C) Image representing the arrangement of mouse LAMP-1 around STM (WT): RFP, and *ΔompA*: RFP (MOI=20) in RAW264.7 cells at 15-, 30-, and 120-minutes post-infection. The percent co-localization (in log_2 scale) between the bacteria and mouse LAMP-1 has been represented as a vertical bar graph. Scale bar = 5µm, (n≥60, N=2, Unpaired student's t-test (Two-tailed)).

Figure 2.

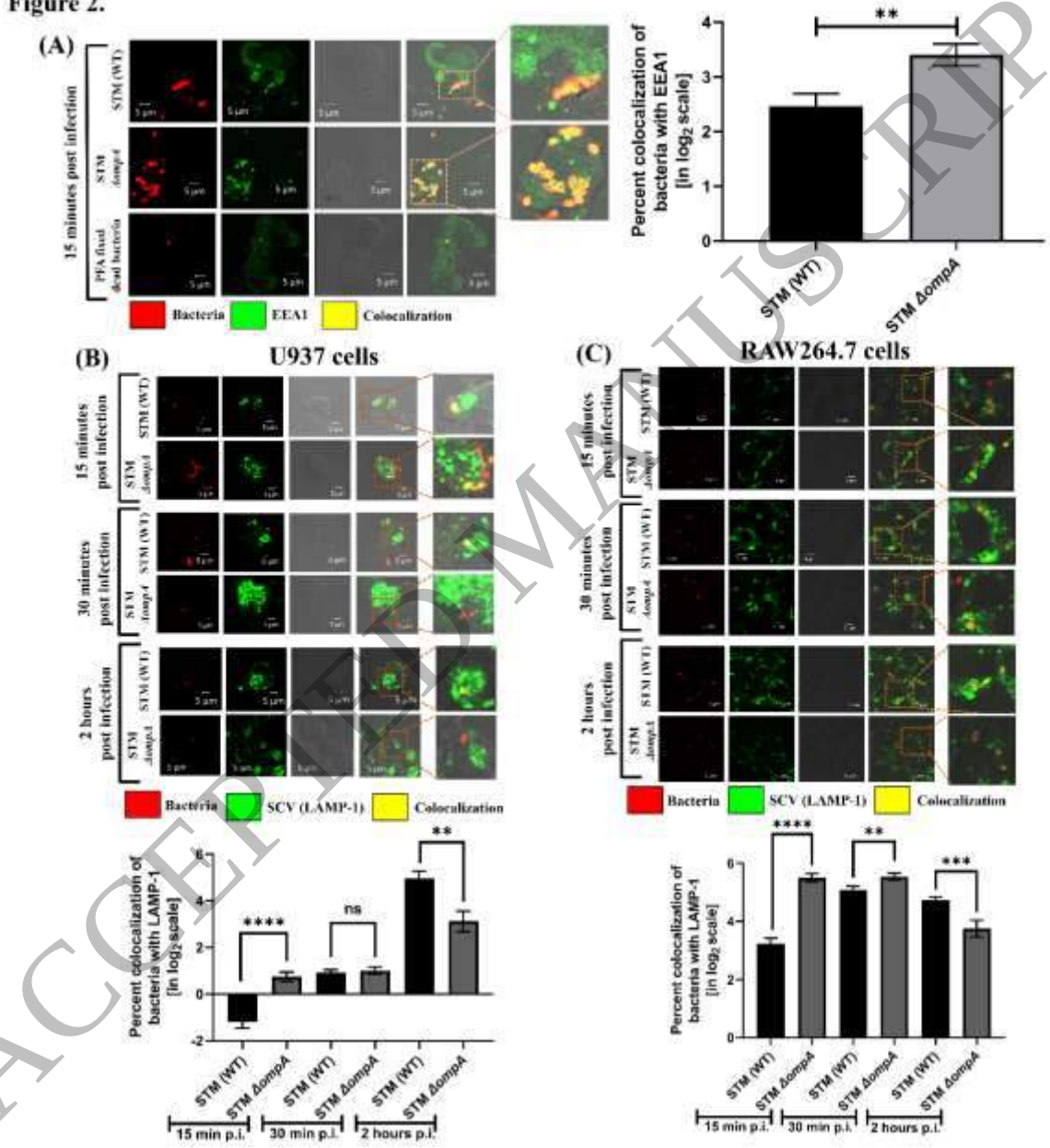

(P) **< 0.005, *(P)* ***< 0.0005, *(P)* ****< 0.0001, ns= non-significant, (Unpaired student's t-test (Two-tailed)).

Figure 3. *Salmonella* Typhimurium utilizes OmpA to interact with host LAMP-1 (SCV) during infection in macrophages.

(A) Representative image of the interaction between *Salmonella* Typhimurium OmpA with host LAMP-1 in RAW 264.7 cells (MOI=20) at 2-, 6-, and 16-hours post-infection. Intracellular *Salmonella* were stained with anti-*Salmonella* OmpA primary antibody. A vertical bar graph represents the co-localization coefficient between the *Salmonella* OmpA and mouse LAMP-1. Scale bar = 5µm, (n=50, N=2, One-way ANOVA with Tukey's multiple comparison test). Data are represented in mean ± SEM. (B) Co-immunoprecipitation depicting the interaction between the mouse LAMP-1 and *Salmonella* OmpA in RAW264.7 cells at 2-, 6-, and 16-hours post-infection (N=3). (C) Co-immunoprecipitation to represent the interaction between mouse LAMP-1 and OmpA of STM (WT), *ΔompA*, *ΔsifA*, *ΔsifA*:*ompA* in RAW264.7 cells at 16-hours post-infection (N=3). (D) Representative image of intracellular localization of STM (WT), *ΔompA*, *ΔsifA*, and *ΔsifA*:*ompA* in RAW264.7 cells (MOI=10) at 16 hours post-infection. A vertical bar graph represents the percentage of co-localization (in $\log_2$ scale) between *Salmonella* and LAMP-1. Scale bar = 5µm, (n=50, N=2, One-way ANOVA with Tukey's multiple comparison test). Intracellular bacteria was stained with anti-*Salmonella* LPS antibody. Data are represented in mean ± SEM. (E) Intracellular proliferation of STM (WT), *ΔompA*, *ΔsifA*, and *ΔsifA*:*ompA* in RAW 264.7 cells (MOI=10). (n=3, N=2, One-way ANOVA with Tukey's multiple comparison test). Data are represented as mean ± SEM.

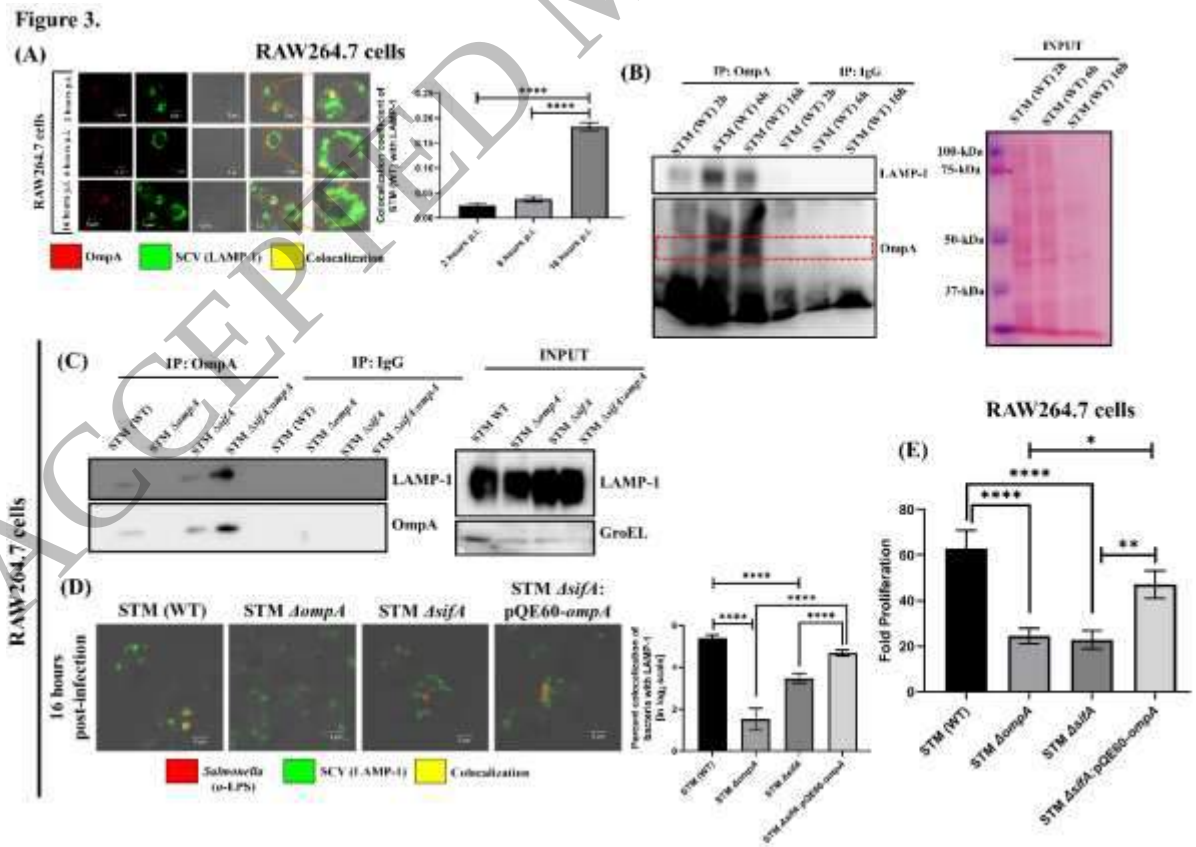

(P) *< 0.05, *(P)* **< 0.005, *(P)* ****< 0.0001, ns= non-significant, (One-way ANOVA with Tukey's multiple comparison).

Figure 4. Introducing mutation in the extracellular loops doesn't alter the function of OmpA *Salmonella* Typhimurium.

(A) The β barrel structure of *Salmonella* Typhimurium OmpA with extracellular loops (Loop1, Loop2, Loop3, and Loop4) obtained by SWISS-MODEL software. Comparison between the extracellular loop sequences of *Escherichia coli* K1 and *Salmonella* Typhimurium. Two different mutations were introduced in loop1 (L1-1 and L1-2) and loop2 (L2-1 and L2-2) separately. Two single mutations (L3-1 and L4-1) were introduced in loop3 (L3) and loop4 (L4). (B) The dot plots (SSC-A vs. DiBAC4) and histograms (Count vs. DiBAC4) representing the outer membrane porosity of STM (WT), *ΔompA*, *ΔompA*: pQE60-*ompA*, *ΔompA*: pQE60-*ompA*-L1-1, *ΔompA*: pQE60-*ompA*-L1-2, *ΔompA*: pQE60-*ompA*-L2-1, *ΔompA*: pQE60-*ompA*-L2-2, *ΔompA*: pQE60-*ompA*-L3-1, and *ΔompA*: pQE60-*ompA*-L4-1 growing in acidic F media for 12 hours post-inoculation using $DiBAC_4$ by flow cytometry. The percent population (in log_2 scale) of $DiBAC_4$-positive bacterial cells has been represented as a vertical bar graph (n=5, N=2, One-way ANOVA with Sidak's multiple comparison test). (C) Densitometric plot representing the intracellular acidification of STM (WT), *ΔompA*, *ΔompA*: pQE60-*ompA*, *ΔompA*: pQE60-*ompA*-L1-1, *ΔompA*: pQE60-*ompA*-L1-2, *ΔompA*: pQE60-*ompA*-L2-1, *ΔompA*: pQE60-*ompA*-L2-2, *ΔompA*: pQE60-*ompA*-L3-1, and *ΔompA*: pQE60-*ompA*-L4-1 incubated in phosphate buffer of pH=5, using BCECF-AM (Concentration- 20 μM) by flow cytometry. The ratio of BCECF-AM (MFI) at 488 (FITC) and 405 (AmCyan) nm has been represented as a vertical bar graph (n=3, N=2, One-way ANOVA with Tukey's multiple comparison test). Data are represented as mean ± SEM. (D) The transcript level expression of *sifA* in STM (WT), *ΔompA*, *ΔompA*: pQE60-*ompA*, *ΔompA*: pQE60-*ompA*-L1-1, *ΔompA*: pQE60-*ompA*-L1-2, *ΔompA*: pQE60-*ompA*-L2-1, *ΔompA*: pQE60-*ompA*-L2-2, *ΔompA*: pQE60-*ompA*-L3-1, and *ΔompA*: pQE60-*ompA*-L4-1 growing in SPI-2 inducing acidic F-media for 8 hours by RT-qPCR (n=3, N=3). Data are represented as mean ± SEM.

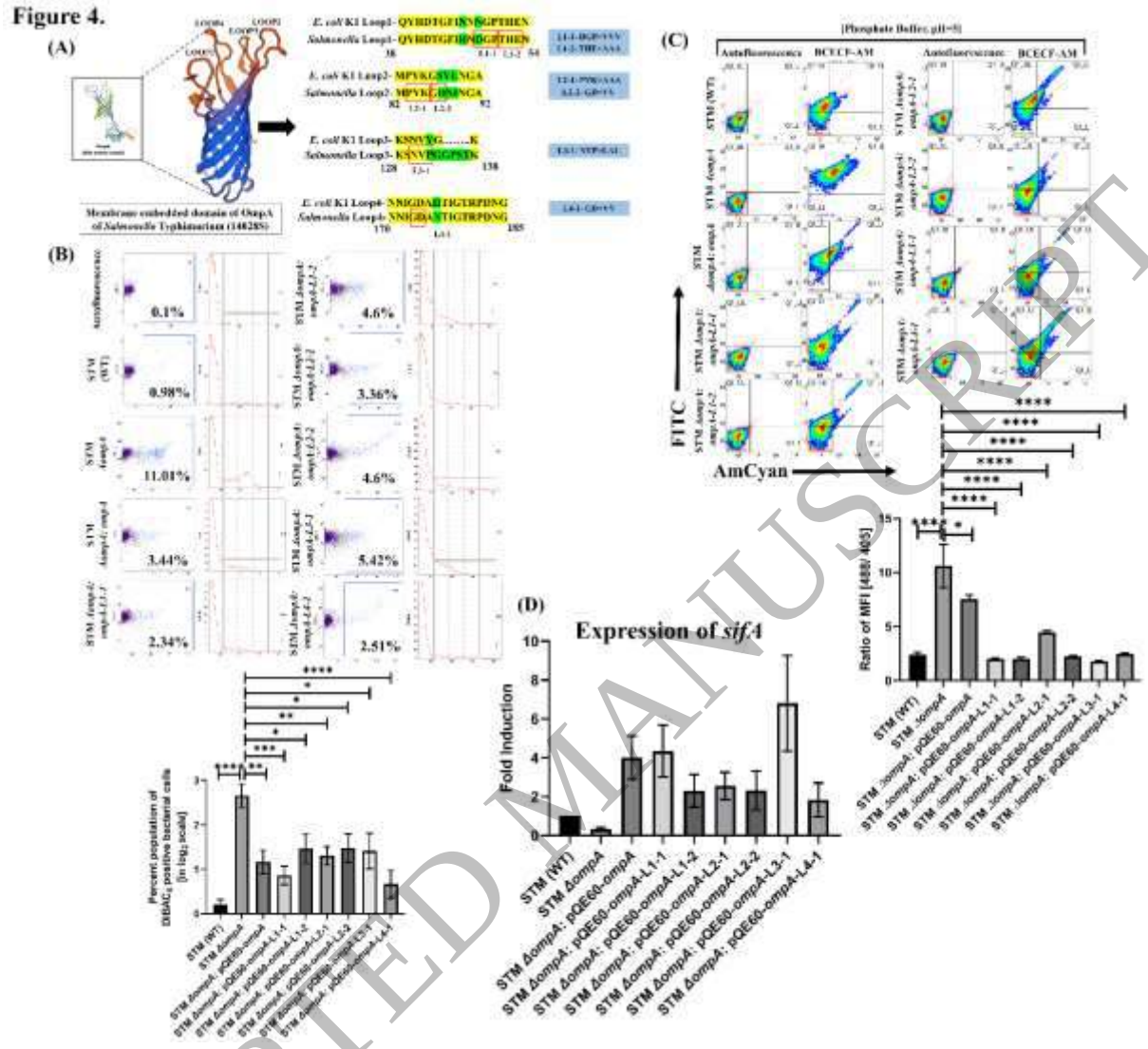

*(P) *< 0.05, (P) **< 0.005, (P) ***< 0.0005, (P) ****< 0.0001*, ns= non-significant. (One-way ANOVA with Tukey's/Sidak's multiple comparison test)

Figure 5. Mutation in the extracellular loops of OmpA releases the bacteria into the cytosol of macrophages but is insufficient for lysosomal activation.

(A) Image representing the recruitment of LAMP-1 around STM (WT), *ΔompA*, *ΔompA*: pQE60-*ompA*, *ΔompA*: pQE60-*ompA*-L1-1, *ΔompA*: pQE60-*ompA*-L1-2, *ΔompA*: pQE60-*ompA*-L2-1, *ΔompA*: pQE60-*ompA*-L2-2, *ΔompA*: pQE60-*ompA*-L3-1, and *ΔompA*: pQE60-*ompA*-L4-1 (MOI=20) in RAW264.7 cells at 16 hours post-infection. The percent co-localization (in $\log_2$ scale) of bacteria with LAMP-1 has been represented as a bar graph. Scale bar = 5µm, (n=100, N=3, One-way ANOVA with Tukey's multiple comparison test). (B) Chloroquine resistance assay of STM (WT), *ΔompA*, *ΔompA*: pQE60-*ompA*, *ΔompA*: pQE60-*ompA*-L1-1, *ΔompA*: pQE60-*ompA*-L1-2, *ΔompA*: pQE60-*ompA*-L2-1, *ΔompA*: pQE60-*ompA*-L2-2, *ΔompA*: pQE60-*ompA*-L3-1, and *ΔompA*: pQE60-*ompA*-L4-1 (MOI=10) infecting RAW264.7 cells at 16 hours post-infection (n=3,

One-way ANOVA with Tukey's multiple comparison test). (C) Confocal images representing the fusion of lysosomes with STM (WT), *ΔompA*, *ΔompA*: pQE60-*ompA*, *ΔompA*: pQE60-*ompA*-L1-1, *ΔompA*: pQE60-*ompA*-L1-2, *ΔompA*: pQE60-*ompA*-L2-1, *ΔompA*: pQE60-*ompA*-L2-2, *ΔompA*: pQE60-*ompA*-L3-1, and *ΔompA*: pQE60-*ompA*-L4-1 (MOI=20) in RAW264.7 cells (pre-treated with Texas red ovalbumin) at 16 hours post-infection. The co-localization coefficient of bacteria with lysosomes has been represented in a vertical graph. Scale bar = 5μm, (n=100, N=2, One-way ANOVA with Tukey's multiple comparison test). (D) Confocal images representing the fusion of lysosomes with STM (WT), *ΔompA*, *ΔsifA*, *ΔompAΔsifA*, *ΔompAΔsifA*: pQE60-*ompA*, *ΔompAΔsifA*: pQE60-*ompA*-L1-1, *ΔompAΔsifA*: pQE60-*ompA*-L1-2, *ΔompAΔsifA*: pQE60-*ompA*-L2-1, *ΔompAΔsifA*: pQE60-*ompA*-L2-2, *ΔompAΔsifA*: pQE60-*ompA*-L3-1, and *ΔompAΔsifA*: pQE60-*ompA*-L4-1 (MOI=20) in RAW264.7 cells (pre-treated with Texas red ovalbumin) at 16 hours post-infection. The co-localization coefficient of bacteria with lysosomes has been represented as a vertical graph. Scale bar = 5μm, (n≥50, N=2, One-way ANOVA with Tukey's multiple comparison test). (E) Intracellular survival of STM (WT), *ΔompA*, *ΔompA*: pQE60-*ompA*, *ΔompA*: pQE60-*ompA*-L1-1, *ΔompA*: pQE60-*ompA*-L1-2, *ΔompA*: pQE60-*ompA*-L2-1, *ΔompA*: pQE60-*ompA*-L2-2, *ΔompA*: pQE60-*ompA*-L3-1 and *ΔompA*: pQE60-*ompA*-L4-1 (MOI=10) in RAW264.7 cells at 16 hours post-infection (n=3, N=3, One-way ANOVA with Tukey's multiple comparison test). Data are represented as mean ± SEM.

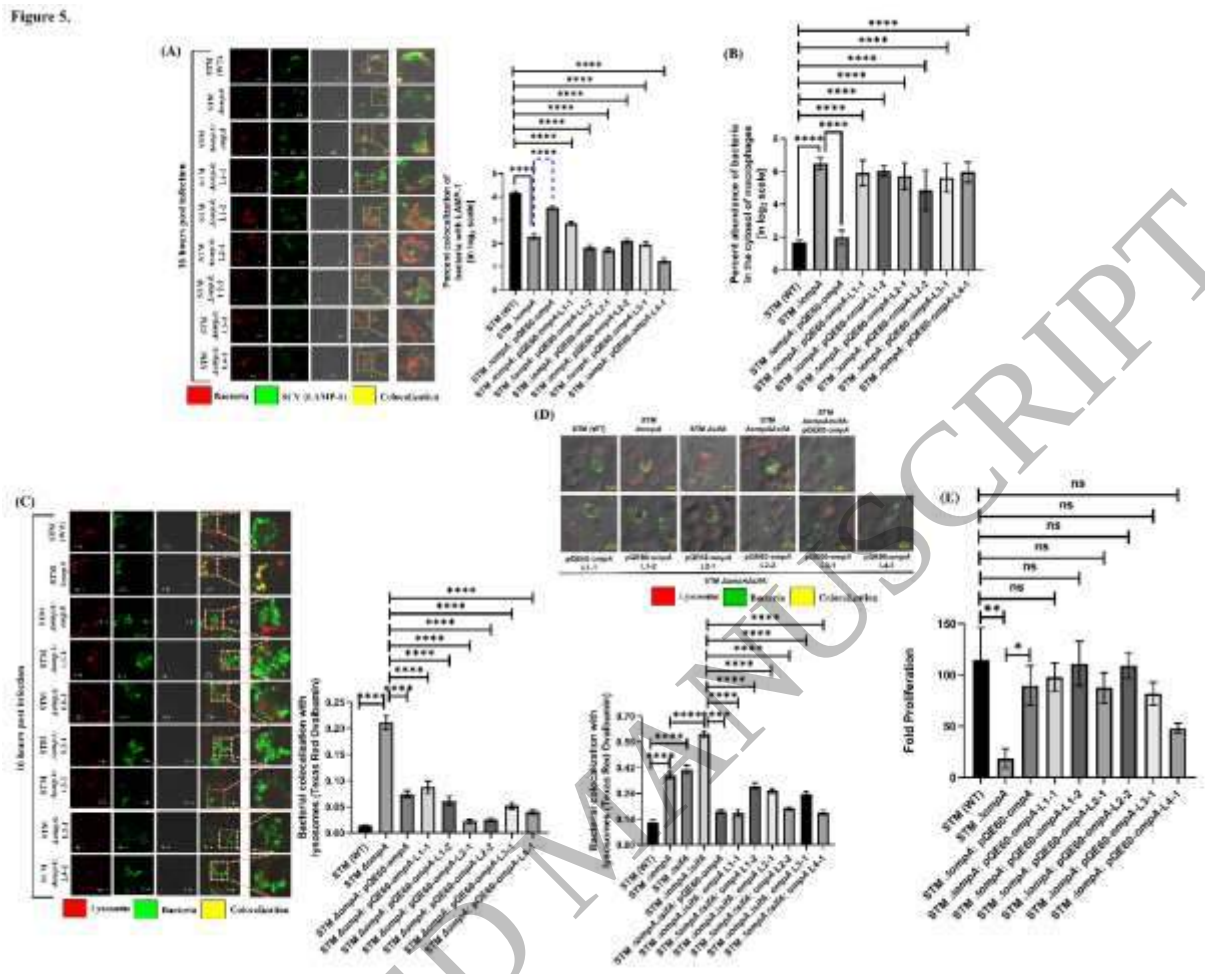

(P) *< 0.05, *(P)* **< 0.005, *(P)* ***< 0.0005, *(P)* ****< 0.0001, ns= non-significant, (One-way ANOVA with Tukey's multiple comparison test).

Figure 6. (Graphical Abstract)

The hypothetical working model of SCV damage by STM *ΔompA* and OmpA loop mutants and subsequent escape from the host lysosomal surveillance.

(A) During the immediate early stage of infection, the membrane of SCV is decorated with early endosomal marker- EEA-1 (Early Endosome Antigen-1). As the time passes, EEA-1 is replaced with LAMP-1. STM (WT) staying inside the LAMP-1$^+$ SCV down-regulates lysosomal biogenesis and suppresses host autophagy machinery in a *sifA*-dependent manner. The down-regulation of lysosome biogenesis facilitates the successful proliferation of the bacteria inside the SCV within the macrophages. (B) During the immediate early stage of infection, STM *ΔompA* stays within the EEA-1$^+$ vacuoles. With an increase in time, STM *ΔompA* cannot retain the LAMP-1 pool around the SCV and comes into the cytosol of macrophages. The cytosolic population of STM *ΔompA* activates host autophagy machinery. After being colocalized with syntaxin 17 and LC3B, a significantly higher fraction of cytosolic STM *ΔompA* is targeted to the lysosomes, which reduced

the intracellular survival of *ompA*$^{-}$ *Salmonella*. (C) Introducing mutations in the extracellular loops hampers the stability of SCV and releases the OmpA loop mutants into the cytosol of macrophages. The cytosolic population OmpA loop mutants activated the host autophagy machinery. However, the cytosolic population of the loop mutants escaped the lysosomal fusion in a *sifA*-independent manner and survived in the cytosol of macrophages.

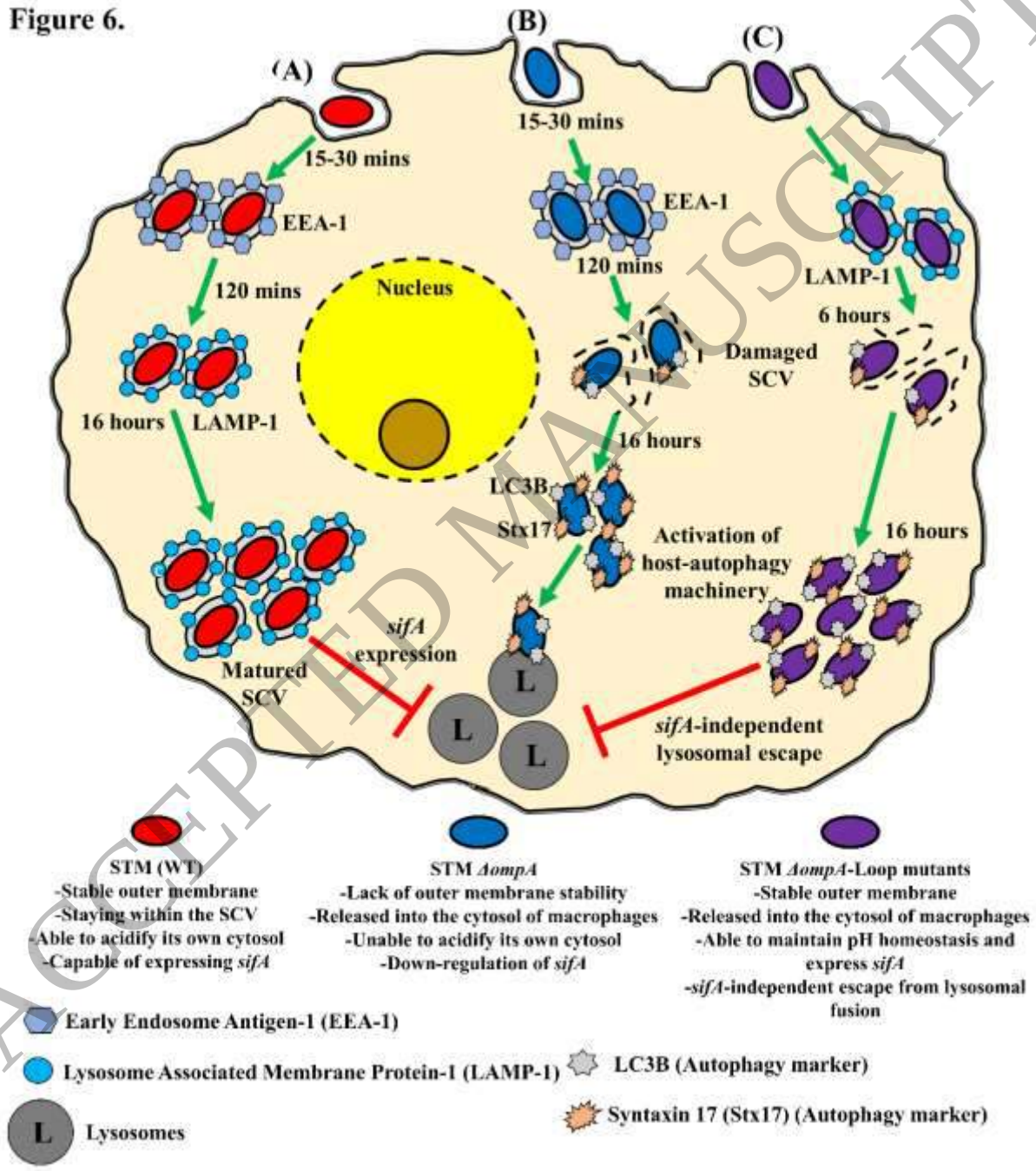

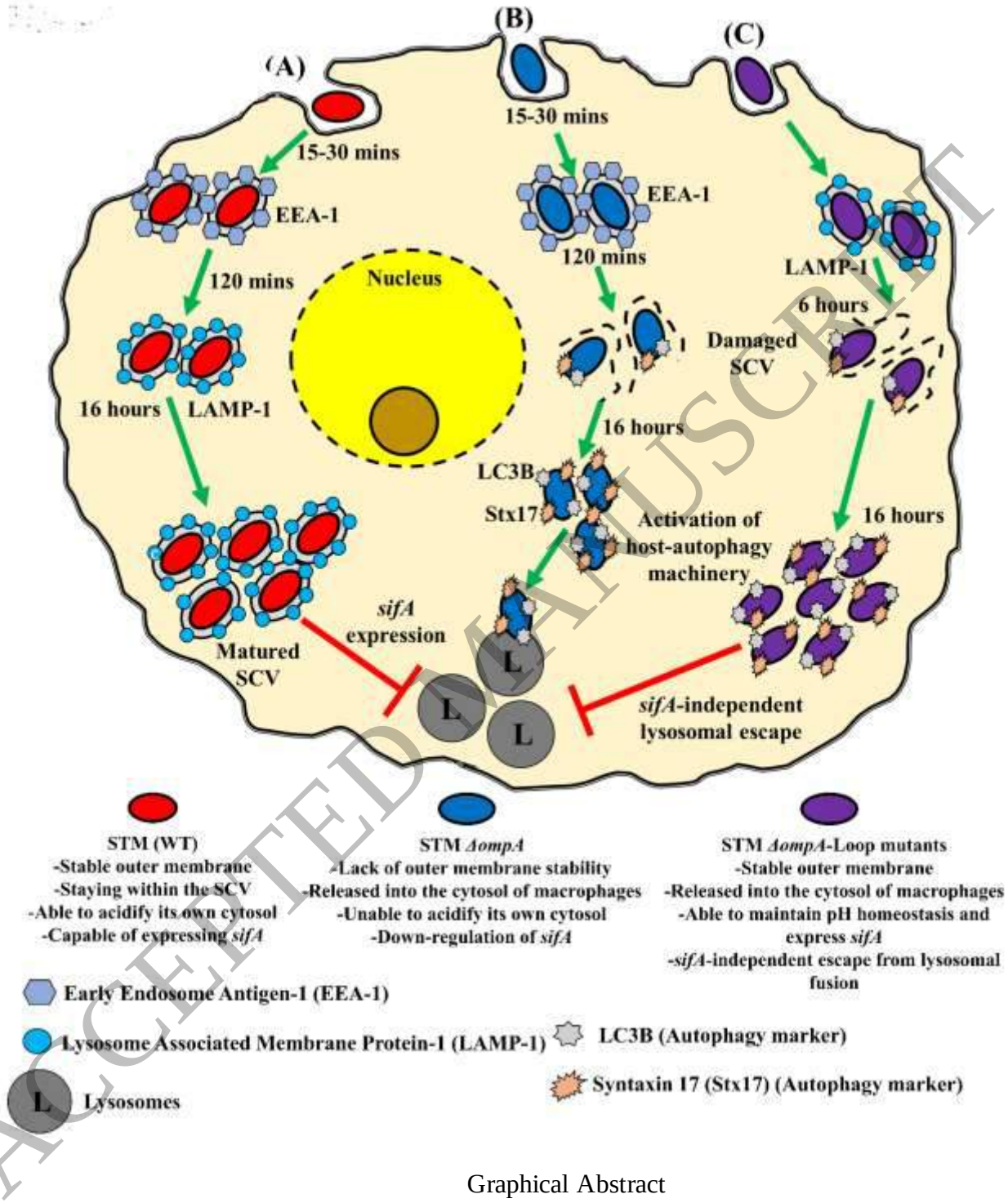

Graphical Abstract

DOI: 10.1093/infdis/jiae376